MODELLING OF THE EFFECTS OF POTHOLES ON MOTOR VEHICLE STRUCTURES

Emmanuel Matsika

2001

MODELLING OF THE EFFECTS OF POTHOLES ON MOTOR VEHICLE STRUCTURES

By

Emmanuel Matsika

A dissertation submitted to the University of Zambia in partial fulfilment of the requirements for the award of the degree of Master of Engineering in Thermofluids

University of Zambia

Department of Mechanical Engineering

Lusaka, Zambia

2001

DECLARATION

I, Emmanuel Matsika, declare that the dissertation represents my own work, and that it has not previously been submitted for a degree at this or another university.

Signed: 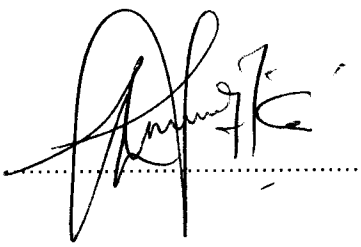 .....

Name: Emmanuel Matsika

Date: 16/2/2001.....

To my parents

APPROVAL PAGE

The University of Zambia approves this dissertation of Emmanuel Matsika as partial fulfillment of the requirements for the award of the degree of Master of Engineering in Thermofluids Engineering.

Name	Signature	Date
DR. EFFORD CLIVE CHIRWA		17 JANUARY 2001
External Examiner		
Dr S.B. ICANTANGA		16/02/2001
Supervisor and Internal Examiner		
DR. L. SIAMINWE		20/02/2001
Internal Examiner		
PROF F.D YAMBA		20/02/2001
Dissertation Chairperson		

ACKNOWLEDGEMENTS

First and foremost, I would like to thank my supervisors, Dr. S. B. Kanyanga and Dr. A. N. Ng'andu for their tireless guidance during the time I was doing the project work and also during the dissertation write up.

In addition, I would like to acknowledge the support rendered by ZCCM Limited through the Kalulushi Technical Services which facilitated for practical work to be carried out. The assistance being in form of vibration analysis equipment and skilled manpower. I am particularly indebted to Mr. Gibson Kabaso and Mr. Chipaela.

The acknowledgements would not be complete without recognising the financial aid from the MHO program of the Netherlands' Ministry of Education.

My gratitude also goes to my classmates and friends for the sincere and positive advice on both academic and social affairs. These are Mr. Edwin Luwaya, Mr. Satnam Virdy, Mr. Grain M. Munakaampe, Mr. Paulos J. Nyirenda and Mr. Moffat Mwanza. I am indebted to my brothers, sisters and my parents for their moral support and encouragement.

The running of the developed software and the writing of the dissertation would have been very difficult without the expert input of the School of Engineering Network Administrator, Mr. Lukwesa Katongo, who was ready to sort out problems even at awkward times. My sincere gratitude goes to him too.

My gratitude also goes to Faith L. Bryant for the encouragement during dissertation writing.

Finally and the most important, I would like to thank God the Almighty for seeing me through the period of study. I know that without Him, I could have done nothing.

Emmanuel Matsika, February 2001

CONTENTS

LIST OF TABLES

Page

LIST OF FIGURES

LIST OF SYMBOLS

		Units
A_a	vibration amplification factor	dimensionless
c_c	suspension critical damping coefficient	[Ns/m]
c_{sh}	suspension damping coefficient	[Ns/m]
c_{tr}	tyre damping coefficient	[Ns/m]
d	diameter of a suspension component, generally	[m]
D_w	vehicle wheel diameter	[m]
D_s	wire diameter of coil spring	[m]
E	modulus of elasticity	[N/m^2]
f_{nus}	frequency of unsprung mass	[Hz]
G	modulus of rigidity of an automobile springs	[N/m^2]
h_{sp}	height of the shock pad	[m]
I	moment of inertia of a vehicle	[kgm^{-2}]
I_y	moment of inertia of the leaf spring cross section	[m^4]
J	polar moment of inertia of the circular section of a bar	[m^4]
k_s	vehicle spring stiffness	[N/m]
k_{tr}	tyre stiffness	[N/m]
l	limiting ripple length	[m]
L	length of the effective part of the torsion bar	[m]
l_a	length of the lever arm	[m]
l_f	distance of the front axle to the centre of gravity of the vehicle	[m]
l_r	distance of the rear axle to the centre of gravity of the vehicle	[m]
l_s	length of a leaf spring	[m]
l_w	pothole length	[m]
l_{wb}	vehicle wheel base	[m]
m_c	coupling mass of a vehicle	[kg]
m_s	sprung mass of a vehicle	[kg]
m_{sf}	front sprung mass of a vehicle	[kg]
m_{sr}	rear sprung mass of a vehicle	[kg]
m_{us}	unsprung mass of a vehicle	[kg]
m_{usf}	front unsprung mass of a vehicle	[kg]

m_{usr}	rear unsprung mass of a vehicle	[kg]
n	the number of active coils or leaves of a coil or leaf spring	dimensionless
n_c	calculated factor of safety	dimensionless
n_d	design factor of safety	dimensionless
P_d	maximum dynamic force	[N]
P_{dus}	maximum dynamic force on the unsprung mass	[N]
p	vehicle roll	dimensionless
q	vehicle pitch	dimensionless
r	vehicle wheel diameter	[m]
r	vehicle yaw	dimensionless
r_l	spring rate of a leaf spring	[m]
R_t	ratio of the duration of the impulse to the natural time of a mass	dimensionless
S_e	endurance limit of a material	[N/m^2]
S_{se}	torsional endurance limit of a material	[N/m^2]
S_{sy}	torsional or shear yield strength	[N/m^2]
S_{te}	tensile endurance limit of a material	[N/m^2]
S_{ut}	ultimate tensile strength of a material	[N/m^2]
S_y	tensile yield strength of a material	[N/m^2]
t	time elapsed after impulse	[s]
t_n	natural period of vibration of a given mass	[s]
t_o	duration of impulse	[s]
t_{ns}	the natural time of the sprung mass	[s]
t_{nus}	the natural time of the unsprung mass	[s]
t_s	thickness of a leaf spring	[m]
T	moment or torque applied on the torsion bar	[Nm]
V	vehicle velocity	[ms^{-1}]
w	leaf spring width	[m]
x_d	pothole depth	[m]
x_f	transmitted vertical displacement of the front sprung mass due to the rear wheel hitting a pothole	[m]
x_r	transmitted vertical displacement of the rear sprung mass due to the front wheel hitting a pothole	[m]
X	vehicle jerk motion	dimensionless
Y	vehicle snaking motion	dimensionless

z	vehicle bounce motion	dimensionless
Z_o	tyre initial displacement	[m]
Z_{of}	the initial displacement of the front sprung mass due transferred vertical motion of the rear sprung mass through pitching	[m]
Z_{or}	the initial displacement of the rear sprung mass due transferred vertical motion of the rear sprung mass through pitching	[m]
Z_{ousf}	the initial displacement of the front unsprung mass due to transferred vertical motion of the rear unsprung mass through pitching	[m]
Z_{ousf}	the initial displacement of the rear unsprung mass due to transferred vertical motion of the front unsprung mass through pitching	[m]
$\ddot{z}_s$	vertical acceleration of the sprung mass	[m/s^2]
$\ddot{z}_{us}$	vertical acceleration of the unsprung mass	[m/s^2]
α	upward inclination of a suspension transverse link, or of the shock absorber, with the horizontal	[radians]
α_s	product of ζ_{sh} and ω_{ns}	[radians]
α_{us}	product of ζ_{tr} and ω_{nus}	[radians]
β	wind-up angle of a suspension lower transverse link	[radians]
δ	static deflection	[m]
ϕ_s	sprung mass vibration response phase angle	[radians]
ϕ_{us}	unsprung mass vibration response phase angle	[radians]
φ	vehicle pitch angle	[radians]
θ	angular deflection of a torsion bar	[radians]
σ	stress in a material	[N/m^2]
σ_a	amplitude stress in a material	[N/m^2]
σ_m	mean stress in a material	[N/m^2]
τ	shear or torsion stress in a material	[N/m^2]
ω	circular frequency	[radians/s]
ω_n	natural circular frequency	[radians/s]
ω_{ns}	sprung mass natural circular frequency	[radians/s]
ω_{nus}	unsprung mass natural circular frequency	[radians/s]
ζ_{sh}	shock absorber damping ratio	dimensionless
ζ_{tr}	equivalent tyre damping ratio	dimensionless

ABSTRACT

The objective of this work was to investigate the effects of the impulses induced by potholes on motor vehicle structures. MATLAB computer package was used to develop a computer program to carry out the tasks. This was done with a view to make recommendations in the nature and frequency of maintenance or replacement of vulnerable parts of the vehicle structure. Further, recommendations were made that vehicle manufacturers should consider in the design of vehicles intended for areas where potholes exist.

Mathematical models of the vehicle suspension systems were used to predict the dynamic forces induced. Stress analysis was performed on selected most susceptible parts of the vehicle. These included wheel bearings, linkage pins and associated bushings, springs and shock absorbers and related fastenings. The parts were chosen following verbal interviews with auto-mechanics in garages and indeed from the experience of the author while working in the transport section of a company. This study only considered stress analysis.

In order to practically determine the vibration responses (acceleration and displacement) of the vehicle and the waveform that best approximates the exciting and excited motion when a wheel hits a pothole, on-vehicle vibration tests were carried out using a two-axle Toyota Corolla 1.5 GL saloon car. The experimental results were found to be lower than the simulated ones.

Simulated results showed that for the car used as a case study, each wheel could be treated separately as a quarter car. The investigation on potholes showed that the pothole length determines the vehicle velocity at which resonance occurs while the magnitude of the induced force is influenced strongly by the pothole depth. In addition and to some extent, the velocity affects the force as it determines the value of the dynamic load factor. For the saloon car used, it was shown that the critical speed (resonance velocity) for both the sprung and unsprung masses fell within 4 to 10 km/h and 40 to 55 km/h for the sprung and unsprung masses, respectively. Since most driving is up to a maximum of 50 km/h around towns and residential areas, the issue of potholes has to be seriously addressed.

The load on the unsprung mass was found to be much higher than that on the sprung mass. Therefore, in the design of suspension parts, emphasis should be put on the unsprung mass components. For the vehicle user, more frequent replacements of suspension parts was recommended, while for the manufacturer, redesigning of some suspension components was recommended.

The results also showed that the suspension geometry, load path characteristics and components materials' mechanical properties dictate the failure mechanism of the vulnerable parts.

CHAPTER 1

1.0 Background and Problem Statement

The problem of potholes in Africa, and Zambia in particular, is of great concern. By August 1997, of the 12,000 km of the economically viable roads in Zambia, only 20 percent were in good condition [1]. Although serious efforts are being made to repair these roads through the National Roads Board, many roads within towns and countryside remain in bad condition.

Currently, most of the vehicles are manufactured in developed countries where roads are generally in good condition. Such vehicles are therefore prone to damage caused by bad roads. The damage thus caused increases,

- Vehicle running costs
- Possibilities of road accidents which may result in loss of property or life
- Transportation time, thus reducing a vehicle's productivity

Even though there may not be available data in Zambia on the effects of potholes on vehicle running costs, a report from the University of Dayton [2], USA indicates that motorists average more than $100 (ZMK260, 000.00 at December 1999 rates) a year in motor vehicle repairs. With Zambian road conditions, the figures would be expected to be much higher.

This study endeavours to fill the gap in knowledge about the effects of potholes on vehicle structures.

1.1 Literature Review

Although a number of studies have been conducted to investigate the vibrational effects of road irregularities, very little has been done particularly on the effects of potholes. Some investigators have treated an irregular road surface as a sinusoidal wave [3]. In fact, most of the data on vehicle ride comfort criteria by the International Standard Organisation (ISO) is based on sinusoidal input [4]. Wong [4] has treated an irregular road as being made up of finite lengths. The height of the foot of the vehicle tyre from a reference and its related derivatives (vertical velocity and acceleration) have been treated as continuous functions of time and are known for a given road profile. The responses

of the sprung and unsprung masses are obtained using numerical procedures based on Taylor's series. Further, the general expressions of the maximum displacement of the sprung and unsprung masses for a continuous sinusoidal road profile have been indicated. Numerical procedures may not be appropriate for pothole analysis because they are often applied to a particular road with a known profile.

Kabondo [5] looked at the subject using an approximation of a pothole as a sinusoidal wave. The author limited himself to the conventional suspension system of a Land Rover 109. No experiments were carried out to validate his computer model. The report does not show how the pothole parameters affect the induced acceleration, and hence the force. Further, it does not indicate the results from the model and how they can be used to make deductions.

The type of suspension system on a vehicle has a bearing on the way the force from the road is transmitted into the vehicle body structure. This is due to differing geometrical configurations [6]. When carrying out stress analysis of the structural members of the suspension and the vehicle structures, conventional calculations dealing with the whole structure [7] or Finite Element Methods (FEM) [8] are employed. The latter are used when the shape of a component is complex.

Due to the tedious calculations involved in most engineering problems, computers are employed. One such tool which has been used by scientists, engineers and mathematicians is a package called MATLAB [9],[10]. Simulations can be carried out using the package. However, there is an allowance for users to develop their own programs using M-files. This was the approach used in this study.

In the absence of information in literature on the effects of potholes on motor vehicle structures, this work is an attempt to make a contribution to the subject.

1.2 Objectives of the Study

The objectives of the study are:

1. To model the effects of the impulses induced by potholes on motor vehicle structures.
2. T determine the waveform which approximates the response to a vehicle wheel hitting a pothole
3. To establish the effects of potholes on motor vehicle structures and thereafter to make recommendations on the nature and frequency of maintenance or replacement/repair.

4. To make recommendations on considerations to be made when designing a vehicle which is to be used where potholes are relatively many and severe.

1.3 Scope of the Study

The state of the road is one of the factors which affect rate at which the state of a vehicle deteriorates. An irregular road surface tends to induce vibrations whose effects on the vehicle "sprung mass" are significantly reduced by the suspension system. The function of the suspension system is therefore to isolate the vehicle structure and occupants from shocks and vibrations generated by the road surface (but maintaining stability, steering control and overall handling precision of the vehicle in its dynamic behaviour).

Road surface irregularities responsible for inducement of vibrations include waviness, bumps, ruts and cracks. While other road irregularities exist, this study focuses on the effects of potholes on motor vehicle structures. A pothole is an undesirable hole created on a road surface. For a vehicle that is moving on a flat road, the sprung and unsprung masses vibrate at their natural frequencies. When any wheel hits a pothole, a forced vibration is induced whose magnitude is dependent on the forward velocity of the vehicle and pothole parameters. Depending on the magnitude, duration and frequency of such disturbances, structural damage and/or fatigue failure can result in the suspension system (unsprung mass), and in the actual vehicle structure (sprung mass) depending on how much force is transmitted from the road surface. Such effects of potholes increase the running costs of a vehicle and the possibilities of accidents due to sudden failure.

The response of the vehicle suspension and body to a disturbance like a pothole is complex. In this work, a proper understanding of the problem was achieved by using a "quarter car" analysis.

The failure of a number of vehicle parts most prone to pothole damage was analysed. The choice of the parts was based on the verbal questioning of auto-mechanics, workshops and the experience gained by the author while working in a motor vehicle workshop. The following are the parts analysed; springs, bushes, pins related to the bushes, wheel bearings, shock absorbers and shock pads.

MATLAB [9],[10] was used to develop a program to determine the vibration responses, forces and stresses in the suspension members. Only MacPherson Strut and Double Wishbone types of

independent suspensions were considered, while dead and live axles were considered for the conventional (rigid axle) type.

In this work, only conventional methods of calculating loads and stresses were employed.

1.4 Dissertation Layout

Following this introductory chapter, Chapter 2 of the dissertation considers the general dynamics of a motor vehicle with particular attention to how the theory of vibration analysis can be used to determine the responses of the sprung and unsprung masses when a wheel hits a pothole. The next two chapters, 3 and 4, deal with types of suspension systems and failure of vehicle suspension parts, respectively.

As part of this work, an experimental investigation was carried out with a saloon car. The details of the experiments together with the findings are presented in Chapter 5.

In order to carry out theoretical analysis on potholes, MATLAB was used. This mathematical tool is introduced in Chapter 6. Further, an introduction to the programs developed for the pothole analysis is made. The chapter ends with a section on the input parameters used for the theoretical study of the saloon car mentioned earlier.

In Chapter 7, the results of the work carried out are presented and discussed, while the conclusions from this work and recommendations for future work are presented in Chapter 8.

CHAPTER 2

VEHICLE DYNAMICS AND VIBRATION ANALYSIS

2.0 Introduction

This chapter considers the general dynamics of a motor vehicle with particular attention to how the theory of vibration analysis can be used to determine the responses of the sprung and unsprung masses when a wheel hits a pothole.

Before considering the motions of a vehicle that are relevant to this study, the general dynamics need to be considered. Presented in Figure 2.1 are the general dynamics of a motor vehicle.

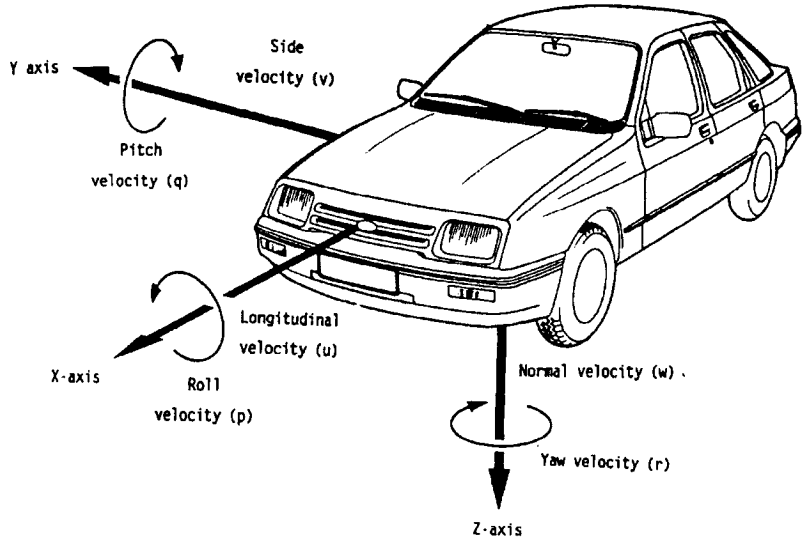

Figure 2.1: Possible Degrees of Freedom on the Three Axes of a Motor Vehicle
(Source: D. Bastow and Howard, Car Suspension and Handling[6])

There are two forms of movements observed from Figure 2.1:
Translational: **X** - jerk; **Y** – snake; **Z** – bounce
Rotational: **p**– roll; **q** – pitch; **r** - yaw

The interaction of these motions, each with its own velocity, acceleration and frequency, makes the sprung vehicle one of the most complex systems in the field of dynamics with at least seventeen degrees of freedom. In this study, only the effects of bounce are analysed as they are considered to

be the relevant ones. Nevertheless, superposition of the vertical motion of the front and rear wheels due to pitching has been taken into account.

2.1 Bounce (Z) and Pitch (q)

Pure bounce: This occurs when front and rear spring masses are equal and springs have identical natural frequencies and rates, and motions are in phase. While weight distribution and springs can be pre-designed, ripples cannot be controlled, hence pitching takes place.

Guest's Theorem [11] states that when a rigid body (such as vehicle body) is mounted on springs, and one set of the springs (such as front ones) are subjected to a vertical force, the resulting effects are the vertical oscillations in both front and rear springs. Contrary to this theorem, springs can be so placed at conjugate points that movement in one spring does not result in movement in the other. This, however, is not practical due to varying load conditions. In this study, it was initially assumed that the conjugate points coincide exactly with wheel centres. Hence front wheels move independently of the rear ones.

The following assumptions were made in the analyses of the models:

(i) Most car suspensions are designed using Guest's Theorem [11]. Therefore, the front and rear wheels can be treated as independent.

(ii) If the spring force is assumed proportional to the vertical displacement of the vehicle, and that the damping force, is proportional to the corresponding linear velocity, then the system can be treated as a linear one. Hence, the principle of superposition is valid.

(iii) Shimmy and tramp motions will be neglected in the mathematical treatment of rigid axle suspensions. This is due to the high complexities associated with the mathematical analysis involved. Moreover, these motions are usually self-excited, not necessarily due to road unevenness. Shimmy occurs when a spinning wheel is subjected to an angular displacement, producing a force which tends to move the axis of rotation in a direction 90^{o} to the original displacement. Tramp is the transverse rocking action of a beam axle when one side of the beam is displaced vertically.

(iv) Wheels oscillate faster than the body. Hence, the two can be treated as separate systems [6]. This is only valid for transient vibration when the system is vibrating at its natural frequency.

(v) Automobile suspension systems are complex with many degrees of freedom. To consider the effect of potholes, a quarter car model shown in Figure 2.2 is used.

(vi) The sprung mass is replaced by dynamically equivalent systems of point masses that may be assumed to be joined by rigid rods of zero mass. This is only true if the total mass is the same, the centre of gravity is in the same position, and the moments of inertia are unchanged.

(vii) Since the front and rear wheels each carry approximately the same mass, with the same spring rate and damping coefficient, they can be considered to be independent.

Initially, a quarter car analysis is carried out. Later, the effect of pitching is included.

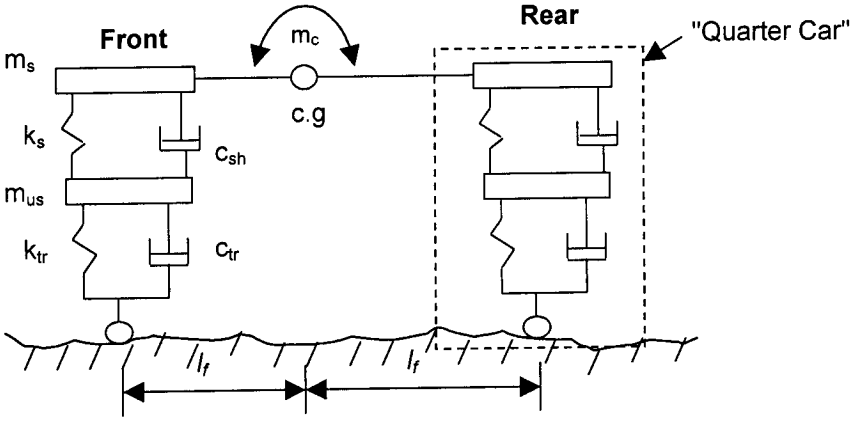

Figure 2.2 Two-dimensional model of bounce and pitch

2.2 Vibration Analysis

Because a vehicle is suspended on springs, it is relevant to study the vibration of a vehicle and to establish how this would assist in solving the problem at hand.

The waveforms that can be used to approximate the excitation due to a pothole are the clipped sine, square, triangular and rectangular waves. The choice of the profile to be used in this study is based on practical results of an experiment conducted during the study. The principle of superposition, which helps in obtaining the overall response of the vehicle, is also considered.

The requirements to carry out the vibration analysis in this study are:

- Parameters of the suspension system, wheel size inclusive
- Velocity of the motor vehicle
- Type of road profile and pothole parameters

In order to obtain the governing equations of a given dynamic model, Newton's Second Law of Motion is employed [3]. The vibration analysis procedure employed involves the following:

1. Mathematical Modelling
2. Derivation of the governing equations
3. Solution of the equations
4. Interpretation of results

2.2.1 Pothole Approximation

A typical pothole takes an elliptical shape, with the longer dimension (length) being in the longitudinal direction of the road. The shorter dimension (width) is in the transverse direction.

Assuming the response to be sinusoidal, the displacement of the sprung and unsprung masses can therefore be expressed thus [4];

$$z(t) = Z_o \sin(\omega t + \phi) \qquad (2.1)$$

The assumption in based on the fact that in most studies, depressions on the road surface have been taken to be sinusoidal [4].

A forcing function can be continuous. However, in this analysis, it was assumed that only one pothole is encountered at a time. Therefore, a transient response is expected as a pothole represents a sudden non-periodic excitation. A transient response takes place at the natural frequency while the amplitude varies depending on the nature of excitation.

It should be noted that when the wheel width is greater than the pothole width, no vibration response is expected. This is because the base of the tyre completely covers the pothole. Thus, the base does not undergo an initial vertical displacement necessary to induce vibrations. Consequently, no analysis is carried out for such a situation.

2.2.2 "Quarter Car Analysis" of the Pothole Study

According to the theory of quarter car analysis [4], the natural frequencies of the sprung and unsprung masses respectively are given by:

$$\omega_{ns} = \sqrt{\frac{k_s k_{tr} / (k_s + k_{tr})}{m_s}} \qquad (2.2a)$$

$$\omega_{nus} = \sqrt{\frac{k_s + k_{tr}}{m_{us}}} \qquad (2.2b)$$

The wide separation between the natural frequencies of the unsprung and sprung masses is important when a wheel hits a pothole. It enables the treatment of the two as separate vibrating systems. The impulse from the road sets the wheel in oscillation at its own natural frequency. For the sprung mass, the excitation will be the vibration of the unsprung mass [4]. The governing equations of motion are given as follows:

Sprung Mass System

$$m_s \ddot{z}_s + c_{sh} \dot{z}_s + k_s z_s = 0 \qquad (2.3a)$$

Replacing the mass, and spring constant with natural frequencies yields,

$$\ddot{z}_s + 2\zeta_{sh} \omega_{ns} \dot{z} + \omega_{ns}{}^2 z_s = 0 \qquad (2.3b)$$

Unsprung Mass System

$$m_{us} \ddot{z} + c_{tr} \dot{z} + k_{tr} z_{us} = 0 \qquad (2.4a)$$

Replacing the mass, and spring constant with natural frequencies yields,

$$\ddot{z}_{us} + 2\zeta_{tr} \omega_{nus} \dot{z}_{us} + \omega_{nus}{}^2 z_{us} = 0 \qquad (2.4b)$$

If the road profile is sinusoidal, the responses of the sprung and unsprung masses can be determined using the classical methods in vibration analysis. For a two-degree-of-freedom system, with the damping of the tyre neglected [4], the vibration amplitudes of the sprung mass, Z_s, and unsprung mass, Z_{us}, are expressed respectively by:

$$z_s = Z_o \sqrt{\frac{A_2}{B_2 + C_2}} \qquad (2.5a)$$

$$z_{us} = Z_o \sqrt{\frac{A_3}{B_2 + C_2}} \qquad (2.5b)$$

where,

$$A_2 = (k_s k_{tr})^2 + (c_{sh} k_{tr} \omega)^2$$

$$B_2 = [(k_s - m_s\omega^2)(k_{tr} - m_{us}\omega^2) - m_s k_s \omega^2]^2$$

$$C_2 = (c_{sh} k_{tr} \omega)^2 [m_s \omega^2 + m_{us} \omega^2 - k_{tr}]$$

$$A_3 = [(k_{tr}(k_s - m_s\omega^2)]^2 + (c_{sh} k_{tr} \omega)^2$$

If the vehicle wheel rolls on continuous undulations, the circular frequency of excitation is equal to $2\pi V / l_w$, where V is the vehicle speed and l_w is the wavelength of the road profile.

Since the vibration of the two masses is being considered separately, Z_s and Z_{us} are taken as the initial displacements of the sprung and unsprung masses respectively. Since most suspension systems are designed for the underdamped condition [3], the solutions of equations 2.3b and 2.4b are determined for $0 < \zeta_{sh} < 1$. Hence, the displacement responses are given by;

$$z_s(t) = Z_s e^{-\alpha_s t} \sin(\omega_{ds} t + \Phi_s) \qquad (2.6a)$$

$$z_{us}(t) = Z_{us} e^{-\alpha_{us} t} \sin(\omega_{dus} t + \Phi_{us}) \qquad (2.6b)$$

Usually in such analyses, the tyre damping effect is neglected [4] giving,

$$z_{us}(t) = Z_{us} \sin(\omega_{nus} t + \phi_{us}) \qquad (2.7)$$

Differentiating these equations twice, the acceleration response is given by $\ddot{z}_s(t)$ and $\ddot{z}_{us}(t)$, respectively.

From the equations of displacement and acceleration, the maximum values of displacement and acceleration are determined. The maximum acceleration is used in Newton's Second Law of motion to calculate the maximum dynamic force induced by the pothole on each mass.

2.2.3 Wheel Contact of a Motor Vehicle

Wheel contact with the road surface is obviously desirable at all times. In practice though, it is not uncommon for the wheel(s) to lose contact. The lower limit to the length of the ripple, *l*, that can be traversed by a car at any given speed is expressed as follows [4],

$$l = \frac{V}{f_{nus}} \sqrt{\frac{m_{us}}{m_s}} \qquad (2.8)$$

The assumptions taken in order to analyse wheel contact are:

1. The car is travelling at such a high speed that the inertia of the relatively large sprung body prevents any appreciable vertical movement.
2. The wheel dimensions are ignored at this stage.
3. The ripple (pothole) will be considered sinusoidal as earlier assumed.
4. The road is flat and horizontal with the pothole being the only road irregularity at the position of interest.

2.2.3.1 Loss of Wheel Contact

If the wavelength of the ripple is larger than the diameter of the wheel, D_w, then loss of contact may occur and a transient vibration takes place. The limiting wavelength for forced excitation at any vehicle speed can be expressed mathematically as:

$$l = D_w \qquad (2.9)$$

This condition is shown in Figure 2.3.

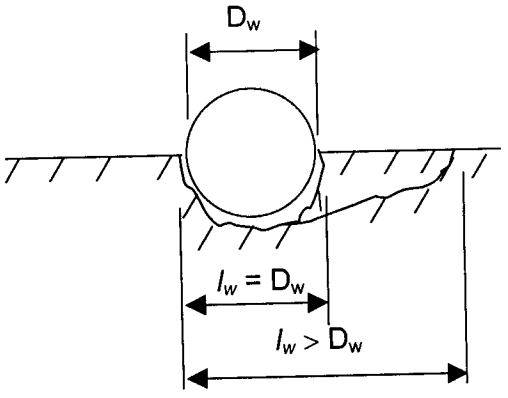

Figure 2.3: Condition expressed by Equation 2.9

What is most important is to determine the initial displacement of the bottom surface of the tyre. Combining the equations of loss of contact, 2.8 and 2.9, the following cases occur:

Case 1 $D_w < l_w < l$, as shown in Figure 2.4.

In this case, wheel contact is lost and the magnitude of Z_o will be equal to the static deflection of the unsprung mass. Therefore, the initial displacement is given by,

$Z_o = \delta$, where $\delta = (m_{us} * g) / k_s$

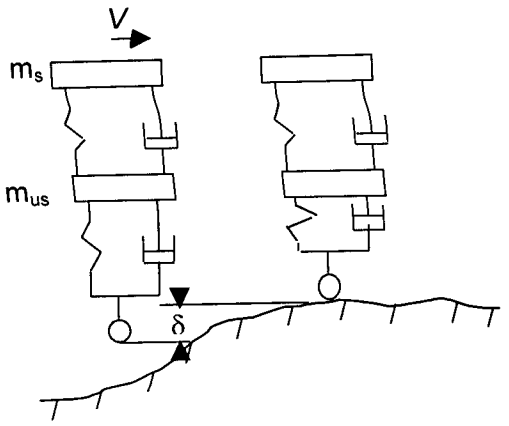

Figure 2.4: Representation of Case 1

Case 2 $l_w \leq D_w$, even if $l_w > l$

The magnitude of the impulse can be deduced from Figure 2.5 as follows:

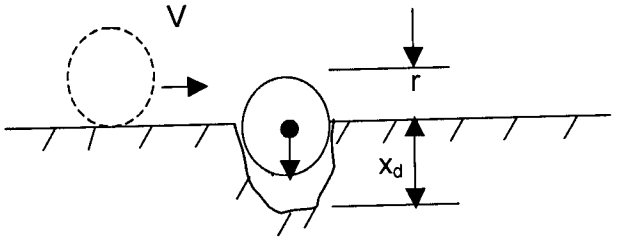

Figure 2.5a: A Condition for Case 2

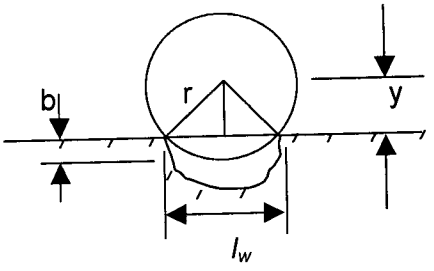

Figure 2.5b:Alternate Condition for Case 2

From Figure 2.5a, if $l_w = D_w$, but $x_d > r$, then $Z_o = r$. However, if $x_d < r$, $Z_o = x_d$.

If $l_w < D_w$, and $b < x_d$, using Pythagoras' theorem,

$$b = r - y = r - \sqrt{r^2 - \left(\frac{l_w}{2}\right)^2} \qquad (2.10)$$

Hence the magnitude of the displacement is $Z_o = b = r - y$. If, however, $l_w < D_w$ and $b > x_d$, then $Z_o = x_d$

Case 3 If $D_w < l_w$ and $l_w > l$ then

$Z_o = x_d$

2.2.3.2 The Effect of the Width of the Wheel

If the width of the wheel is greater than or equal to the width of the pothole, then there will be no vibration response from the system. Such potholes can be ignored when it comes to simulation of effects of potholes on vehicle structures.

2.2.4 Superposition of the Response Due to Interaction of Disturbance (Input) On Front And Rear Wheels

Usually, when the front wheel hits a pothole, the rear one does also. So, if the excitation input for the front wheel is given by z (t), the rear one is given by z(t+Δt); where $\Delta t = l_{wb}/ V$ is the time lapse from the time the front wheel hits the pothole to the time the rear one does. The overall response is obtained by superposition of the individual responses.

In order to determine the displacement of the rear suspension due to the front wheel hitting a pothole, Figure 2.6 below is considered.

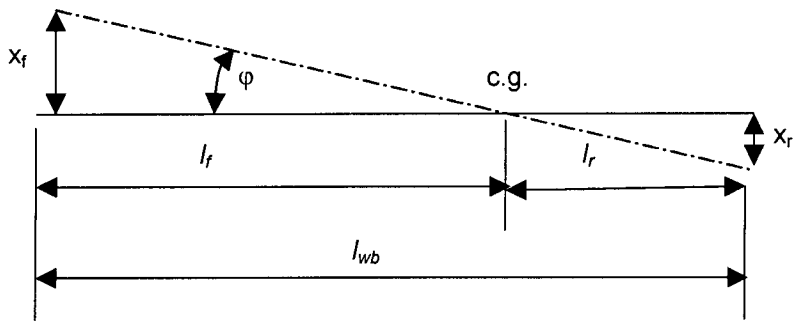

Figure 2.6: Effect of vertical displacement of one end of the vehicle on the other end

The displacement $x_f \approx l_f \varphi$. Therefore, $\varphi = x_f / l_f$ *(2.11)*

Similarly, $x_r \approx l_r \varphi$

Using the expression of φ in Equation 2.11, the displacement $x_r = l_r (x_f / l_f)$,

Therefore, the initial displacement of the rear sprung mass due to the vertical motion of the front part is given by; $Z_{or} = x_r = l_r (x_f / l_f)$ *(2.12a)*

Using the amplitude equations for a two-degree-of-freedom vibrating system [4], the corresponding initial displacement of the unsprung mass is expressed as;

$$Z_{ousr} = (k_s * Z_{sf}) / (-m_{us} * \omega_{nus}^2 + k_s + k_{tr}) \quad (2.12b)$$

Similarly, the displacement of the front sprung mass y_f due to a displacement y_r at the rear is given by $y_f = l_f (y_r / l_r)$. Therefore, the initial displacement of the front sprung mass due to the vertical motion of the rear part is given by; $Z_{of} = y_f = y_r (l_f / l_r)$ *(2.13a)*

Similarly, the unsprung mass displacement is expressed as;

$$Z_{ousf} = (k_s * Z_{sf}) / (-m_{us} * \omega_{nus}^2 + k_s + k_{tr}) \quad (2.13b)$$

Each of the displacements is used as the initial displacement on the sprung and unsprung masses at the respective sides (front and rear).

Front Side (Subscript " *f* ")

$$z_{sf} = Z_o \sqrt{\frac{A_{2f}}{B_{2f} + C_{2f}}} \quad (2.13a)$$

$$z_{usf} = Z_o \sqrt{\frac{A_{3f}}{B_{2f} + C_{2f}}} \quad (2.13b)$$

The response is given by

$$z_{sf} = Z_{sf} e^{-\alpha_{sf} t} \sin(\omega_{dsf} t + \phi_{sf}) + Z_{of} e^{-\alpha_{sf}(t+\Delta t)} \sin(\omega_{dsf}(t + \Delta t) + \phi_{sf}) \quad (2.14)$$

Neglecting the tyre damping,

$$z_{usf} = Z_{usf} \sin(\omega_{nusf} t) + Z_{of} \sin(\omega_{nusf}(t + \Delta t)) \quad (2.15)$$

Rear Side (Subscript "*r* ")

$$z_{sr} = Z_o \sqrt{\frac{A_{2r}}{B_{2r} + C_{2r}}} \quad (2.16a)$$

$$z_{usr} = Z_o \sqrt{\frac{A_{3r}}{B_{2r} + C_{2r}}} \quad (2.16b)$$

The response is given by:

$$z_{sr} = Z_{sr} e^{-\alpha_{sr} t} \sin(\omega_{dsr} t + \phi_{sr}) + Z_{or} e^{-\alpha_{sr}(t-\Delta t)} \sin(\omega_{dsr}(t - \Delta t) + \phi_{sr}) \quad (2.17)$$

$$z_{usr} = Z_{usr} \sin(\omega_{nusr} t) + Z_{or} \sin[\omega_{nusr}(t - \Delta t)] \quad (2.18)$$

2.3 Determination of the Induced Force

In the determination of the dynamic force on the wheel and body, the dynamic load factor or amplification factor, A_a, is employed. It is given by the ratio of the maximum deflection of the given mass, $z(t)_{max}$, to the static deflection, δ. Therefore, it is necessary to know the ratio R_t of the duration of the impulse to the natural time of the vibrating mass. For the pothole situation, the duration of the impulse (shock), t_o, is assumed to be given by the time it takes for the wheel to pass over the second half part of the pothole [12]. Hence,

$$t_o = 0.5\,(l_w/V) \qquad (2.19)$$

The time periods for natural oscillation for the sprung and unsprung masses respectively are given by;

$$t_{ns} = (2\pi)/\omega_{ns}\ , \text{ and } \quad t_{nus} = (2\pi)/\omega_{nus} \qquad (2.20)$$

Using the graph of the amplification factor or dynamic load factor, A_a, against time ratio, R_t, [3] the amplification factor corresponding to each data set is determined. Figure 2.7 shows the typical graph.

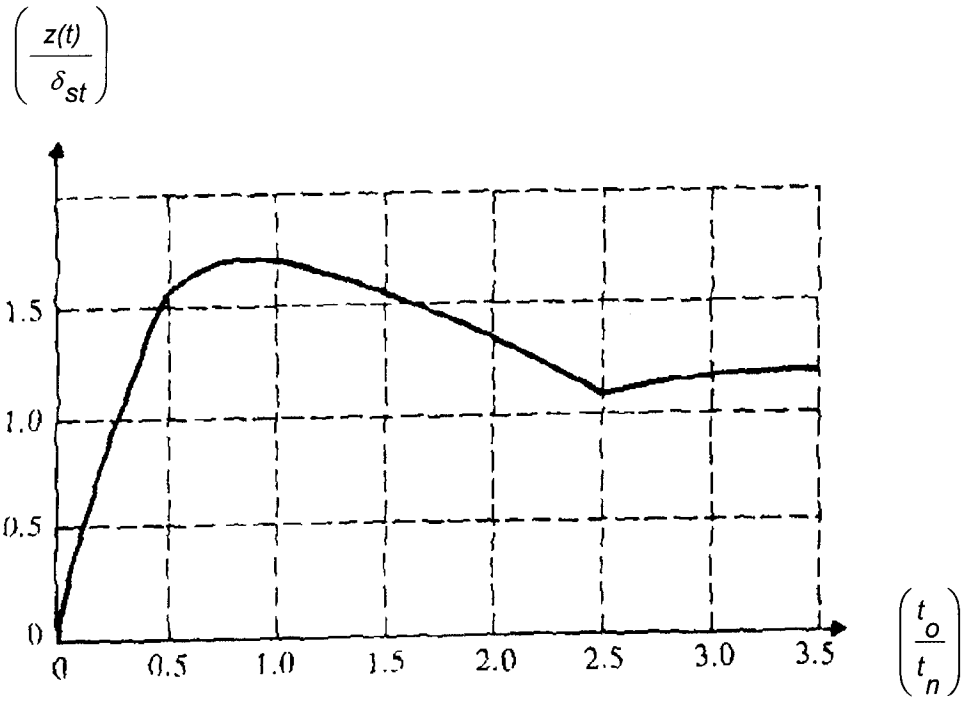

Figure 2.7: Amplification Factor Vs Time Ratio [3].

The maximum dynamic load, P_d, is given by:

$$P_{dus} = A_a m_{us} \ddot{z}_{us\ max} \quad \textit{(unsprung mass)} \qquad (2.21)$$

$$P_{ds} = A_a m_s \ddot{z}_{s\ max} \quad \textit{(sprung mass)} \qquad (2.22)$$

The force from the unsprung mass is taken as the one transmitted up through the suspension system. It does not necessarily represent the force on the base of the tyre, which is expected to be higher than P_s. This is because part of the load on the tyre periphery is used to deform the tyre and is absorbed in the suspension system.

The acceleration equations presented in this chapter are used to determine the acceleration vibration response of the sprung and unsprung masses of a vehicle. For quarter car analysis, the equations that do not take superposition into account are used. On the other hand, the equations where superposition is taken into account are applied to a two-axle vehicle model. The response for the quarter car analysis is compared with the superimposed consideration in order to find out the extent to which the vertical motion of the front and rear sides of the vehicle affect each other. If there is little effect, a quarter car model can be applied to describe the response at each wheel.

The equations of displacement are used to study the vibration response of the two masses. Thus, the time it takes for the vibration to die out can be determined. Further, when the graph of maximum displacement against vehicle speed is plotted for a case with particular pothole and vehicle suspension parameters, it is possible to determine the speed at which resonance occurs for each spring-mass system.

CHAPTER 3

VEHICLE SUSPENSION SYSTEMS

3.0 Introduction

Now that the expression of the force induced by a pothole has been established, it is important to understand the way the force is transmitted to the various other members. This chapter deals with establishment of the expressions for the forces transmitted in the suspension system of the Double Wishbone and MacPherson strut for independent systems. It also looks at the conventional system where leaf springs are employed.

3.1 The Chassis and Unibody Construction

The suspension members are connected to the vehicle body in two ways; either through a chassis (frame) or directly using unibody (integral) construction [13].

3.1.1 The Frame

The frame is designed to support various units of the transmission and body rigidly, and to keep them in correct positions. The material normally used for the frame is cold rolled open-hearth steel cold pressed into channels. Heavy trucks usually use frames made of I-beams. The stresses that the frame has to withstand are [13]:

1. Bending which occurs due to the rising and falling of the front and rear axle.
2. Torsional (twisting) stresses caused by the tendency of different corners to rise and fall independent of others.
3. Lozenging; i.e. forcing of the rectangular frame into a diamond shape (this usually happens when cornering).
4. Forces due to acceleration and braking.

3.1.2 The Integrated Construction

The integrated or unibody construction is a design in which the frame is eliminated and the body is so constructed that it has sufficient strength and stiffness to carry the loads normally taken by the frame. The whole structure is built up of light metal pressings secured together, usually by welding. Suitable strengthening sections are placed at points of maximum load such as engine and suspension mountings. The integral construction is normally confined to passenger cars [6,13].

The current study does not include details on chassis loading since it is not one of the major components affected by potholes.

3.2 Types of Suspension Systems

The force from the wheel is transmitted to the suspension system via the wheel drum and the wheel bearing. It is worthwhile to note that the load path to the structure depends largely on the type of suspension and the suspension geometry [13]. Suspension systems can be divided into two major categories. These are conventional and independent systems.

1. Beam or Rigid Axle Suspensions (Conventional Suspensions)

In this type of suspension system,

(i). The two pairs of wheels are mounted on a rigid axle.

(ii). The beams can either be "live" (with a differential) or "dead" (without a differential).

(iii). The chassis is supported on the axle through leaf springs.

(iv). The wheels experience the same magnitude of angular motion in the vertical plane.

2. Independent Suspensions

This is a method of elastically supporting the chassis on road wheels without the intermediary of rigid axles. Thus, wheels move independently. In this type of system,

(i). The wheels are not interdependent.

(ii). The body is supported through shock absorbers and coil or torsion springs.

(iii). Some independent systems execute parallel (or approximate) up and down motion such that the gyroscopic effect is reduced. This solves the wheel wobble or shimmy problem experienced in conventional suspension systems.

In Zambia, the most predominant independent suspension systems in use are the MacPherson strut and Double-wishbone. In fact, world-wide, over the years, many other types of independent systems have been discarded for a variety of reasons, with only these two being widely used [6]. They are mostly used in passenger cars and as front suspensions in certain vans. On the other hand, dependent suspension systems are common in light and heavy vehicles. The springs employed in independent and dependent suspensions are coil and leaf springs respectively. In both cases, however, telescopic hydraulic shock absorbers are normally incorporated [6].

The factors that affect the magnitude of the shock transmitted into the suspension system are tyre diameter, flexibility of the tyre sidewall, the contact area of the tyre/road interface and the unsprung mass. On the other hand, the factors which affect the amplitude of wheel motion and the load transmitted to the body structure through spring seats and suspension attachment points are the spring rate, the damping effects of the shock absorber and the ratio of the sprung to the unsprung mass.

For different degrees of freedom, the distribution of the masses, the attachment of the wheels and the balancing of the spring rates make fundamental contributions to the behaviour of the vehicle under dynamic conditions. The type of the suspension and its geometry determines the actual magnitude of the induced forces. The variables which affect the suspension geometry are toe setting, camber angle, castor angle, mechanical trail and wheel off set (scrub radius).

When dealing with models of suspension systems, sometimes the damping effect of the spring can be neglected in cases where the shock absorber damping coefficient is much higher than that due to the spring [6] (the body is assumed to be rigid). The natural frequency of the sprung mass is a significant factor in the behaviour of the suspension system on the road. It determines the rate at which the energy stored by a compressed spring is transmitted back into the body structure – the residual effects of crossing a bump or pothole [6].

3.2.1 The Load Path

It is important to understand how the force is transmitted to the various other members. This also entails establishing the expressions for the forces and the resulting stresses. Only expressions giving the forces from the wheel and the suspension system up to the frame or body are considered in this work. In the conventional suspension system, laminated leaf springs are usually used as shown in Figure 3.1.

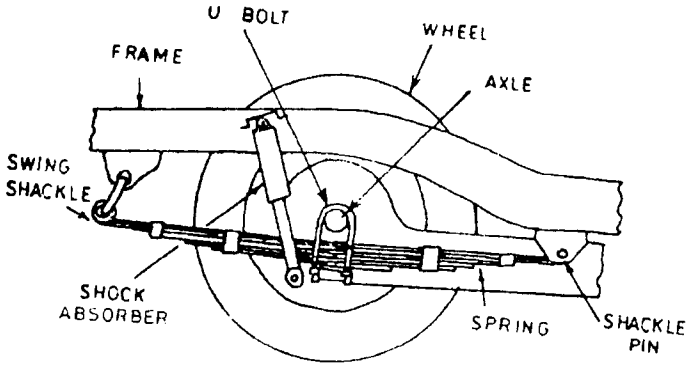

Figure 3.1: Laminated Spring Assembly

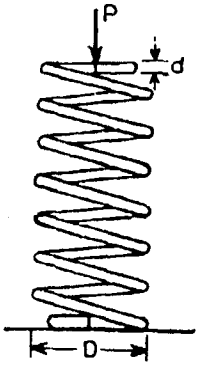

Figure 3. 2: A Coil Spring

Independent systems use coil springs of the type shown in Figure 3.2. The vehicle weight is supported through the spring, control arm, knuckle, spindle, hub, wheel and wheel tower as shown in Figure 3.3. If the front suspension is equipped with torsion bars, the load is absorbed through the lower control arms. The torsion bar is either connected from the inboard end of the lower control arm pivot to the vehicle frame at a point parallel to the rear engine mounting or connected between the outer end of the lower control arm and the front cross member.

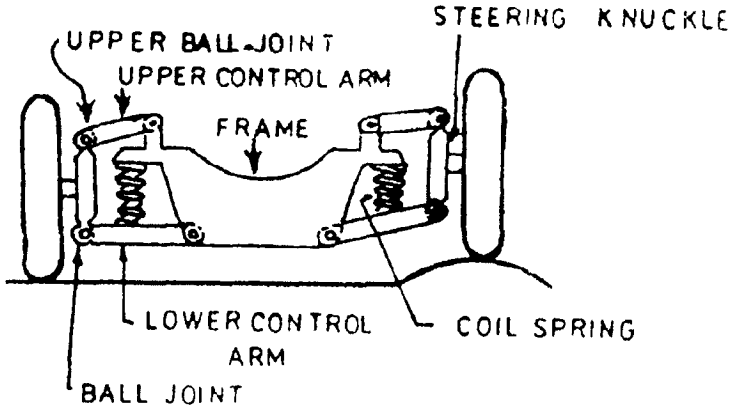

Figure 3.3: An Independent Suspension (Double Wishbone)

The ball joint on either the upper or lower end of the spring loaded control arm is called a weight carrying ball joint. When it fastens to the knuckle above the control arm, it is called a tension ball joint because the body tends to pull the joint from the knuckle. When the control arm is located above the ball joint, it pushes the ball joint into the spindle and is thus called a compression ball joint.

In both the MacPherson and Double-wishbone suspensions, the transverse link is connected to the body by rubber bushes and connected to the stub axle by a ball joint as shown in Figures 3.3 and 3.4. In the latter, the kingpin is tilted inwards at the top to assist in obtaining centre point steering without excessive camber (i.e. assists the camber angle). The angle between the centre line of the kingpin and the vertical is known as the kingpin inclination angle and its value is usually between 5° and 10° [14]. This also represents the angle of inclination of the load path from the wheel to the bearing above the shock pad as discussed later in Section 3.4.2.

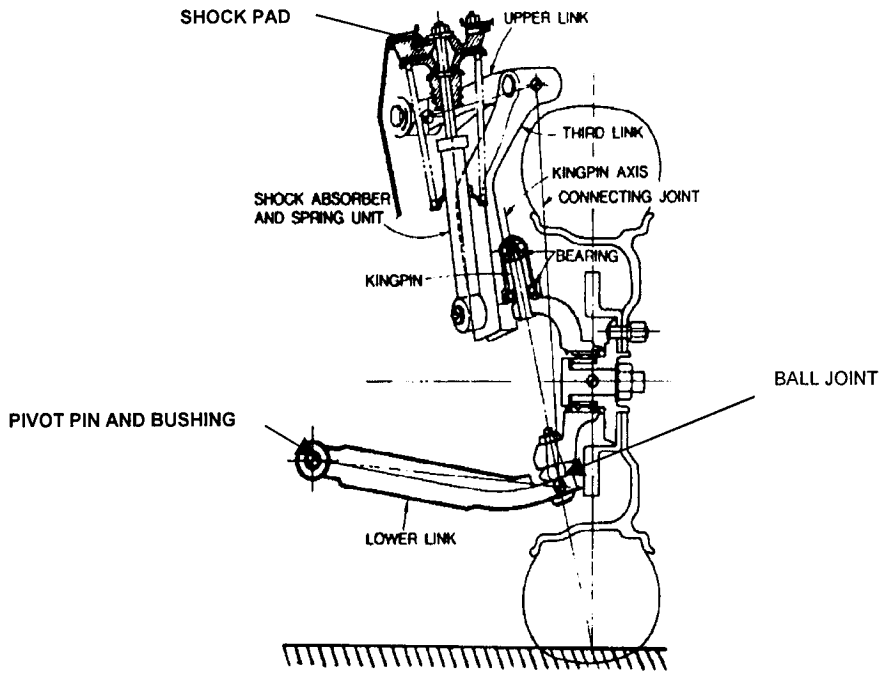

Figure 3.4: A complete assembly of a strut

3.3 The Suspension Shock Absorber (Damper)

Rubber bushings are used between control arms, hangers and knuckles to help absorb road shocks, provide deflection and reduce noise. Shock absorbers are installed on a suspension system to improve ride, vehicle controllability and vehicle handling by rapidly dampening the oscillation. This is common in almost all types of suspension systems. Without damping, a vibration once excited would persist indefinitely. In practice, damping exists in three forms; friction, viscous and that due to air resistance. Since damping due to friction and air is small compared to the viscous one, the bulk of damping is viscous damping [6].

In rear axles, shock absorbers are connected between the spring seat on the rear axle housing and the frame. The position of the shock absorber for an independent suspension varies due to the diversity of the suspension geometry. Generally, the damping coefficient, c_{sh}, of the shock absorber is expressed as:

$$c_{sh} = \zeta_{sh}\left(2\sqrt{k_s m_s}\right) \qquad (3.1)$$

where the critical damping constant, $c_c = 2\sqrt{k_s m_s}$

Worn shock absorbers can result in a loss of control. The function of the shock absorber is to keep the tyres on the ground. A worn shock absorber allows the tyres to bounce excessively causing a reduced grip on the road and dangerous steering instability. This can result in loss of control or even roll-over of the vehicle.

Further, worn shock absorbers can cause damage to tyres and other components: The bouncing allowed by worn shock absorbers can result in abnormal wear of the tyre tread. The pattern is usually called cupping and results in an uneven tread which must be replaced. The bouncing of the vehicle can also damage other suspension components such as bushings and springs. This bouncing can be subtle and undetectable by the average driver or it can be dramatic and obvious.

3.3.1 Types of Hydraulic Dampers

Apart from hydro-pneumatic and hydro-elastic suspensions, in which diaphragms move the fluid, hydraulic dampers depend upon pistons working in cylinders for developing the pressures necessary to provide the damping forces. These cylinders can be made as either lever-arm devices or telescopic tubes. Vane type hydraulic dampers were also made for some time but have now been abandoned because they were not reliable [13]. The three main types of the lever-arm dampers have now given way almost universally to telescopic devices that are dealt with in more detail below.

3.3.1.1 Telescopic Dampers

The objective in damper valve design is to maintain consistent laminar flow characteristics throughout the operating range of loads and input velocities. A damper valve is an orifice which opens according to the stroke and internal pressure generated to create a specifically tailored resistance curve. The most commonly used form of hydraulic damper now is the telescopic double or twin-tube type. This combines the action of fluid passing through a piston in a cylinder with the displacement of fluid into a concentric chamber as shown in Figure 3.5.

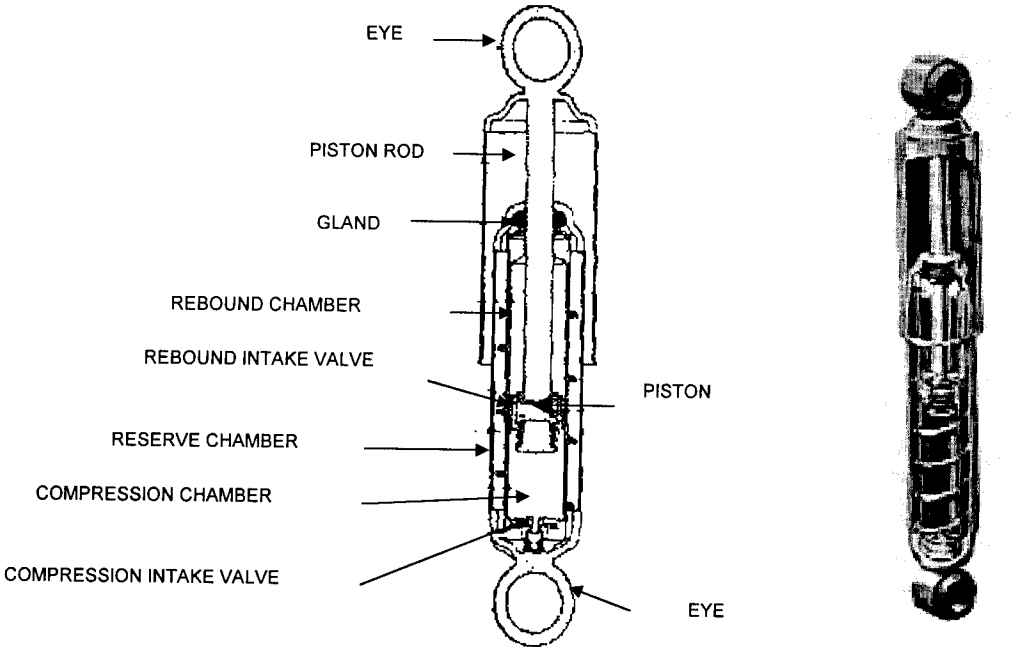

Figure 3.5: A Telescopic Shock Absorber

Excessive loads on the damper can result in much higher damper pressures being developed, hence higher forces if the limit travel is exceeded. In turn, this leads to premature failure of the device. Dynamic Loads on the damper are transmitted from the road surface in the form of vertical acceleration. Typical values of the acceleration of the unsprung mass vary from 20 to 30 g's [6,15].

In the Double wishbone and MacPherson suspension system, the top end of the shock absorber is connected to the vehicle body through a shock pad that assists in damping the forces from the wheel. Figure 3.4 shows a complete suspension assembly of a strut.

3.4 Mechanics of an Independent Suspension

Before one can consider the forces in the various members of the suspension system, it is necessary to understand the geometry of the suspension and the associated motions when the wheel is displaced.

3.4.1 Double Transverse Link (Double Wishbone)

The spring is mounted on such a system in three ways:

(i) Coil Spring mounted between the lower link and the vehicle body.

(ii) Coil Spring mounted between the upper link and the vehicle body.

(iii) Torsion bar fitted at the pivot of the lower link.

Only (i) and (iii) are dealt with in detail here as (i) and (ii) can be analysed in a similar manner.

(a) Coil Spring mounted between the lower link and the vehicle body

Figure 3.6 shows a double-transverse-link independent suspension. The action of a vertical force R is considered as this represents the induced force due to the wheel hitting a pothole on a straight road.

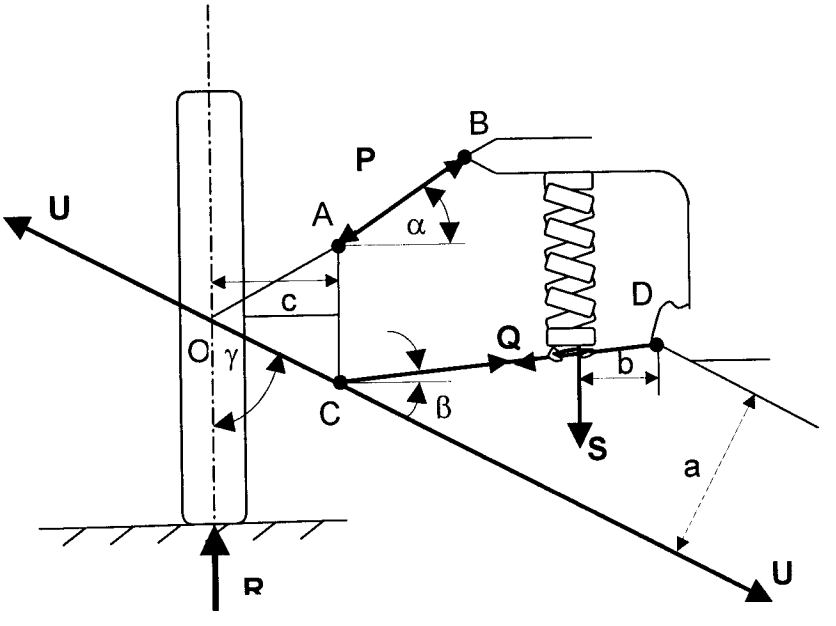

Figure 3.6: The Geometry of a Double Transverse Link Independent Suspension

For the equilibrium of the stub axle assembly represented by length c,

$P \cos \alpha = U \sin \gamma$

This gives, $U = (P \cos \alpha)/ \sin \gamma$ *(3.2)*

In a similar manner, $P = R/(\sin \gamma + \cos \alpha \cot \gamma)$ *(3.3)*

This equation gives the force in the link AB as well as the force on pivot A.

Substituting for P in Equation 3.2,

$U = R/(\sin \gamma \tan \alpha + \cos \gamma)$ *(3.4)*

This force acts on the pivot C in the direction shown in Figure 3.6.

$\sum M_D = 0$ gives $Sb = Ua$

$S = U a / b = R a / b (\sin\gamma \tan \alpha + \cos \gamma)$ *(3.5)*

This expression gives the force in the spring.

Now,

$$Q = U \sin(\gamma - \beta) = R \frac{\sin(\gamma - \beta)}{\sin\gamma \tan\alpha + \cos\gamma} \qquad (3.6)$$

This represents the force in the link CD.

(b) Torsion Bar Fitted at the Pivot of the Lower Link

Considering Figure 3.7, the most important parameters are the moment at B and the angle of rotation of link CB about B, θ_{CB}. The torsion bar is fitted at B parallel to the longitudinal axis of the vehicle (i.e. perpendicular to the plane of sheet of paper).

In the case of a wheel hitting a pothole, the maximum displacement along the axis through which P_W acts can be geometrically related to the movement of link CB. This helps in obtaining θ_{CB} knowing the initial position of link CB.

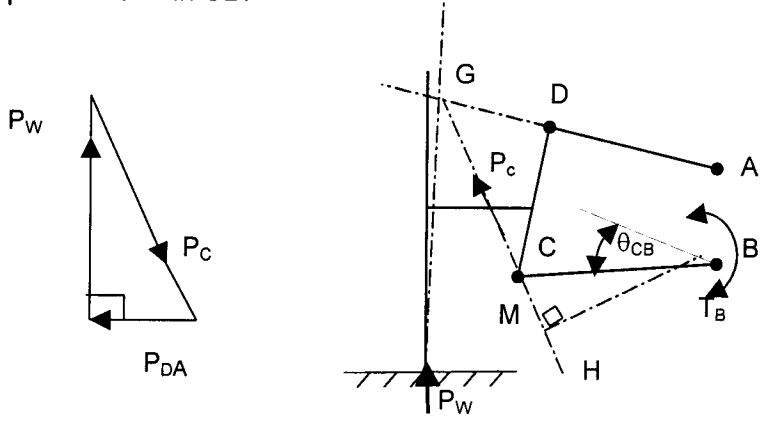

Figure 3.7: The Geometry of a Double Wishbone System with a Torsion bar

The torque (T_B) is given by:

$$T_B = P_C * MB \qquad (3.7)$$

3.4.2 The Strut Suspension (MacPherson Strut)

The strut suspension system has gained popularity over the years. It is used for both front and rear systems. Figure 3.8 shows the geometrical construction of the suspension with the forces on it.

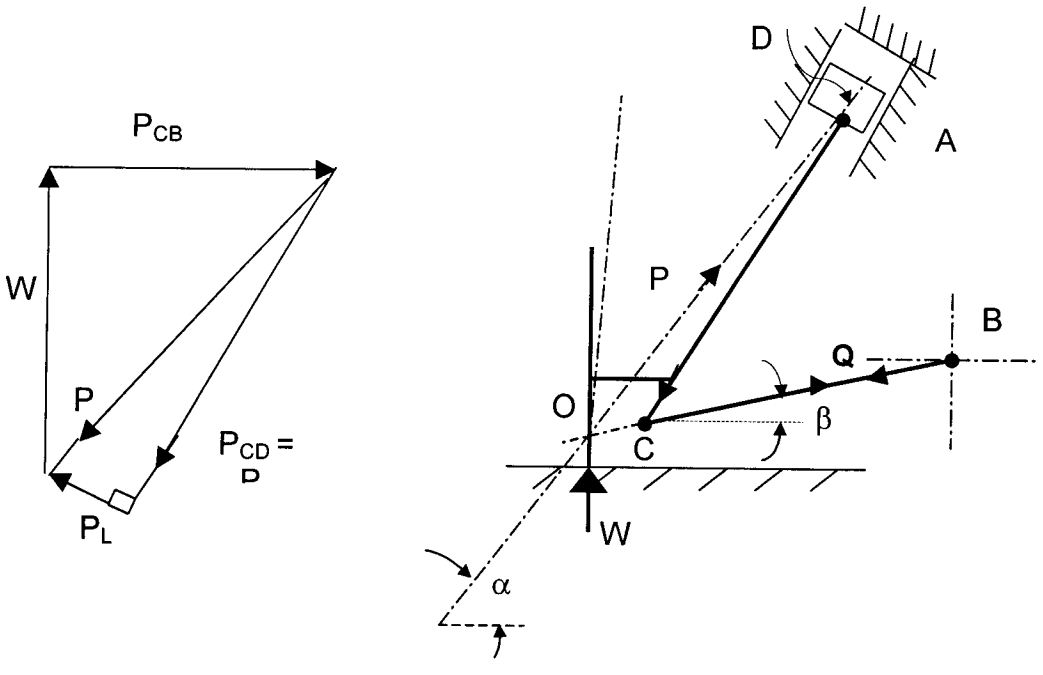

Figure 3.8: The Geometry of a MacPherson Strut and the Force Vector

The strut is considered as a piston sliding in guides at A. The forces acting on the wheel/stub axle/strut assembly are at the ground/wheel contact point W, force P_{CB} in link CB and the force P acting at the top of the piston. Interaction occurs at O. Force P is resolved into two components namely,

- $P_{CD} = P_s$, which is parallel to the strut, along CD.
- P_L, which is normal to the strut (acting at the top of the mounting). This is not a desirable force as it gives high bearing loads in the strut bearings and piston. The higher the ground force, the higher is this force too.

Considering Figure 3.9, the loads P_B and P_P acting on the bearing and the piston can lead to high friction forces that oppose the sliding of the strut.

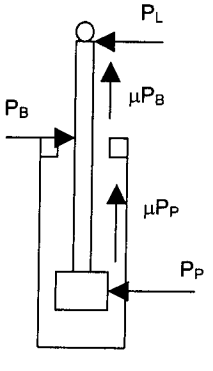

Figure 3.9: Effect of the Lateral Force on the Shock Absorber

3.4.2.1 Force Analysis of a MacPherson Strut

From Figure 3.8, let P_{OD} = force acting in OD

P_s = Spring force

P_L = Lateral force in shock absorber

From the equilibrium of the forces horizontally, Q cosβ =P cosα

$$\text{Hence}, Q = P\frac{\cos\alpha}{\cos\beta} \qquad (3.8)$$

Vertically,

$$W = P\sin\alpha + P\cos\alpha\tan\beta$$

$$\text{Therefore}, P = \frac{W}{\sin\alpha + \cos\alpha\tan\beta} \qquad (3.9)$$

This is the force along OD.

Substituting P in Equation 3.8,

$$Q = \frac{W}{(\tan\alpha + \tan\beta)\cos\beta} = \frac{W}{\sin\beta + \cos\beta\tan\alpha} \qquad (3.10)$$

Therefore, Force in link CB = Q = P_{CB}

Force in link DC = P_s = P_{CD}

Force at D = P

Force at B = Q

The force components of P are given by:

$$P_L = P\sin(90 - \alpha) \qquad (3.11.a)$$

$$P_s = P\cos(90 - \alpha) \qquad (3.11b)$$

Since in the Double Wishbone and MacPherson Strut a shock pad separates the shock absorber from the body, the force acting on the pad is equal to the one calculated as acting on the unsprung mass. It is quite common for a shock pad to fail prematurely due to excessive forces transmitted from the road surface. In this study, the maximum dynamic load acting on the pad is given by P_{ds} which was discussed in Section 2.3 of Chapter 2.

3.5 Conventional Suspension Systems

As already stated, a number of arrangements of conventional suspension systems exit. This section considers typical front and rear axles.

3.5.1 The Front Axle

In the front, conventional suspension systems usually employ dead axles. The front hubs rotate on anti-friction taper-roller bearings while the king-pin forms the pivot on which the steering knuckle assembly is hinged as shown in Figure 3.10.

Front axles are subjected to two types of stresses namely, bending and shear stresses. In the static condition, the axle may be considered as a beam supported vertically upward at the ends. The bending moment thus caused is zero at the point of support and rises linearly to a maximum at the point of loading. It remains constant thereafter.

Therefore, the maximum bending moment, $M_b = W\ l_b$, Nm

Where, W = the load on one wheel

l_b = the distance between the centre of the wheel and the spring pad.

Under dynamic conditions, the vertical bending moment is increased due to road roughness. The front axle also experiences a bending moment in the horizontal plane because of resistance to motion. This is of a nature similar to the vertical one but of very small magnitude and hence can be neglected except in situations when it is comparatively large [13].

The resistance to motion also causes a torque in the case of the drop-type front axle. Thus, the portions beyond the spring pads are subjected to combined bending and torsion. The drop-type front axle is mostly used in medium and heavy vehicles. The magnitude of the torque is given by,

$$T_r = R\delta.$$

where, R = Resistance to motion

δ = Drop from the spindle axis to the centre of the section

The torque due to resistance is lower for the section between the spring pads. In this portion, bending predominates whereas at the steering head, torsion predominates. Hence, an I-beam is used for the portion where the bending moment predominates and is gradually changed to circular, oval or rectangular at the steering head [13].

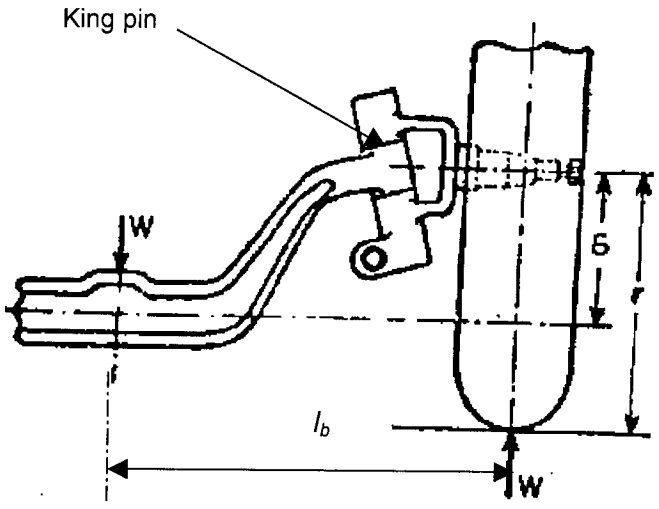

Figure 3.10: Drop-type front axle

3.5.1.1Bearing Loads on the Front Axle

Figure 3.11 shows the forces and the reaction on the steering knuckle when the vehicle is stationary. The thrust load and knuckle-pin-bearing load can be expressed in terms of the reaction of the wheel on the wheel spindle.

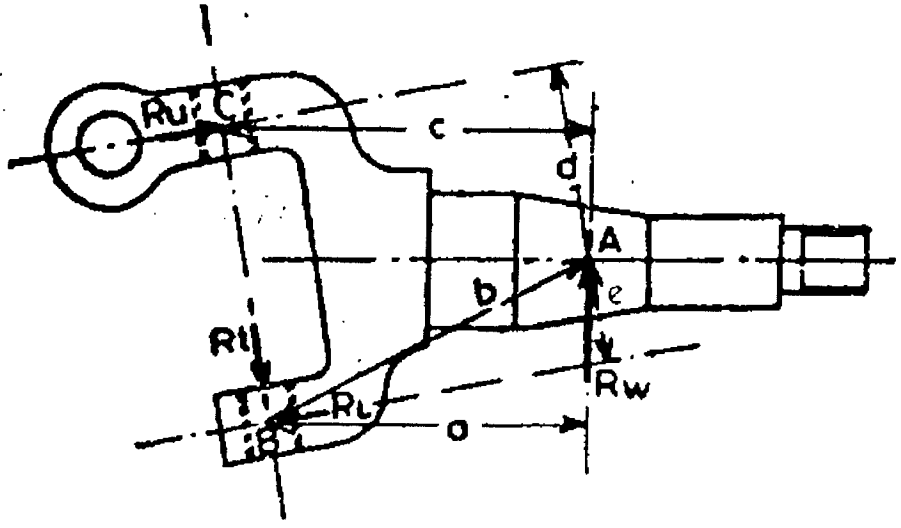

Figure 3.11: The Forces and the Reaction on the Steering Knuckle

Let, R_w= W = the reaction of the wheel on the spindle, which acts vertically through the centre of the tyre on the ground ($R_w = P_{dus}$, the dynamic load on the unsprung mass)

R_u = the load on the upper knuckle -pin bearing

R_t = the load on the thrust bearing

R_L = the load on the lower knuckle-pin

B and C represent the centre of the lower and upper knuckle-pin bearings respectively.

Now, $\Sigma M_c = 0$, gives $R_w c - R_L (d+e) = 0$

$$R_L = \frac{c}{(d+e)} R_w = \frac{c}{d+e} P_{dus} \qquad (3.12)$$

Similarly, $\Sigma M_B = 0$ gives, $R_w a - R_u (d+e) = 0$

or

$$R_u = \frac{a}{(d+e)} R_w = \frac{a}{(d+e)} P_{dus} \qquad (3.13)$$

Again, $\Sigma M_A = 0$ (where A is a point on the spindle axis in the centre of the wheel) gives,

$R_t b - R_l - R_u d = 0$, or $R_t b = R_l e + R_u d$

Substituting the expressions of R_t and R_u,

$$R_t = \frac{ce + ad}{b(d+e)} R_w = \frac{ce + ad}{b(d+e)} P_{dus} \qquad (3.14)$$

3.5.2 The Rear Axle

There are two types of axles considered under this section; the "live" axle and the "dead" one. Both carry part of the vehicle weight, but the latter also transmits torque to the driving wheels.

3.5.2.1 The Live Axle

There are three types of live axles:

i) Semi-floating Axle

The semi-floating axle is used on most rear drive passenger cars and light commercial vehicles. In this case, the differential casing is carried by bearings mounted in the differential carrier. The inner ends of the axle shafts transmit only turning torque and are not acted upon by any other force hence

the term floating. The stresses caused by the operation of the differential are taken up by the axle housing. The outer ends of the axle shafts are supported in the axle housing by a single bearing and the wheels are keyed on a taper portion at these ends. Therefore, the axle shafts take the bending moments caused by skidding, turning and wobbling of the wheels. Nevertheless, this has no relevance to this study and is not discussed any further.

The axle on the other hand takes the entire weight of the vehicle. This is what is relevant to this work as the point of action of the vehicle weight is the same as that of the force induced by a pothole.

(ii) Three-quarter Floating Axle

Although not usually employed, this type of rear axle is used on medium and commercial vehicles and some passenger cars. In this case, a bearing on the axle shafts supports the wheels. The axle shafts take the stresses caused by turning, skidding and wobbling of the wheels similarly to the semi-floating axle. However, the axle housing carries 75 percent of the vehicle weight while the axle shaft carries the remaining load [13].

(iii) Full-floating Axle

Full-floating axles are used mostly on heavy trucks. In this case, two tapered roller bearings are placed between the outside of the axle housing and the wheel hub. The wheels are driven through dogs or splines at the end of the axle shaft. In this case, the axle shafts transmit only the driving torque. The axle housing through the wheel bearings takes the stresses caused by turning, skidding and wobbling of the wheels. It also takes up the entire weight of the vehicle [13].

3.5.2.2 The Dead Axle

As already alluded to, the dead axle is similar to the live one. Therefore, the vertical loading of the bearings is much the same way [13]. Hence, the expressions for the live axle vertical loading of the bearings apply to the dead one as well.

3.5.3 Analysis of the Stresses Due to a Vertical Force on a Wheel

This section considers the wheel bearings, which are the most vulnerable parts of the wheel assembly.

3.5.3.1 Bearing Loads Due to Vertical Forces on the Rear Axle

In this section, the expressions of the bearing loads for the semi-floating and full-floating axles are presented. The three-quarter type of axle has not been included as it is not usually employed [13].

(a) Semi-floating Type

The bearing loads due to a vertical load on the axle are shown in Figure 3.12. When a vehicle is going round a bend, the side load is considered. In this study, a straight road is assumed and hence the side load is equal to zero

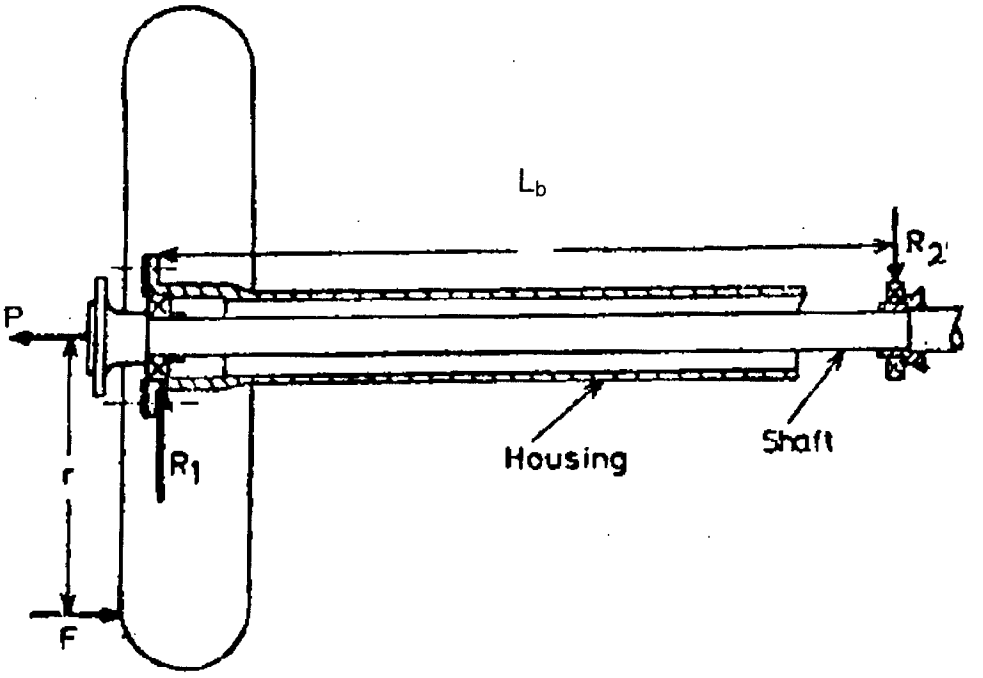

Figure 3.12: The Bearing Loads on a Semi-floating Axle

Where, L_b = the distance between bearings

In this case, though R_1 and R_2 are equal in magnitude, they act in opposite directions.

$$R_1 = R_2 = W \qquad (3.15)$$

(b) Full-floating Type

Figure 3.13 shows bearing loads due to a vertical load on a full-floating axle.

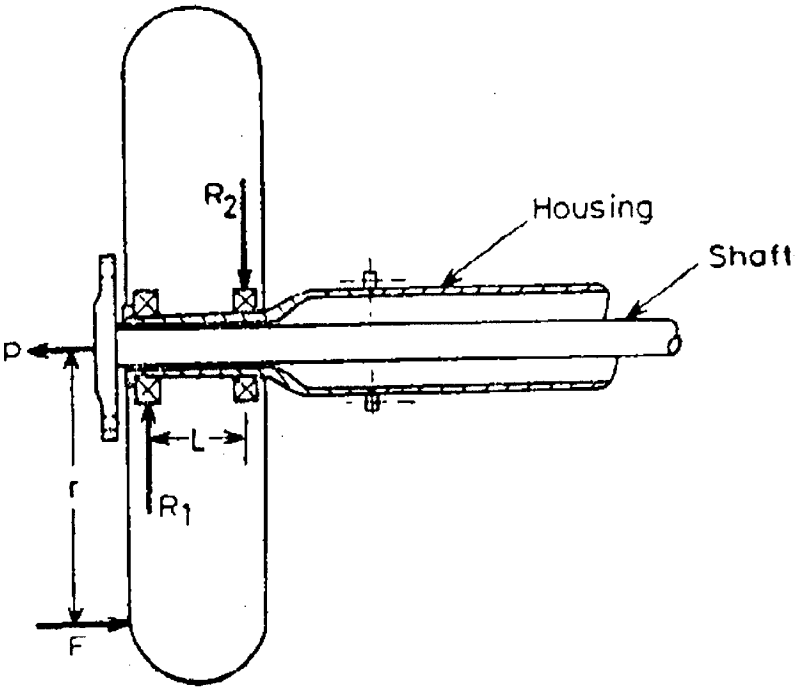

Figure 3.13: Bearing Loads on Full-floating Axle

Where, F = horizontal force at the rim of the wheel (equal to zero on straight road)

L = distance between the centres of the wheel bearings

R_1 and R_2 = radial reactions of the bearings on the wheel hub

The reactions R_1 and R_2 can be assumed equal assuming that the vertical force W is acting at the centre of the wheel surface.

Therefore,

$$R_1 = R_2 = {}^1/_2\, W \qquad (3.16)$$

3.6 Concluding Remarks

The force expressions determined in this chapter are used to calculate the stresses in the members at the points of interest as discussed in the next chapter. The calculated stresses are compared with

the design allowable stresses in order to establish whether a member fails. However, for bearings, the design load is compared with the calculated load in order to determine the possibility of failure.

For simplicity and clarity, the details of the load path for conventional suspension systems are combined with failure of suspension components in the next chapter.

CHAPTER 4

FAILURE OF VEHICLE SUSPENSION PARTS

4.0 Introduction

This chapter deals with the failure of some suspension members. Both static and fatigue failure are considered. The modes of failure under consideration are bending, torsion and shearing depending on the loading of a component.

The failure of parts deemed most susceptible to pothole damage is analysed in two ways. These are:

1. Addition of the static load and the maximum dynamic load to give a total load that is used to calculate the stresses based on static loading principles. This assumes an isolated case of a pothole on a road.
2. Taking into account the repeated loading stemming from a vehicle hitting other potholes during its exploitation period. This constitutes fatigue loading, and hence fatigue failure is expected.

In the following sections, the forces are denoted generally. However, when analysing a particular suspension system, the relevant expressions determined in Chapter 3 are used.

4.1 Static Failure of Various Suspension Members

As already stated in Chapter 3, the most common suspension systems in use are the MacPherson Strut and Double Wishbone types of independent suspensions, and the dead and live axles for the conventional type. Therefore, only these are dealt with in the following sections. It should be noted that to each of the dynamic loads presented, a static load, $m_s g$, is added to account for the vehicle weight at the given side of the wheel.

4.1.1 Suspension Springs

Suspension springs are used to cushion the shock from road obstacles through the wheels to the vehicle body. The common springs in use in the automobile industry are:

(a) Laminated or leaf springs
(b) Coil springs
(c) Torsion bar springs
(d) Air springs
(e) Volute springs, and
(f) Rubber springs

Being most predominant in Zambia, the first three are the only ones dealt with in detail in this work.

1. Laminated or Leaf Springs

The commonly used leaf spring is the semi-elliptic type. It has one main leaf spring connected at the end with brackets as shown in Figure 3.1. The main spring is held together with various shorter ones using a centre bolt. A leaf spring is considered equivalent to two cantilever beams loaded at two ends [13]. The upper part of the leaf experiences tension while the lower one experiences compression.

Practically, leaf springs fail due to fatigue that always starts on the tension side of the spring because the tensile strength of a material is less than its compressive strength [13]. The average stress is approximately half ($^1/_2$) of the maximum as the stress varies linearly from the surface to the neutral axis.

For analysis, Figure 4.1 is considered [12].

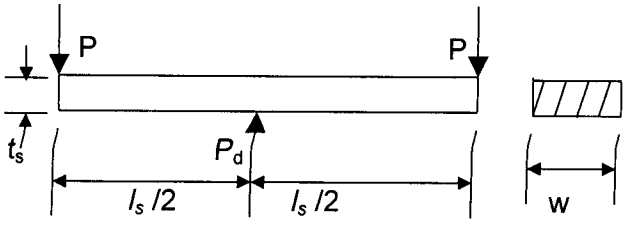

Figure 4.1: A Leaf Spring Used for Analysis

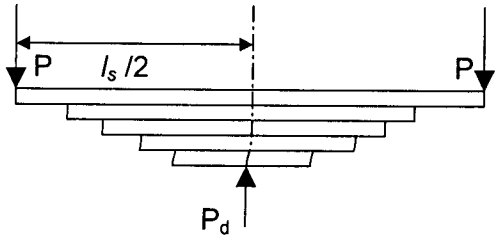

Figure 4.2: A Multi-leaf Spring

Let P = load on each end, N. The spring can be considered as a cantilever of length l_s /2 carrying a load at the end. The deflection of the spring is given by [13]

$$\delta = \frac{P_d l_s^{\,3}}{6EI} = \frac{2P_d l_s^{\,3}}{Ewt_s^{\,3}}, m \qquad (4.1)$$

At a distance x from the end of the spring, the bending moment is given by

$$M_x = P_d x, \quad Nm \qquad (4.2)$$

The stress due to bending is given by:

$$\sigma_x = \frac{M_x y}{I} = \frac{P_d x \frac{t_s}{2}}{\frac{wt_s^{\,3}}{12}} = \frac{6P_d x}{wt_s^{\,2}}, N/m^2 \qquad (4.3)$$

Where y = maximum distance of fibre from the axis = t_s / 2, and I is the area moment of inertia.

In order to have uniform stress throughout the length, multi-leaf-springs, shown in Figure 4.2, are used, where all springs undergo equal deflection due to the load on the top leaf. If n is the number of leaves, then the static deflection is given by:

$$\delta = \frac{2P_d l_s^3}{Enwt_s^3}, m \qquad (4.4)$$

Mathematically, it has been found that the deflection increases by 50 percent if the length of the spring decreases uniformly, each leaf overlapping its neighbour by an amount $l_s/2n$ [5] as shown in Figure 4.2 [13]. Thus,

$$\delta = \frac{3P_d l_s^3}{Enwt_s^3}, \ m \qquad (4.5)$$

However, due to interleaf friction, deflection becomes smaller giving,

$$\delta = \frac{2.85P_d l_s^3}{Enwt_s^3}, \ m \qquad (4.6)$$

The rate of the spring, r_l, is given by:

$$r_l = \frac{Total\ load\ on\ the\ spring}{Maximum\ deflection} = \frac{2P_d}{\delta} = \frac{Enbt^3}{1.425l^3}, N/m \qquad (4.7)$$

In addition, the maximum bending stress is given by:

$$\sigma_b = 1.05 \frac{\delta t_s E}{l_s^2}, N/m^2 \qquad (4.8)$$

In the above equation, t_s was assumed equal for the n leaves. However, in normal practice, t_s varies. Hence, there are "graded springs". This is in order to have equal maximum stress. For graded springs the term nt_s^3 is replaced by Σt_s^3, giving,

$$\delta = \frac{2.85P_d l_s^3}{EP_d \Sigma t_s^3}, m \qquad (4.9)$$

$$r_l = \frac{Ew\Sigma w_s^3}{1.425l_s^3}, N/m \qquad (4.10)$$

An initial curvature or "camber" is given to the springs so that they are substantially straight when under full static load. To overcome the difference in the stresses due to curvature, nipping is done. Nipping is an assembly where the thinner leaf is curved to a smaller radius than the thicker one. The initial stress due to nipping is taken into account when carrying out calculations. This stress adds to the initial positive stress, and overcomes the initial negative stress.

In the semi-elliptic type leaf spring assembly, the springs are usually supported off centre (asymmetrical springs) as shown in Figure 4.3.

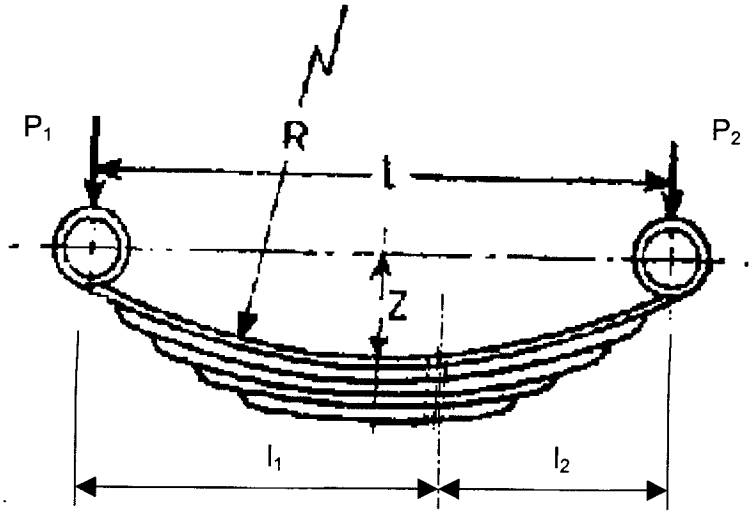

Figure 4.3: Asymmetrical Spring

From Figure 4.3,

$$P_1 = \frac{l_2}{l_s} P_d, N \qquad (4.11a)$$

$$P_2 = \frac{l_1}{l_s} P_d, N \qquad (4.11b)$$

$$\delta = \delta_1 - \frac{l_1}{l}(\delta_2 - \delta_1), m \qquad (4.12)$$

Where δ is the deflection at the centre bolt, while δ_1 and δ_2 are the deflections under load P_1 and P_2 respectively.

The forces at the ends of the leaf spring become the loads on the shackle pins and the related bushes. On the other hand, the load on the shock absorber is approximately equal to the load on the unsprung mass but taking into account the angle of tilt of the damper.

2 Coil Springs

Mainly subjected to torsion, coil springs fail by shear. The stress varies uniformly from a maximum at the surface to zero at the centre of the circular cross section. The average stress is given by,

$$\sigma_{average} = {}^{2}/_{3}\,\sigma, N/m^2 \qquad (4.13)$$

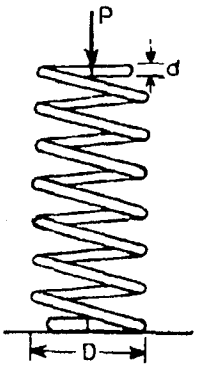

Figure 4.4: Main Parameters of a Coil Spring

Automobile springs are designed based on close coil helical springs [16]. Under the load P,

$$\delta = \frac{8nPD^3}{Gd^4}, m = \frac{\pi D^2 n\tau}{Gd}, m \qquad (4.14)$$

Therefore,

$$\tau = \frac{Gd\delta}{\pi D^2 n}, N/m^2 = \frac{8PD}{\pi d^3}, N/m^2 \qquad (4.15)$$

3 Torsion bar Spring

A torsion bar spring can either be hollow or solid. It is a bar of spring steel anchored to the frame at one end while the other end is freely supported and connected to a lever arm. The lever arm is pin-jointed to the axle spindle or steering head. Principally, the mode of loading of torsion-bar springs is

the same as that of coil springs. Torsion bars are designed under maximum dynamic load (bump load) considerations and the corresponding stress. Let W be the load on the lever arm of the torsion bar causing the moment T on the torsion bar.

The angular deflection of the bar under the torsion moment is given by,

$$\theta = \frac{TL}{GJ} = \frac{32TL}{\pi d^4 G}, radians \qquad (4.16)$$

The maximum torsional stress produced is given by,

$$\tau_{max} = \frac{T_{max}}{J}\frac{d}{2} = \frac{16T_{max}}{\pi d^3}, N/m^2 \qquad (4.17a)$$

The maximum shear stress can also be expressed as,

$$\tau_{max} = \frac{G\theta_{max} d}{2L}, N/m^2 \qquad (4.17b)$$

If the arm of the torsion bar is inclined upward considerably instead of making it horizontal, the increase in deflection with increase in load is smaller. When the arm is horizontal, the movement of the vehicle body is equal to the movement of the free end of the arm around its fulcrum. Figure 4.5 shows diagrammatically a torsion-bar arm extending upwards. Line *OY* represents the position of the arm in the unloaded state; *OX* represents its position under maximum bump load and *OZ* represents its position under maximum static load.

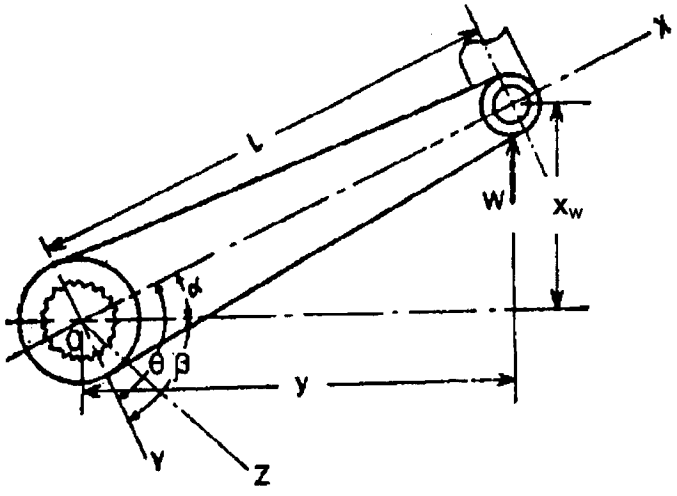

Figure 4.5: Torsion bar extending upwards

Where x_w = linear deflection from the horizontal = l sinα

y = effective arm length = l cosα

The angular rate of deflection is given by

$$r_a = \frac{W_{max}}{\theta_{max}}, N \quad per \quad radian$$

The monent on the torsion bar can be expressed as

$$T = r_a\theta = r_a(\alpha + \beta), \quad where \quad (\alpha + \beta) = \theta$$

and $$\alpha = arc\ sin\frac{x_s}{l}$$

the load, $$W = \frac{T}{y} = \frac{T}{l\cos\alpha} = \frac{r_a(\alpha + \beta)}{l\cos\alpha}, N \qquad (4.18)$$

For both springs, the material usually used has a tensile strength of 600 MPa to 1350 MPa [17].

4.1.2 Suspension Linkage Bushes

Usually, a metallic bushing is employed in the bracket where the pin at the end of the suspension linkage is pivoted. If the load on the bushing exceeds the proof stress of the metal, then the bearing may fail. Consequently, this may affect the performance of the system. The rubber bushing at the end eyes of a shock absorber can be treated in the same way. This also applies to bushes in shackle pins of a leaf spring. The bush can be assumed to be loaded in two ways, point loading and distributed loading. Reference is made to Figure 3.4.

4.1.2.1 Failure of a Bush Assuming a Point Load

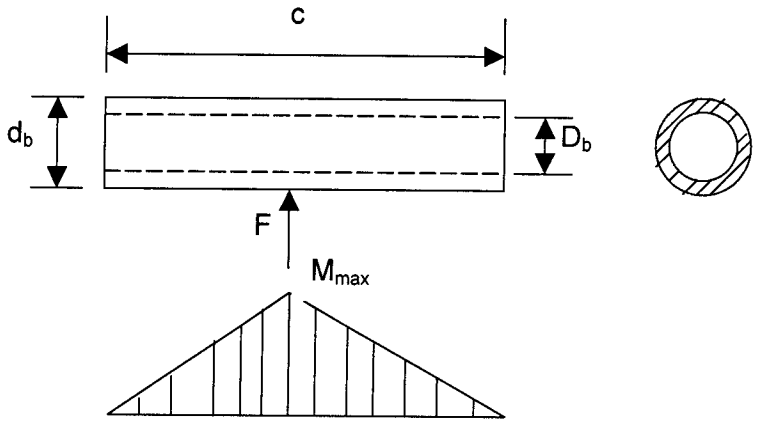

Figure 4.6 Loading and Bending Moment Diagram of a bushing

Assuming the load on the bushing to be F;

the maximum bending moment on the bushing is given by $M_{max} = F\frac{c}{2}$

The maximum stress is given by $\sigma_{max} = \frac{cD_b}{4I} F_{max}$. *(4.19)*

where, $I = \pi (D_b^4 - d_b^4) /32$; D_b and d_b are the outer and inner diameters of the bush respectively.

The factor of safely is given by,

$$n_c = \frac{\sigma_{max}}{S_y} \qquad (4.20)$$

where S_y is the yield stress of the material. If n_d = the design factor of safety, failure of the bush occurs when $n_c < n_d$

From the way in which the suspension bushes are constructed, it is not likely that they would fail by bending. Instead, they are likely to fail due to compression as discussed in the next section.

4.1.2.2 The Failure of the Bush Assuming Distributed Load

Assuming a distributed load between the inner and outer surface of the bush in Figure 4.7, the load is given by F. In this case, failure is determined by *crashing* caused by a compressive force.

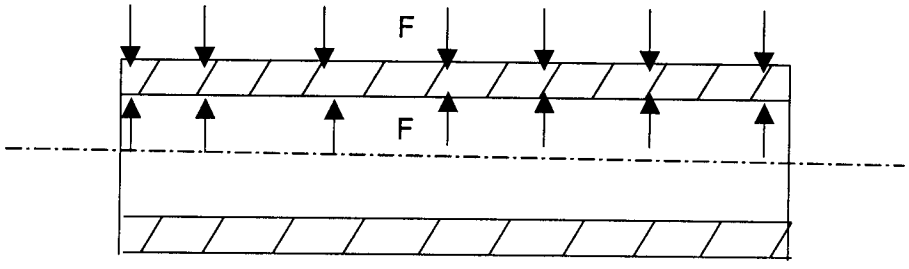

Figure 4.7: Distributed Loading on the bushing

Since this is a bearing, the calculation of the bearing pressure is based on the projected area [18]. The bearing pressure, P_b, is given by,

$$P_b = F / A_b , \qquad (4.21)$$

where $A_b = D_b{*}c$, m^2, as defined in Figure 4.6.

Failure of the bushing occurs when the calculated bearing pressure, P_b, exceeds the allowable pressure. Alternatively, in case the allowable pressure is not given the calculated pressure can be compared with the compressive strength of the bearing material.

Shackle bushes are normally made of bronze with an ultimate strength of 410 MPa [17]. These are used in leaf spring assemblies.

There are, however, components where metal-packed composite bearings are used. These include shock absorber pin bearings, suspension hinges, ball-socket bearings, door-hinge bearings, and steering knuckle bearings [17]. The compressive strength of this material is about 250 MPa while the typical load falls between 20 to 50 MPa [17].

4.1.3 Failure of Suspension Joint Pins

The weakest section of the suspension linkage joint is the pin. The pin connects the linkage to the vehicle body. Its failure means that the linkage would be disconnected from the body and would thus fail to perform its desired function.

4.1.3.1 Failure of a Pin Assuming a Point Load

Assuming a point load on the pin, the following applies.

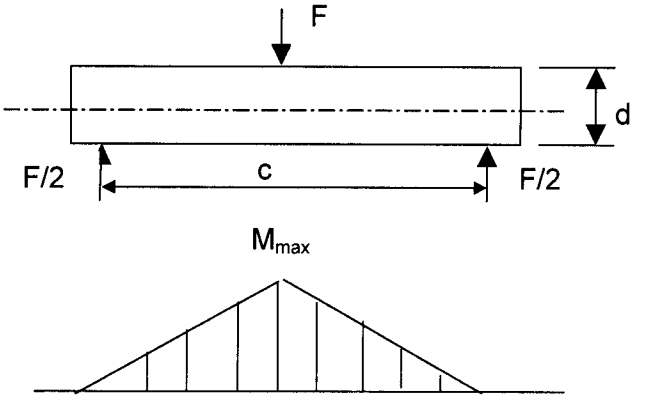

Figure 4.8 Loading and Bending Moment Diagram of a pin

The maximum bending moment is given by $M_{max} = \frac{F}{2} * \frac{c}{2}$

Hence, the maximum bending stress is given by,

$$\sigma_{max} = \frac{M_{max}\frac{d}{2}}{\frac{\pi d^4}{64}} = \frac{32M_{max}}{\pi d^3}, N/m^2 \qquad (4.22)$$

The factor of safety is expressed as $n_c = \frac{\sigma_{max}}{S_y}$ *(4.23)*

If n_d = the design factor of safety, the failure of the pin occurs when $n_c < n_d$

4.1.3.2 Failure of a Pin by shearing

There is also a possibility that the pin would fail due to shear. In that case, the shear force is given by F/2 on each side of the pin. Hence, the shear stress is given by,

$$\tau_{max} = \frac{Shear\ force}{Area} = \frac{\frac{F_{max}}{2}}{\frac{\pi d^2}{4}} = \frac{2F_{max}}{\pi d^2}, N/m^2 \qquad (4.24)$$

The pure torsion failure criterion [19] is employed to determine the possibility of failure of the pin.

$\tau_{max} = \tau_a + \tau_m = S_{sy} = 0.577\ S_y,\ N/m^2$ *(4.25)*

Hence, the pin fails if $\tau_{max} > S_{sy}$.

Although failure of this mode is a possibility, seldom does this occur. Therefore, the failure considered in this work is by bending as discussed in Section 4.1.3.1.

4.1.4 Shock Pad

Made of rubber, and joined to a circular metallic bracket, a *shock pad* usually fails by shearing or compression/tension close to the centre of the bracket. The rubber used has an ultimate strength of about 10 MPa [20]. The maximum shear and tensile stresses are respectively given by,

$$\tau_{max} = \frac{P_{ds}\sin\psi}{A_p}, N/m^2 \qquad (4.26a)$$

$$\sigma_{max} = \frac{P_{ds}\cos\psi}{A_p}, N/m^2 \qquad (4.26b)$$

where A_p is the area of shear corresponding to the contact area of the metallic bracket and the rubber

Normally, the contact area takes a conical shape as shown in Figure 4.9

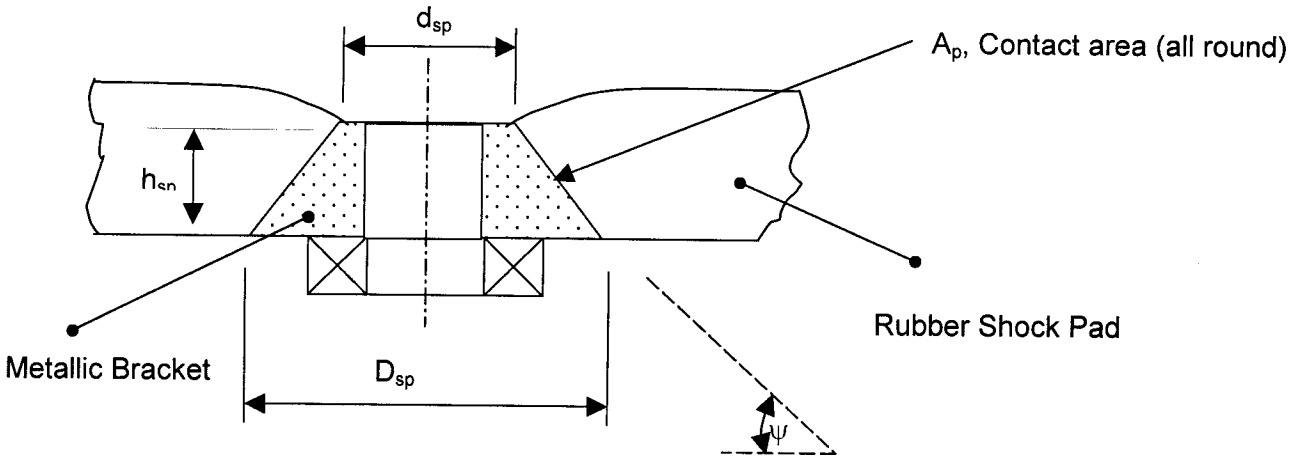

Figure 4.9: Shock Pad

From the geometry, $A_p = \dfrac{\pi(D_{sp}{}^2 - d_{sp}{}^2)}{4\sin\left(\dfrac{\pi}{2} - \psi\right)}, m^2$ *(4.27)*

Replacing Equation 4.27 for A_p in Equations 4.26a and 4.26b gives,

$$\tau_{max} = \frac{4P_{ds}\sin\psi\sin\left(\dfrac{\pi}{2} - \psi\right)}{\pi(D_{sp}{}^2 - d_{sp}{}^2)}, N/m^2 \qquad (4.28a)$$

$$\sigma_{max} = \frac{4P_{ds}\cos\psi\sin\left(\dfrac{\pi}{2} - \psi\right)}{\pi(D_{sp}{}^2 - d_{sp}{}^2)}, N/m^2 \qquad (4.28b)$$

Where $\psi = tan^{-1}\left[h\left(\dfrac{D_{sp} - d_{sp}}{2}\right)\right]$

4.1.5 The Shock Absorber (Damper)

The two most common failures on a damper are,

(i). Damaging of the rubber bushes in the end eyes of the damper.

(ii). The loss of its effectiveness due to excessive damper pressures.

Failure analysis for the first case is carried out in the same way as a bush as shown in Section 4.1. The possibility of failure due to the second reason can be determined by comparing the safe design pressure with the calculated one.

4.1.6 Wheel Bearings

Wheel bearings are designated by the ability to withstand loads. The selection of bearings is usually done by using manufacturers' specifications [17]. Hence, the loads determined through calculations help in choosing the correct bearings.

4.1.6.1 Static and Dynamic Capability

The static load rating, Co, is used as a measure of the capability of a very slow moving or static rolling bearing. Co is the load at which total permanent deformation of rolling elements and races at most highly loaded contact point amounts to 0.0001 of the diameter of the rolling elements [17].

For dynamic loading, the basic load rating, C, is used for calculating the service life of a rotating rolling bearing. C indicates that bearing load at which bearing life is 1 million cycles. In accordance with ISO [17];

$$\text{Service life equation, } L_{10} = \left(\frac{C}{P}\right)^{p}$$

where L_{10} - Nominal service life in millions of revolutions achieved or exceeded by 90 % of a large number of identical bearings

C - Basic load rating in N (determined empirically)

P - Equivalent dynamic bearing load in N

p - Empirical exponential of the service life equation

Since the loading due to a pothole is isolated, the loading can be determined for a static case where the calculated loading on the bearing is compared with C_o in order to determine the possibility of failure.

For the general case of fluctuating stresses, the mean value of the stresses is not zero. This is the case with the condition of the pothole-induced forces. The loading varies from the static load (F_s due to vehicle weight) to the sum of the static load and the maximum dynamic load ($F_s + F_d$).

The endurance limit S_e' or fatigue limit is the maximum stress when no fracture occurs (infinite life). When the fatigue strength of a specimen is determined, it will not be the same for an actual machined member. There are other important factors which affect the strength such as geometry of the part, environmental conditions, etc, which have to be taken into account.

Since the endurance limits are usually the values for a rotating-beam specimen, one may use the following formulae are used to find the endurance limit for [19]:

Reversed torsion: $S_{se}' = 0.58\ S_e'$
Reversed tension: $S_{te}' = 0.85\ S_e'$

For steel, the endurance limit is derived from the tensile test results using the empirical formulae;
$S_e' = 0.5\ S_{ut}$ ($S_{ut} < 1400$ MPa)
$S_e' = 700$ MPa ($S_{ut} \geq 1400$ MPa)
where S_{ut} is the minimum tensile strength.

4.2.1. Endurance-Limit Modifying Factors

The rotating-beam specimen used in the laboratory to determine the endurance limit is prepared very carefully and tested under closely controlled conditions. It is unrealistic to expect the endurance limit of a mechanical or structural member to match the values obtained in the laboratory. To account for the most important of these conditions a variety of modifying factors are employed, each of which is intended to account for a single effect. Using this idea, the following formula is employed,

$$S_e = k_a\, k_b\, k_c\, k_d\, k_e\, k_f\, S_e' \qquad (4.29)$$

where Se = endurance limit of the mechanical element
Se' = endurance limit of the test specimen
k_a = surface factor
k_b = size factor
k_c = load factor

k_d = temperature factor

k_e = stress concentration factor

k_f = miscellaneous-effects factors

In determining the fatigue failure of the vehicle parts, each of the factors is taken into account in order to get S_e [7].

4.2.2 Failure Modes Due to Fluctuating Stresses

In the case of repeated stresses, the minimum value of the stresses σ_{min} is zero as shown in Figure 10(b). Thus, $\sigma_a = \sigma_m = \sigma_{max}/2$. Figure 4.10(c) shows another special case which arises when the mean value σ_m is zero. Therefore, $\sigma_{max} = -\sigma_{min} = \sigma_a$.

For the last case, the value of reversed stresses, the endurance limit and the fatigue strength directly determine the life of the machine member. In the case of other loading situations, special theories have been developed [19], some of which are discussed below.

4.2.2.1 Fluctuating Bending

There are two methods of graphical representation to show how both the mean stress and the stress amplitude influence the fatigue strength: the Goodman's diagram or Smith's diagram, and the Goodman's line.

4.2.2.2 Goodman Line Diagram

For design purposes, the Goodman's failure line is the mostly employed [19]. This is because the dimensions of the part under consideration do not have to be known. Any stress situation under the line is a safe situation. For brittle materials, or for stress concentration where there is no yielding, the ultimate strength, S_{ut}, is used. When the σ_a/σ_m ratio is known from the bending moments on the machine member, dimensions can be determined. The projected line in Figure 4.11 intersects the failure line at A hence determining the values of σ_a and σ_m.

This criterion has been used to determine the possibility of failure of leaf, torsion and coil springs, bushes, pins and welds holding brackets where bushes are pressed. Fatigue strength under combined loading has not been considered here, as the parts in consideration are not expected to be loaded thus.

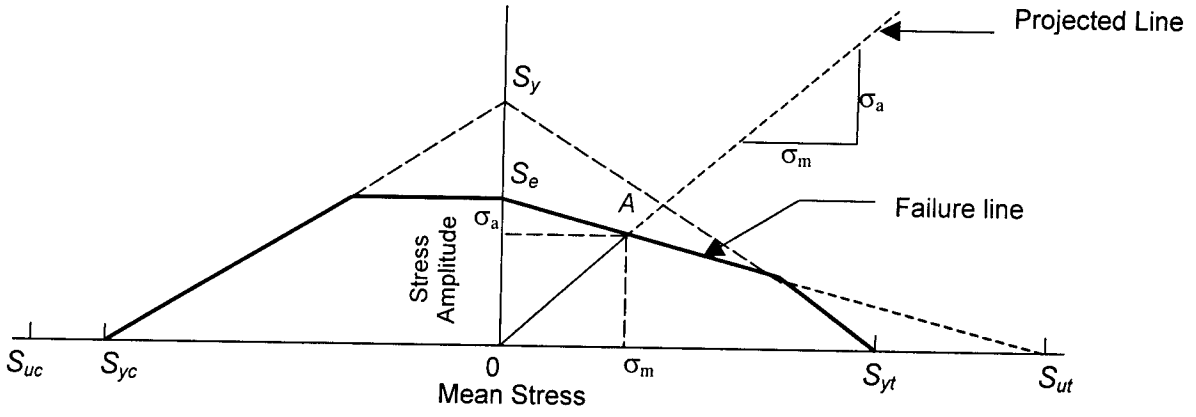

Figure 4.11: The Goodman Failure Line

In order to determine the failure of a machine component, the modified Goodman relationship is employed [7]. Mathematically, it is expressed as,

$$n_c = \frac{S_{ut} S_e}{S_{ut}\sigma_a + S_e \sigma_m} \qquad (4.30)$$

4.2.2.3 Fluctuating Torsion

The torsional endurance limit S_{se} is approximated as $S_{se} = 0.577\ S_e$ [19]. For reversed torsion, it has been observed from experiments that the torsion mean stress τ_m has no effect on the torsional endurance limit S_{se} , therefore, the failure criterion is :

Fatigue Failure Criterion: $\tau_a = S_{se},\ N/m^2$ (4.31)

Let,

$F_a = (F_{max} - F_{min})/2$, which gives the load amplitude

$F_m = F_a + F_{min} = (F_d/2)+F_s$, which gives the mean load.

where F_s = static load, which in this case is the portion of the vehicle weight, mg, acting at a given wheel, and F_d = dynamic load, which in this case caused by a pothole. Using the equations in Chapter 3, the static load on each component is determined by replacing the load reaction on the tyre base with the vehicle load, mg, at that wheel.

4.2.3 Fatigue Failure of Suspension Springs

There are cases when the shock absorber is not that effective due to old age and use. The spring is then prone to failure as it has to take up most of the load.

4.2.3.1 Coil Springs

Mainly subjected to torsion, coil springs fail by shear. In order to determine the stresses in a spring, Figure 4.4 is used.

The amplitude stress is given by, $\tau_a = \frac{8DF_a}{\pi d^3}, N/m^2$ *(4.32)*

The mean stress is given by, $\tau_m = \frac{8DF_m}{\pi d^3}, N/m^2$ *(4.33)*

The failure criterion used is as indicated in Section 4.2.2.3.

4.2.3.2 Leaf Springs

The amplitude stress is given by, $\sigma_a = 1.05\frac{\delta_a t_s E}{l_s^2}, N/m^2$ *(4.34)*

The mean stress is given by, $\sigma_m = 1.05\frac{\delta_m t_s E}{l_s^2}, N/m^2$ *(4.35)*

where δ_a and δ_m are the amplitude and mean displacements respectively.
The Goodman's criterion is used to determine the failure of leaf springs.

4.2.3.3 Torsion bar Springs

The amplitude shear stress is deduced from the amplitude load as,

$$\tau_a = \frac{T_a}{J}\frac{d}{2} = \frac{16T_a}{\pi d^3}, N/m^2 \quad (4.36)$$

While the mean stress is given by,

$$\tau_m = \frac{T_m}{J}\frac{d}{2} = \frac{16T_m}{\pi d^3}, N/m^2 \quad (4.37)$$

4.2.4 Suspension Linkage Bushings

4.2.4.1 Fatigue Failure Assuming a Distributed Load on a Bushing.

The load F in Figure 4.7 is considered compressive on the bushing's thickness. Therefore, the modified Goodman criterion is used to find out the possibility of failure of the bushing.

4.2.5 Suspension Joint Pins

4.2.5.1 Failure of the Pin Assuming a Point Load

Assuming a point load on the pin as indicated in Figure 4.8, the following results,

The mean stress, $\sigma_m = \frac{8cF_m}{\pi d^3} N/m^2$ *(4.39)*

The amplitude stress, $\sigma_a = \frac{8cF_a}{\pi d^3}, N/m^2$ *(4.38)*

The modified Goodman fatigue failure criterion is used to determine the possibility of failure of a pin.

4.2.5.2 Failure of a Suspension Pin by Shearing

From Figure 4.8, the amplitude stress can be expressed as

$$\tau_a = \frac{2F_a}{\pi d^2}, N/m^2 \qquad (4.40)$$

while the mean stress is given by,

$$\tau_m = \frac{2F_m}{\pi d^2}, N/m^2 \qquad (4.41)$$

Using the fatigue shear failure given in Section 4.2.2.3, the possibility of failure of the pin is determined.

4.2.6 Shock Pads

Using Equation 4.28a, the amplitude shear stress in the shock pad can be expressed as,

$$\tau_a = \frac{4\left(\frac{P_{ds}}{2}\right)\sin\psi \sin\left(\frac{\pi}{2}-\psi\right)}{\pi(D_{sp}^2 - d_{sp}^2)}, N/m^2 \qquad (4.42a)$$

while the mean shear stress is given by,

$$\tau_m = \frac{4\left(\frac{P_{ds}}{2} + P_{st}\right)\sin\psi \sin\left(\frac{\pi}{2} - \psi\right)}{\pi(D_{sp}^{\ 2} - d_{sp}^{\ 2})}, N/m^2 \qquad (4.42b)$$

where P_{st} is the static load on the shock pad.

The failure criterion used is that given in Section 4.2.2.3.
Similarly for the tensile stress,

$$\sigma_a = \frac{4\left(\frac{P_{ds}}{2}\right)\cos\psi \sin\left(\frac{\pi}{2} - \psi\right)}{\pi(D_{sp}^{\ 2} - d_{sp}^{\ 2})}, N/m^2 \qquad (4.43a)$$

$$\sigma_m = \frac{4\left(\frac{P_{ds}}{2} + P_{st}\right)\cos\psi \sin\left(\frac{\pi}{2} - \psi\right)}{\pi(D_{sp}^{\ 2} - d_{sp}^{\ 2})}, N/m^2 \qquad (4.43b)$$

Usually, ball joints and suspension members are designed to give stress levels not exceeding 65 % of the yield stress when subjected to a fluctuating load condition [16].

Hence, $n = \frac{1}{0.65} = 1.54$

4.3 Closing Remarks

Although only stress analysis has been considered in this work, it is true that wear occurs and this accelerates the failure of a given part. It is expected that potholes will introduce higher normal loads and relative speeds between moving components. Ultimately, the rate of wear increases thus reducing the size of a given component. Therefore, the actual force that is required to ultimately cause the component to fail is lowered.

This study did not include experimental testing of different components as it was not feasible due to lack of equipment, time and the components themselves.

CHAPTER 5

EXPERIMENTAL INVESTIGATION WITH A SALOON CAR

5.0 Introduction

This chapter deals with the practical work that was carried out in order to determine the vibration responses of a motor vehicle when one wheel hits a pothole. The maximum acceleration is used to determine the maximum induced load while the displacement profile is used to determine the response profile and duration of the impulse. The tests described here were conducted on Kalengwa Road, a good asphalt surface but with potholes at an isolated location, in Kalulushi, in the Copperbelt Province of Zambia.

The response to an excitation of the unsprung and sprung masses of a motor vehicle can be measured using well-positioned accelerometers on the wheel hub and the vehicle body respectively. The accelerometers are connected to an analyser which records the signal either in digital or graphical form.

From the acceleration, the force induced by hitting a pothole can be determined using Newton's Second Law of Motion. On the other hand, the plot of the measured displacement against time gives an idea of the waveform that best approximates the motion of the two masses.

In order to get a good approximation of the magnitude of the acceleration and displacement of masses in question, on-vehicle tests were carried out. The equipment used was from the Zambia Consolidated Copper Mines (ZCCM) - Technical Services in Kalulushi. Only the left side of the vehicle was considered as the car was assumed to be symmetrical about its longitudinal axis.

5.1 Objectives

The objectives of the experiments that were carried out were as follows:

1. To determine the acceleration (vibration response) of a motor vehicle when a wheel hits a pothole.
2. To determine the waveform that best approximates the excitation and response.

5.2 Equipment

The following is the equipment that was used to carry out the experiments;

- IRD Fast Track Mechanalysis Vibration Analysis Machine [21]
- IRD 885 Mechanalysis Vibration Analyser/Balancer [22]
- "3 meters" measuring tape
- Acceleration Transducer (Accelerometer)
- Connecting cables
- Toyota Corolla GL 1.5, 1984 model, with independent McPherson Strut suspension system throughout.

5.3 Procedure

Transducer mountings for the points designated 1 to 4 below were fabricated and mounted on the said points shown in Figure 5.1:

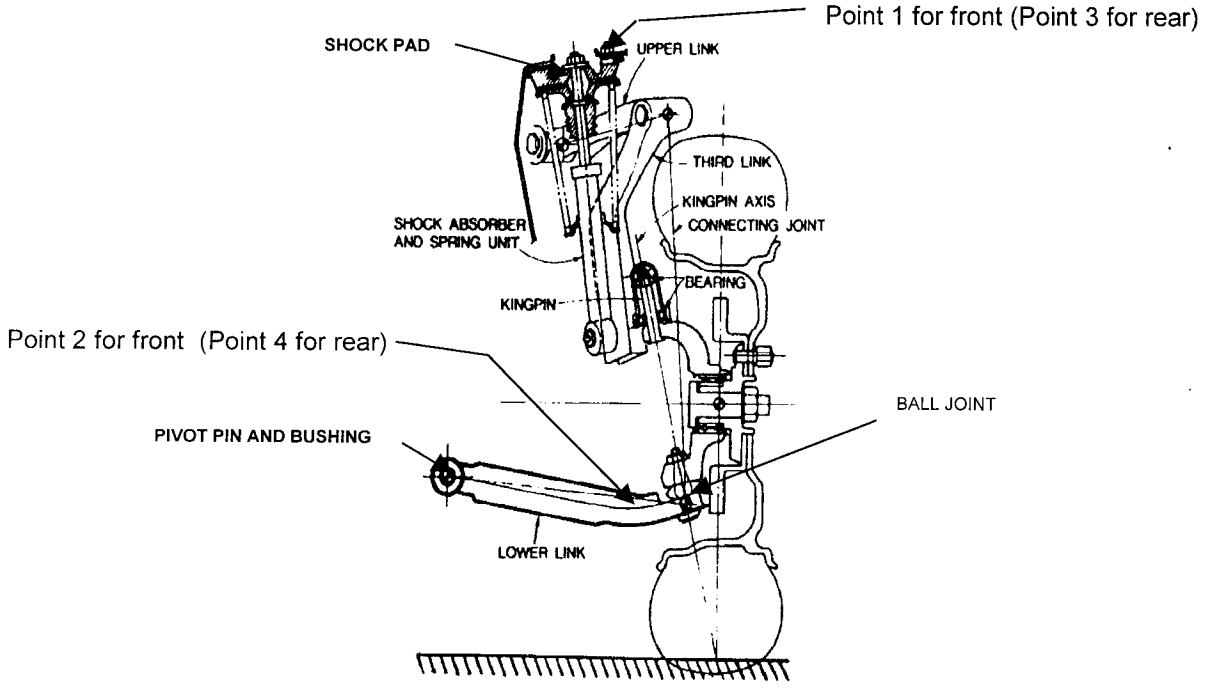

Figure 5.1: Points where the accelerometer was placed on the strut assembly

Point 1: Front top position (vehicle body, representing the sprung mass)

Point 2: Front bottom position (vehicle wheel assembly, representing the unsprung mass)

Point 3: Rear top position (vehicle body, representing the sprung mass)

Point 4: Rear bottom position (vehicle wheel assembly, representing the unsprung mass)

Pothole Parameters

A typical pothole on the road was chosen and the following parameters were measured:

Length (in the direction of the road)	l_w = 110 cm
Width (in the transverse direction)	w = 100 cm
Average Diameter	D = 105 cm
Depth	x_d = 8 cm

Actual Vehicle Parameters

The vehicle parameters that could be measured are given below:

Wheel base	= 2.45 m
Wheel diameter	= 0.56 m
Total Vehicle Mass	= 880 Kg (net) + 145 Kg (driver, passenger and analysis equipment) =1025 Kg

Figure 5.2 shows the path the signal takes from the vehicle the analyser.

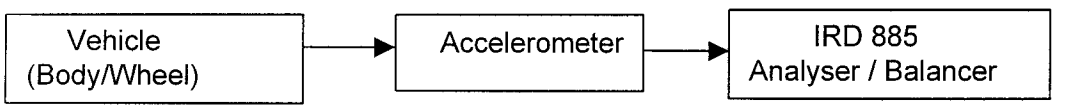

Figure 5.2: The Movement of the signal from the Vehicle to the Analyser

The vibration tests on the vehicle were carried out as follows:

1. A line at a distance of about 2m before the beginning of the selected pothole was marked. This is where the vibration analysis equipment was activated to pick up the response. The mark took into

account the operator reaction (approximately 0.15 seconds). This ensured that the responses at all the speeds were taken without missing the signal during the machine pickup time.

2. A transducer was fastened onto a fabricated rigid steel mounting. The mounting was firmly bolted on an area very close to the top of the left shock absorber (point 1 in Figure 5.1).
3. A cable was connected from the transducer to the analysis equipment held by an operator in the front passenger seat.
4. In order to get the acceleration, the parameters of the analysis equipment were set as follows:
   Analysis Mode: "Time Wave Analysis" (TWA)

Period	976.6 μs
Data Sets	1024
Tot Per	1000 ms (recommended by Technical Services staff)
Frequency	1.00 Hz (recommended since lowest frequency expected was 1Hz)
Amplitude	5.00
Units	g's (acceleration; where 1g=acceleration due to gravity $\approx$ 9.81 m/s^2)
Measurement	Peak to Peak Value of Output signal.

Where:

Period – displays the rate of sampling

Data sets – shows the number of data sets averaged together to create the displayed waveform

Tot per – shows a calculated value of the total time that samples are recorded

Frequency – displays a calculated value of the sampling frequency

Amplitude – gives the amplitude range

Units – shows the choice of response parameter (displacement; velocity; acceleration)

5. From an arbitrary position before the pothole, the vehicle was accelerated to 10 km/h. At that constant speed (without braking), the wheel on the transducer side was passed over the pothole. The analyser was activated at about the 2m mark before the pothole.
6. Having picked up the response, the analyser displayed the signal on the screen. The data/signal was stored, for future down loading. Three readings were taken for each speed.

7. Steps 5 and 6 were repeated for the speeds 20, 30, 40, 50 and 60 km/h. Due to battery charging problems of the analyser, after performing the tests for the six speeds, the signals had to be printed using the provision on the machine. This had to be done at the Technical Services Station that was about 6 - 7 km from the point of the tests. Since the analyser failed to download the data onto a computer as planned due to malfunctions, the integrated signal printout facility was used to print the results.
8. The accelerometer was then fastened to the front bottom mounting (point 2 in Figure 5.1) at a safe and convenient position on the transverse link of the suspension, about 9 cm from the wheel hub, close enough to the wheel without interfering with the motion of the wheel and when cornering. This point represents the vertical motion of the front wheel.
9. Steps 3 - 7 were repeated.
10. The transducer was then fastened to the mounting fitted above the rear shock absorber. This represents point 3 similar to the front top position.
11. Steps 3 - 7 were repeated.
12. Finally, the transducer position was changed to the rear wheel. The transducer mounting was fastened onto the suspension transverse link close enough without the accelerometer interfering with the motion of the wheel. The position was about 9.5 cm from the wheel hub.
13. Steps 3 - 7 were carried out except that only two readings taken per given speed due to restrictions on fuel availability.

In order to measure the displacement profile of the unsprung mass (wheel) and the sprung mass (body), steps 1- 13 were carried out with the following changes:

(a) The analysis mode was changed to "Data History", which plots the overall response of the system verses time. It can be tuned to display only amplitudes at a designated frequency.
The parameters were set as follows:

Amplitude for the sprung mass:	300, for speeds 10, 20 and 30 km/h
	600, for speeds 40 and 50 km/h
	1500, for speed 60 km/h
Amplitude for the unsprung mass;	1500, for speeds 10 and 20 km/h
	3000, for speeds 30, 40, 50 and 60 km/h

(b) Other settings;

Units: μM, h

Period: 3600 seconds

Rate: 40

Filter: Out

Only one run was conducted per given speed for the reason cited earlier. There was an inherent limitation on the equipment in that it could not read both responses at the **same** time. Therefore, a separate run was done for each point for a particular vehicle speed. This would have required that seventy-two runs be done for acceleration. The number does not take into account the more than fifteen failed runs. The response profile obtained for each speed was however enough to determine the waveform of the response. Additionally, and to check the accuracy of each run, extra runs were carried out at:

Front wheel (10, 20 and 30 Km/h)
Rear wheel (40, 2 x 60 Km/h)
Rear body (60 Km/h)

5.4 Calibration of the Vehicle Speedometer

In order to check the accuracy of the speedometer readings, the meter was calibrated.

Place: University of Zambia, Lusaka
Calibration Speed = 40 km/h
Distance = 80 m

5.4.1 Procedure

A distance of 80 m was marked on an asphalt road. At a steady speed of 40 km/h, the vehicle was driven over the marked distance. Using two stopwatches, the time taken to transverse the marked distance was taken. Results were tabulated and a calibration factor was determined to correct the speedometer readings. The calculation of the factor is given in Appendix A.1.

5.5 Determination of the Correction Factor for the Recorded Values of Acceleration

As noticed from the experimental procedure, it was not possible to place the accelerometer on the wheel hub. Thus, it was positioned as a distance from the hub. This introduced an error in the values of acceleration obtained for both the front and rear unsprung masses. In order to take into account the resulting error, a correction factor was determined as shown in Appendix A.2.

5.6 Samples of the Collected Responses

This section presents samples of the acceleration and displacement responses printed from the vibration analysis equipment. Although only three printouts have been displayed for each, there were as many printouts as the runs.

For the acceleration plots, the most important portion is where there is a sudden increase in the fluctuations as shown in Appendix B.1.

The plot for the displacement is rather different from the acceleration plot. Appendix B.2 shows that initially, the plot is almost horizontal (datum). At the point the wheel hits a pothole, there is a sudden rise in the curve up to a maximum before dropping to the datum.

5.7 Derived Results for the Case Study

This section presents the derived data obtained from the readings collected, which are shown in Appendix C. Below is a brief explanation of how each data set is converted.

Velocity

The actual velocity of the vehicle is determined by multiplying the speedometer reading with the calibration factor determined in Appendix A.1.

Acceleration

For the acceleration, the collected data is in g's. Since 1 g $\approx$ 9.81 m/s^2, in order to convert the collected data into m/s^2, each acceleration reading is multiplied by a factor of 9.81. Details of how the means and standard deviations were calculated are presented in Appendix D. In order to obtain the corrected

values of acceleration of the unsprung mass, each recorded value is multiplied by the correction factor determined under Section 5.5.

Table 5.1: Maximum Acceleration when the Front Wheel Hits a Pothole, Front Sprung Mass

Vehicle Speed		Maximum Acceleration (m/s^2)
(km/h)	(m/s)	
10.5	2.92	14.46
21	5.83	16.98
31.5	8.75	20.12
42	11.67	28.93
52.5	14.58	32.07
63	17.50	35.22

Table 5.2: Maximum Acceleration when the Front Wheel Hits a Pothole, Front Unsprung Mass

Vehicle Speed		Maximum Acceleration (m/s^2)	
(km/h)	(m/s)	Recorded	Corrected (Actual)
10.5	2.92	15.40	21.41
21	5.83	30.81	42.83
31.5	8.75	32.07	44.58
42	11.67	45.27	62.93
52.5	14.58	66.66	92.66
63	17.50	55.97	77.80

Table 5.3: Maximum Acceleration when the Rear Wheel Hits a Pothole, Rear Sprung Mass

Vehicle Speed		Maximum Acceleration (m/s^2)
(km/h)	(m/s)	
10.5	2.92	12.26
21	5.83	14.14
31.5	8.75	15.09
42	11.67	18.87
52.5	14.58	26.41
63	17.50	34.90

Table 5.4: Maximum Acceleration when the Rear Wheel Hits a Pothole, Rear Unsprung Mass

Vehicle Speed		Maximum Acceleration (m/s^2)	
(km/h)	(m/s)	Recorded	Corrected (Actual)
10.5	2.92	20.63	26.41
21	5.83	33.96	43.47
31.5	8.75	41.51	53.13
42	11.67	58.48	74.85
52.5	14.58	89.93	115.11
63	17.50	78.29	100.21

5.8 Discussion

Although the experiments were done under difficult conditions, results were obtained which gave a trend from which some conclusions could be made.

Initially, it was decided that the IRD Fast Track Vibration Analysis Equipment be used for the tests. This was despite the fact that it did not have a combined facility for the output printout. The data collected from the tests was to be downloaded onto a computer for printing later. However, the machine malfunctioned after the first set of tests. The data could not therefore be retrieved. It was therefore suggested that the IRD 885 Vibration Analyser / Balancer be used. After the first set of tests, it also malfunctioned. The system program had to be reloaded before it could be used again.

During the tests whose results were collected and are available, 108 runs were successful while 32 were discarded. The other runs which were wasted are those results that could not be retrieved due to the malfunctioning of the machines.

Since the printouts from the machine were much smaller than the downloaded ones, the accuracy of the results was expected to be lower, but without altering the results significantly.
Despite the aforesaid difficulties, tests were conducted using the same IRD 885 machine. The following text discusses the results.

From the data in Section 5.6, graphs shown in Figure 5.3 were plotted. The graphs in Figure 5.2 show the maximum acceleration at each speed, plotted on the same axes for all the four transducer points.

From Figure 5.3, the following can be observed:

1. The increase in vehicle speed increases the acceleration induced by a pothole up to a maximum value for the unsprung mass while it continues to increase for the sprung mass.
2. The rear wheel recorded a higher value of acceleration than the front one. This could be attributed to the additional effect of the front wheel hitting the pothole before the rear wheel. Further, the general design is that the rear suspension is stiffer than the front one [6]. On the contrary, the acceleration values for the front body were higher than the rear one. It could be as a result of the

old spring and shock absorber of the front part being weaker and thus allowing higher load to be transmitted through the suspension system.

The actual data history obtained from the analysis equipment (Appendix D) shows that the motion of the points under examination follows a sinusoidal pattern. Thus, it can be assumed that the input due to the pothole is sinusoidal as well. In this study, therefore, the assumption that a pothole represents a sinusoidal excitation is valid.

The results from the tests carried out can be considered to be approximations due to the following:

1. From the design of the equipment, it was clear that it was suitable for measuring steady state response of stationary equipment with rotating members. This is further supported by the fact that only one channel of the IRD machine could operate at a time. This implies that it was not possible to pick the vibration response of more than one point of a vehicle when it hits a pothole. Consequently, there was need to pass over the same pothole in the same way at the same speed so that the response produced is the same for all runs. Practically, this was difficult to achieve.
2. Maintaining a constant speed as the vehicle passed over the pothole was not practically possible.
3. The line where the wheels ran as they hit the pothole could vary, as each run was unique.
4. Since the transducer could not be placed on the axis of the wheel, it had to be placed at a distance from the axis so as not to interfere with the wheel as it rotates (and also as it corners for the steerable wheels). Further, care had to be taken not to tamper with the original design of the existing structures. For the front and rear wheels, the transducer was placed 9cm and 9.5cm from the wheel axis respectively. If the transducer was placed on the wheel axis, higher responses could have been recorded. This applies to the unsprung masses only.
5. Error in the time to start the machine for response pickup.

The standard errors relating to the measured accelerations are shown in Appendix D. As shown, he standard deviations are much lower than the mean values in most cases. This indicates that the experiments were carried out with reasonable consistency despite the above stated points.

5.9 Concluding Remarks

Despite the problems encountered during the tests, and the limitations of the vibration analysis equipment, the tests can be considered to have been successful.

The following can be concluded:

1. With suitable equipment, it is possible to measure the acceleration and determine the displacement profile of the sprung and unsprung masses of a vehicle when it hits a pothole.
2. The wheel assembly experiences the highest acceleration and hence, the higher force as compared to the vehicle body.
3. Since there is a great difference in acceleration between the wheels and the body, most of the energy from the wheel is dissipated in the suspension system. Therefore, particular attention must be taken on redesigning components constituting the suspension system.
4. The excitation due to a vehicle hitting a pothole can satisfactorily be approximated as a sinusoidal waveform.
5. When a vehicle hits an isolated pothole, the force input can be considered to be a shock one since it happens over a short period of time. Failure of the members is therefore likely to be due to a shock load.

5.10 Graphical Representation of the Derived Results

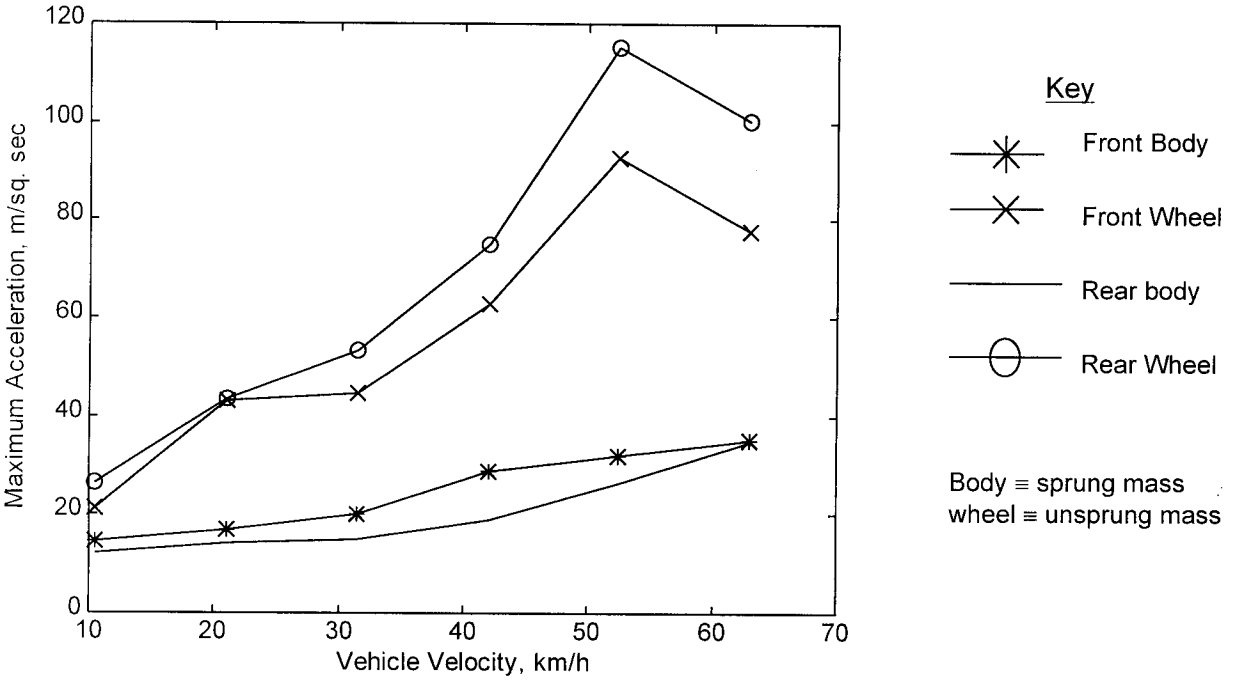

Figure 5.3: Acceleration Vs Vehicle Velocity for Various Accelerometer Positions

CHAPTER 6

THE MATLAB COMPUTER PROGRAM USED IN THE THEORETICAL STUDY

6.0 Introduction

This chapter introduces MATLAB, the mathematical tool used in this study. It further gives a brief description of each program dealing with a specific task.

MATLAB is a computer package for matrix computations. The word MATLAB stands for Matrix Laboratory. This package is written to facilitate easy engineering and scientific calculations. Entirely written in C-language, MATLAB is a complete integrated system, including graphics, programmable macros, a fast interpreter, and many analytical commands. Over the years, MATLAB has improved beyond the "MATLAB Laboratory" to become a versatile scientific "Spread Sheet" for numeric calculations.

Computer simulation of effects of potholes on vehicle structures requires the use of large matrices and vibration response is better represented in graphical form. MATLAB can easily handle large matrices that need no dimensioning. It also has quality graphic capabilities.

6.1 Pothole Program

A MATLAB Program, using M-files, was developed to determine the vibration responses of the vehicle suspension, the loads and stresses of the components of MacPherson, Double Wishbone and Conventional Suspensions systems. For the case study, the vehicle parameters used are those given in Chapter 5.

The responses are used to find the maximum force induced as a result of a vehicle hitting a pothole. The force thus determined is used to find the possibility of failure for the various targeted suspension components (both by static and fatigue failure).

The following are the parts which were selected for failure analysis; Springs, Bushes, Pins (related to the bushes), Wheel Bearings and Shock absorbers.

6.2 Pre-requisites to Accessing MATLAB Pothole Program

Before accessing the package, the user should have all the data related to the suspension system, velocity of the vehicle, type of road profile and pothole parameters. In order to get the fatigue stress and strength of a given vehicle, the user is expected to know:

(i) The mechanical properties of the materials from which the vehicle components being analysed are made.
(ii) The dimensions and design safety factors for each of these components.
(iii) The type and geometry of the suspension system.

6.3 Getting Started

The pothole program is accessed by typing (while in the MATLAB Environment),

>> Potanaly

This results in the display of the introduction of the suspension systems. Once the user gets started, the prompt will appear with instructions appearing at appropriate stages during the computation. Hence this is an interactive program that does not necessarily need a user manual.

6.4 Introduction to the Main MATLAB M-File Programs

The programs below only represent the main ones. There are, however, other sub-programs which complement the main ones. These include those that plot the displacement and acceleration as functions of time. They are important whenever plotting of graphs is required. Other programs not part of the main program were only used to generate data and graphs used to assist in carrying out general investigations on potholes.

Intropot.m

Gives a brief introduction of the main program POTANALY (Pothole Analysis) which is used to determine the vibration responses, induced force and load/stress analysis of vehicle structures.

6.4.1 Programs for Quarter Car Vibration Analysis

The programs in this section were particularly developed so that the case of quarter car analysis and that with superposition of the front and rear sides of a vehicle could be compared. They are not

part of POTANALY. Further, they can be used to observe vibrational characteristics of both the sprung and unsprung masses. The mathematical expressions in Chapter 2 are used.

zdisp.m

Determines the displacement of the sprung and unsprung masses of a vehicle when it hits a pothole. It also plots the graphs of displacement against vehicle velocity for both masses.

z_plot

Plots the maximum displacement of the sprung and unsprung masses of a vehicle when it hits a pothole. This is for particular pothole dimensions at a particular resonance velocity.

z_splots.m

This plots the displacement of the sprung mass against time for various velocities.

zaccel.m

Determines the maximum displacement of the sprung and unsprung masses of a vehicle when it hits a pothole. This is for a particular resonance velocity

zaccelts.m

Determines the maximum acceleration of the sprung and unsprung masses of a vehicle when it hits a pothole. It also plots the graphs of acceleration against vehicle velocity for both masses. Thus, the velocity at which acceleration is a maximum is determined.

6.4.2 Programs for Vibration Analysis with the Front and Rear Wheels Superimposed on Each other

This section deals with the programs which relate to vibration analysis with the ultimate goal of determining the forces on both the sprung and unsprung masses. The programs make use of the mathematical expressions in Chapter two.

dyfact.m

Determines the dynamic load factor at any given speed on the front side of a motor vehicle. The factor was incorporated into the program by interpolating values in Figure 2.7.

forcesf.m

Determination of the maximum dynamic force on the front sprung and unsprung masses of a vehicle when it hits a pothole for velocities 0 - 100km/h. The dynamic load factor, A_a, is taken into account. Newton's Second Law of Motion is employed.

forcesr.m

Determination of the maximum dynamic force on the rear sprung and unsprung masses of a vehicle when it hits a pothole. The dynamic load factor, A_a, is taken into account. Newton's Second Law of Motion is employed.

force_s.m

Determination of the maximum dynamic force on the sprung mass of a vehicle when it hits a pothole. This is for a particular vehicle speed.

force_us.m

Determination of the maximum dynamic force on the unsprung mass of a vehicle when it hits a pothole. This is for a particular vehicle speed.

6.4.3 Determination of the Induced Load and Stresses

The mathematical expressions and failures modes presented in Chapters 3 and 4 were used in developing the following programs.

conven.m

This program analyses the failure of mechanical parts of a conventional suspension system that uses leaf springs. The parts are shackle pins and bushes, and leaf springs.

d_wisbo.m

This program analyses the failure of the mechanical components of a Double Wishbone type of independent suspension. The components are transverse link pins and bushes, and springs (both coil and torsion, whichever is applicable).

MacPher.m

This file analyses the failure of the mechanical components of a MacPherson type of independent suspension. The components are transverse link pins and bushes, and coil springs.

shokpad.m

This program analyses the failure of a shock pad. This is applicable only to MacPherson and Double-wishbone suspension systems.

w_bering

This program analyses the failure of wheel bearings. It is used for all the three types of suspension systems.

Shock.m

Compares the design load and the calculated load to determine failure of the shock absorber. Just like w_bering, it is employed for the suspension systems given.

6.4.4 Miscellaneous

susptrav.m

Determines the suspension travel ratio of the sprung and unsprung masses of a vehicle when it hits a pothole. The graph can be used to compare with a typical one to ascertain the accuracy of the simulations.

6.5 Input Parameters for the Theoretical Study of a Saloon Car

This section presents the parameters which were used for the saloon car used in the experimental work. In addition to the actual vehicle parameters stated in Section 5.3, other parameters were approximated from literature because information could not be obtained from the manufacturers. The source references for the data given are indicated against each given parameter. The results from the simulations using these parameters are presented later in Chapter 7.

6.5.1 Actual Vehicle Parameters

Below are the parameters which were physically measured from the vehicle

Wheel base, l_{wb} = 2.45 m
Wheel diameter, D = 0.56 m
Total Vehicle Mass, M = 1025 kg

6.5.2 Approximated Vehicle Parameters for Vibration Analysis

In order to carry out the vibration analysis on the car, the following parameters were approximated from literature [3, 4, 6]:

Sprung mass, m_s = 276.75 kg (front); m_s = 184.5 kg (rear)
Mass Ratio, m_{us}/m_s = 0.1
Wheel base ratio, l_r / l_f = 1.5
Tyre stiffness, k_{tr} = 176 kN/m
Stiffness ratio, k_{tr} / k_s = 8
Rear spring stiffness, k_r = 22 kN/m
Damping ratio, ζ = 0.3

In the response functions, tyre damping was taken into account. Tyre parameters were approximated from the data given in Appendix E [4].
Type: Radial ply
Size: 165 x 13
Inflation pressure: 30 psi (206.9 kPa)
Damping coefficient: 3.43 kN s / m

6.5.3 Parameters for the Determination of loads and Stresses in Various Suspension Members

The angle of inclination of the strut, α, is taken to be 83°. This is approximated from the kingpin inclination in Chapter 3. From the same chapter, the initial angle of inclination of the transverse link, β, is assumed to be 7°.

In order to determine the possibility of failure of the selected suspension components, mechanical properties of the materials from which the components were made were approximated from literature. Some mechanical properties of the materials for the suspension components are presented in Appendix F [17, 20].

Below are the input parameters for each component:

(i) Shock Absorber

Maximum allowable load = 16480N [3,6,15]. This is calculated using Newton's Second Law of Motion using the maximum acceleration.

(ii) Shock Pads

The material used to make shock pads is rubber as shown in Figure 4.9. The following parameters apply to the shock pad being analysed,

S_{ut} = 10 MPa [20]
Top diameter, d_{sp} = 0.04 m (measured)
Bottom diameter, D_{sp} = 0.055 m (measured)
Height = 0.045 m (measured)

(iii) Coil Spring

High Carbon steel is normally used to make coil springs [17]. The following are the parameters of the coils springs of the car being studied.

S_y = 500 MPa [17,9]
S_{ut} = 700 MPa [16,17,20]
G = 73575 MPa [6]
n = 4 coils (counted)
Coil mean diameter = 0.13 m (measured)
Wire diameter = 0.01 m (measured)

(iv) Transverse Link Pin

Usually, alloy steel is used to make these pins [18]. In the study, the following parameters apply,

S_y = 300 MPa [20]
S_{ut} = 500 MPa [20]
d = 0.035 m (measured diameter)
Length = 0.07m

(v) Rubber Bushes

Rubber bushes are treated like bearings. Therefore, metal-packed materials are employed [17]. Typical allowable compressive stresses range from 20 to 50 MPa. Presented below are the *parameters for the rubber bushes used in the simulation in this work.*

Length = 0.07 m (measured)
Outer diameter = 0.040 m (measured)
Inner diameter = 0.035 m (measured)
S_{ut} = 20 MPa [17],

(vi) Wheel Bearings

Like the shock absorber, the maximum load of 16480N is approximated from literature.

Generally, in the determination of failure of the above mentioned components, the following assumptions are made,

(a) The general reliability for all components has been assumed to be 0.9 [7].
(b) The factor of safety for all suspension parts is assumed to be 1.54 to 2 [16]

CHAPTER 7

RESULTS AND DISCUSSION

7.0 Introduction

This chapter presents the findings from the vibration and force analyses and failure investigations of the selected suspension components of the car used in this work. It ends with a discussion of the results giving explanations on the observed results and indicating what deductions can be made.

7.1 Vibration and Force Results from the Case Study

7.1.1 Comparison between the Induced Force for a Quarter Car and a Situation where Superposition is taken into Account

This comparison is necessary in order to determine the extent to which the superposition of the front and rear sides of the car goes. Further, this would assist in establishing whether a quarter car analysis is adequate in determining the maximum loads induced by a pothole.

Figures 7.1, 7.2, 7.3 and 7.4 show a comparison between the maximum induced force for a quarter car and the situation where superposition is taken into account. The first two figures consider the front sprung and unsprung masses respectively while the last two consider the corresponding rear masses.

The graphs indicate that for the car used in this work, there is very little difference between the two situations being considered because the motion on each side does not have a strong impact on the maximum force generated. Therefore, a quarter car is adequate to obtain the maximum loads on a given wheel position. This may not necessarily be the case for all vehicles due to the difference in the suspension types and their parameters, as well as differing positions of the centre of gravity.

7.1.2 Comparison Between the Induced Force of the Sprung and Unsprung Masses for a Quarter Car with the Dynamic Load Factor Considered

In order to compare how much force is transmitted from the road to the sprung and unsprung masses, graphs in Figures 7.5 and 7.6 where plotted. Knowledge of this comparison would assist in establishing where much emphasis should be placed in the design or redesign of the vehicle structures (i.e. whether sprung-mass or unsprung-mass-related structures).

Figure 7.5 compares the forces on the front sprung and unsprung masses of the car while the Figure 7.6 compares the rear ones. The figures reveal that the force on the unsprung mass is much higher than on the sprung one. They also show that the maximum force on the sprung mass occurs at a lower vehicle velocity than on the unsprung mass. This was expected because the sprung mass has a lower natural frequency than the unsprung mass. Therefore, its resonance occurs at a lower velocity, which is directly proportional to the frequency of excitation.

The maximum load on the front sprung mass is 3.47 kN occurring at 4 km/h while the maximum load on the unsprung mass is 15.77 kN occurring at 47 km/h. The maximum load on the rear sprung mass is 4.43 kN occurring at 6km/h while the load on the unsprung mass is 17.01 kN occurring at 48 km/h.

Further, the two figures reveal that for both the sprung and unsprung masses, the maximum force is higher for the rear than the front. This is attributed to the difference in the suspension properties and the adding up effect at the rear. By design, the front spring stiffness is lower than the rear while the front sprung mass is higher than the rear one [13]. Nevertheless, the unsprung mass is assumed to be the same for both.

The loads on the unsprung mass are used as the input to the wheel and the suspension system. On the other hand, the load on the sprung mass is used as the input into the body at the point of connection of the suspension to the body. In this study, it is equal to the force that acts on the shock pad for independent suspension systems.

7.1.3 Comparison Between the Induced Force for a Quarter Car When the Dynamic Load Factor is taken into account and when it is not.

As discussed in Chapter 2, the amplification factor or dynamic load factor, has a bearing on the actual maximum dynamic load on the vibrating mass. From Figure 2.7, it can be observed that the factor can range from 0 to 1.725. Therefore, it can either increase the normal load for A_a greater than one, or reduce the load when A_a is less than one. In order to determine how the factor affects the load in this work, graphs for the situation when the factor is taken into account and when it is not were plotted. Figures 7.7,7.8, 7.9 and 7.10 show the comparison between the force obtained when the dynamic load factor, A_a, is taken into account and when it is not. All the figures consider a

quarter car. The first two figures represent the front sprung and unsprung masses while the last two are for the rear corresponding masses.

Table 7.1 shows the maximum loads for different situations for a quarter car using the case study of a saloon car.

Table 7.1: Maximum Loads on the Sprung and Unsprung Masses with and without the Dynamic Load Factor, A_a

Car	Mass	Induced Force Without A_a, (kN)	Induced Force With A_a, (kN)	Resonance Velocity, (km/h)
Front	Sprung	2.22	3.47	4
	Unsprung	9.71	15.77	47
Rear	Sprung	2.81	4.43	6
	Unsprung	10.47	17.01	48

From the graphs shown in Figures 7.7 to 7.10, the dynamic load factor is greater than one at most velocities. However, at the resonance, and most critical, velocities, the factor is always greater than one. This is revealed by the higher values of the load where the factor is taken into account in Table 7.1. The observations may not always be the same for all vehicles as the value of A_a depends on the natural frequency of the vibrating body and the duration of impulse.

7.2 The Effects of Pothole Dimensions on the Induced Force

In order to determine the relationship that exists between pothole dimensions and the induced force (or acceleration), the front side of the car was considered. Only the front was considered as the pattern of results, and hence deductions are expected to be the same for both the car front and rear. A quarter car was considered.

7.2.1 Induced Force Vs Pothole Depth

Arbitrary pothole lengths were chosen, D > l_w=0.4 m and D < l_w=0.8 m, with varying pothole depth from 0.02 to 0.3m as shown in Figures 7.11 and 7.12. The limit of 0.3m is approximated from Appendix G [23].

(a) When l_w = 0.4m while varying the pothole depth; the induced force increases linearly with increasing pothole depth. However, at about pothole depth 0.085m, the value of the force

remains constant despite the increase in pothole depth. This can be explained by the geometrical relationship that exists between the wheel and pothole size as shown in Section 2.2.3. Since the wheel diameter is greater than the pothole length, a condition is encountered when the wheel sits on the edges of the potholes restricting it from going further down into the pothole. Under such circumstances, the wheel does not touch the pothole bottom. Therefore, the initial displacement, Z_o, is always given by the value of b as indicated in Section 2.2.3.

(b) When l_w = 0.8m while varying the pothole depth; the induced force increases linearly with increasing pothole depth continuously. This is unlike when D < l_w where the pothole size limits the initial displacement of the wheel. The practical maximum value of the pothole depth is 0.3m up to which the analysis was done.

It can be observed that for the unsprung mass, the graphs of the two cases are superimposed up to where the force is constant for the condition when D > l_w = 0.4 m. For the sprung mass, however, the forces when D > l_w = 0.4 m are lower than when D < l_w = 0.8 m. This is because the time ratio, t_o/t_n, upon which the dynamic load factor, A_a, depends, is appreciably different for the two cases.

7.2.2 Induced Force Vs Pothole Length

Similar to the previous section, arbitrary pothole depths, x = 0.1 m and x = 0.15 m, with varying pothole length from 0.2 m to 1.2 m, were chosen as shown in Figures 7.13 and 7.14. The limit of 1.2m is approximated from the consideration in Appendix G.

(a) When x = 0.1m while varying the pothole length, the induced force on the unsprung mass increases with increasing pothole length from l_w = 0.2 to about 0.5 m after which an increase in the pothole length has no effect on the value of the force. The initial increase to a constant value is due to the strong interaction between the pothole and wheel dimensions when D < l_w and the satisfaction of Case 1 as discussed in Section 2.2.3.

(b) The pattern of the plot for the condition when x = 0.15m is much the same as the one when x = 0.1m. The only difference arises in the constant value of the force which is higher for x = 0.15m than for x = 0.1m. This is consistent with the deductions made from Figures 7.11 and 7.12.

7.2.3 Resonance Velocity Vs Pothole Length

Figure 7.15 shows that the resonance velocity increases linearly with increasing pothole length. Despite the change in pothole depth, the two lines are superimposed. This indicates that the resonance velocity does not depend on the pothole depth, but increases with increasing length.

7.3 Validation of Theoretical Results

Since, as already stated, most of the vehicle parameters were approximated, it is necessary to determine the extent to which these results can be relied upon. For this reason, the simulated results from this work are compared with experimental results, and in some cases further supported by existing simulations. The theoretical and practical results for vibrations and forces have been compared. Although a force transducer was not used to determine the practical forces, the forces were calculated from the practical values of acceleration using Newton's Second Law of Motion [3].

7.3.1 Suspension Travel Ratio Vs Frequency

In order to check the reliability of the theoretical computation, the suspension travel ratio was plotted against frequency on a log scale as shown in Figure 7.16. A mass ratio of $m_{us}/m_s \approx 0.1$ was used to compare with a similar existing simulation, Figure 7.17[4]. The two graphs agree in that the suspension travel ratio increases with frequency up to the natural frequency of the sprung mass (1.22 Hz in this case) after which it goes down to a minimum. Finally, the ratio increases with frequency to a maximum at the natural frequency of the unsprung mass (13.25 Hz in this case). Beyond that, the suspension travel reduces with increasing frequency. Since the frequency is a direct function of the vehicle velocity in pothole analysis, this agrees with the fact that at higher velocities than the resonant one, the displacements, and thus induced loads, of both the sprung and unsprung masses reduce as shown in Figures 7.5 and 7.6. The fact that the results from this work are similar to those of an existing simulation shows that the approximations made for vehicle parameters were reasonable and, therefore, the vibration results obtained are reasonable.

7.3.2 Comparison between the Induced Acceleration Vs Vehicle Velocity for Theoretical and Experimental Results

Figures 7.18 and 7.19 compare the theoretical and practical results for the front and rear unsprung masses. Theoretical values are about five times higher than the practical ones. If smooth curves were drawn using the plotted points in Figure 7.19, it would be shown that while the practical result indicates that the maximum acceleration is attained at about 52km/h, the computer simulated one

indicates 47km/h. The smooth curves were actually drawn during the course of the work. Only six points were plotted for the simulated results in order to correspond to the six velocities at which the experiments were carried. In this way, a good comparison could be made between the two results.

The discrepancy in the values and the velocity at which resonance occurs could be attributed to the assumptions made in the theoretical models in Chapter 2. The variations in the experimental results are reasonably small to assume that the experiments were done with reasonable consistency as shown in Appendix D.

Despite the previously mentioned disparities, it is still possible to observe in Figures 7.18 and 7.19 that there exits a resonance velocity at which the induced acceleration, and hence the force, is maximum.

7.3.3 Comparison between the Induced Force Vs Vehicle Velocity for Theoretical and Experimental Results

The trend of the graphs in Figures 7.20 and 7.21 (car front and rear respectively) is similar to that of the acceleration in the previous section. On both front and rear, maximum force theoretically occurs at about 47km/h while practically, it occurs at about 52km/h. For the front unsprung mass at the practical maximum resonance velocity, the theoretical force is about 3.5 times higher than the practical, while it is 3 times for the rear unsprung mass. Again this indicates that the simulated values are much higher. Since the parameters used in the theoretical model were estimated, it is likely that this would be responsible for the large difference between theoretical and experimental predictions.

7.3.4 The Profile of the Response from the Experimental Work

Reference is made to the results discussed in Section 5.5. It can be observed that the response to a vehicle hitting a pothole can be approximated to be sinusoidal because the sample simulated response shown in Figure 7.22 also shows a similar pattern as those in Appendix B.1. Further, the acceleration response is as typically given in existing simulations [4]. This confirms the assumption in which the input for the simulated case in this work was taken to be sinusoidal. There is a difference though between the response in Figure 7.22 and that shown in the literature in that the former shows a dying response. This is because it has been assumed that only one pothole is encountered at a given time, resulting in a transient response.

The experimental profile shows that the response is not exactly sinusoidal, but an approximation. Therefore, although the principles that govern the treatment of a road as a sinusoid (Chapter 1) can be used in the analysis of potholes, the response may not be exactly sinusoidal. This is attributed to the strong interaction between the wheel and pothole dimensions. Therefore, there would be need for more experimental work to determine reliable correction factors to be used in the model.

This assumption is further supported by the approximately half sine experimental displacement profiles shown in Appendix B.2.

7.4 Failure of Selected Suspension Components

Using the maximum induced forces (P_{dus} and P_{ds}) calculated for the case of the saloon in Section 6.5, the possibility of failure of the selected components was determined. Table 7.2 shows the results obtained using the program "Potanaly" based on theoretical loads. In order to generate this table, the user prepares a blank one with only the top row and the left column filled in. Then as the program runs, the user completes the table. This is because the decision on whether a component fails or not is highlighted as the program is being executed.

Table 7.2: Failure of components for the Saloon Car, Front Side (Theoretical)

Component	Failure Mode	Component Fails?	Static/Fatigue Failure
Transverse link bushing	Max. Bearing pressure/compression stress	Yes	Static
Transverse link pin	Maximum bending moment	Yes	Static
Coil Spring	Maximum torsional stress	Yes	Static
Shock Pad	Maximum shear stress	Yes	Fatigue
	Maximum tensile/compressive stress	Yes	Fatigue
Shock Absorber	Maximum Axial Load	Yes	N/A
Wheel bearing	Maximum radial load	Yes	N/A

The simulations for the above table were carried out using the pothole dimensions as those for the experiments (i.e. l_w = 1.1m, x_d = 0.08m). The resonance velocity of 47km/h for the unsprung mass was used to determine the load. Table 7.2 shows that for the same pothole dimensions and vehicle parameters, all the components fail.

Just like in the case of vibration analysis, approximated mechanical properties of the various suspension components were used. This is because it was very difficulty to obtain the exact properties both from literature and vehicle manufacturers. Hence the predictions are approximations. Appendix F [17, 20] shows some of the tables from which the data was approximated.

Using the accelerations obtained experimentally, the equivalent forces were approximated using Newton's Second Law of Motion. This is because the loads could not be determined experimentally. Similarly to Table 7.2, the possibility of failure of the components due to the experimental loads was tabulated. The results are shown in Table 7.3.

Table 7.3: Failure of components for the Saloon Car, Front Side (Practical)

Component	**Failure Mode**	**Component Fails?**	**Static/Fatigue Failure**
Transverse link bushing	Max. Bearing pressure/compression stress	No	Static
Transverse link pin	Maximum bending moment	No	Static
Coil Spring	Maximum torsional stress	Yes	Static
Shock Pad	Maximum shear stress	Yes	Fatigue
	Maximum tensile/compressive stress	Yes	Fatigue
Shock Absorber	Maximum Axial Load	No	N/A
Wheel bearing	Maximum radial load	No	N/A

Table 7.3 shows that all the components except the coil spring and shock pad do not fail. This shows a significant difference from the theoretical predictions in Table 7.2. The difference arises due to the fact that the practical loads are lower than the theoretical ones (Section 7.3.3). Since practically the shock pad actually failed, this shows that the practical loads more likely indicate the reality than the theoretical, although the spring did not fail.

7.5 Discussion

The case presented is a typical example. Generally, the magnitude of the maximum acceleration, and hence induced force, and the velocity at which resonance occurs is dependent on the vehicle parameters as well. These include the tyre and suspension stiffness, the sprung and unsprung masses at the wheel of interest. This is because the circular frequency, ω, is a function of the velocity of the vehicle. On the other hand, the natural frequency of each mass involved is a function of the spring stiffness and the mass of the oscillating body. Although only the case of MacPherson struts used on the saloon vehicle studied in this work has been presented, the program "Potanaly" can be used to analyse double-wishbone (independent suspension) and the conventional type, which uses beam axles with leaf springs.

7.5.1 Vibration and Force Analysis

7.5.1.1 Comparison between Quarter Car and Superimposed Responses

The comparison between the maximum induced force considering a quarter car and the effect of superposition shows that there is very little difference between the two. Therefore, for a vehicle similar to the one analysed in this work, the less complicated quarter car analysis can be carried out, thus reducing on computational time, but without compromising the accuracy of the results obtained.

7.5.1.2 The Effect of the Dynamic Load Factor on the Induced Force

The value of A_a varies from 0 to 1.725 [3]. Therefore, when the calculated value of the force is multiplied by the factor, there are three possibilities,

(i) The load is lowered when $A_a < 1$

(ii) The load is increased when $A_a > 1$

(iii) There is no change in the load when the value of $A_a = 1$.

For this study, the dynamic load factor is greater than 1 at most velocities. However, at the resonance, and most critical, velocities, the factor is always greater than one. This may not always be the case. However, it is expected that for most saloons the value of the factor would be greater than one. This in itself compounds the problem as the load is amplified, the more reason why the issue of potholes must be seriously addressed.

7.5.1.3 The Effects of Pothole Dimensions on the Induced Force

From the results obtained, it can be seen that the initial vertical displacement, which is a function of the pothole depth, directly affects the magnitude of the force on the wheel. An increase in the initial displacement increases the vertical acceleration of the unsprung mass. Hence the induced force increases in the same manner.

The velocity at which resonance occurs is dependent on the pothole length assuming that the vehicle suspension parameters are kept constant. The longer the pothole length, the higher will be the velocity at which resonance takes place. Hence, it does not necessarily mean that when one is driving at a low velocity they are safe from pothole effects. (This gives the more reason why the issue of potholes must be addressed). However, a change in the mass and spring stiffness changes the natural frequency of either the sprung or unsprung mass and hence the velocity at which resonance occurs.

7.5.1.4 Other Remarks

For both the practical and theoretical investigations, the acceleration (and hence induced force) is higher for the rear part of the vehicle. This is also shown in the experimental data in Tables 5.2 and 5.4. In this case, the maximum values of acceleration are 66.66 m/s^2 and 89.93 m/s^2 for the front and rear sides, respectively. The difference between the two sides can be attributed to the difference in the design parameters of the two and the 'adding-up' effect (i.e. coupling). In normal design, the rear suspension has a larger stiffness than the front one [13]. Hence, the natural frequency is higher which consequently increases the acceleration.

More emphasis has to be given to the unsprung mass components and not the sprung ones since the induced force of the former is many times larger than the latter (Figures 7.5 and 7.6). Further, resonance of the sprung mass occurs at very low velocities (1 to 6km/h in this case). Most driving takes place at much higher velocities.

It is worthwhile noting that the forces determined in this work only indicate the load on the sprung and unsprung masses, not necessarily the force on the tyre periphery. The actual load is expected to be higher since some of it is absorbed by the tyre deformation.

Finally, the result for the condition when the wheel width is greater than the pothole width indicated that there was no vibration response, and hence no vertical load is induced.

7.5.2 Failure of Suspension Components

For a particular case, a table similar to Table 7.2 can be generated. The table can assist in determining which components are likely to fail. Further, it assists in knowing the components which require redesigning. Alternatively, it would assist in determining the tolerable size of pothole below which a particular vehicle is "safe" to drive on at all speeds.

From Table 7.2, it shows that theoretically, the suspension components being considered would all fail under the practical conditions of l_w = 1.1m, and x_d = 0.08m. However, Table 7.3 shows that for practical loads under the same pothole parameters, only the coil spring and shock pad would fail. It is very common to find potholes which are much deeper than the 0.08m used during experiments. This means that at the resonance velocity in similar circumstances, deeper potholes would generate higher loads that would cause the other components to fail.

It is most likely that the experimental results are close to reality because while 5 out of 6 experimental predictions are correct, only 1 out of 6 theoretical predictions are correct. Therefore, in order to get results that are close to the practical values, there would be need to correct the resonance velocity and the force induced. In this case, when carrying out simulations, the maximum force would have to be calculated at (47 + 5) km/h (i.e. to corrected to the practical 52km/h). The forces evaluated at this corrected velocity are divided by 3.5 and 3 to get the practical values for the front and rear sides, respectively. These are the loads to be used in the determination of the possibility of failure of the suspension components.

7.5.3 General Remarks

The current work has not considered a case for trucks and buses. This is because the mode of analysing the effects is much the same way as that of the case presented as long as they are two-

axle vehicles. Articulated vehicles have not been considered as this would be beyond the intended scope of this work.

For heavy vehicles, the maximum loads are usually much higher due to the suspension parameters [24]. Examples are the simulated dynamic tyre forces for a step of 0.10m, which are presented in Appendix H [24].

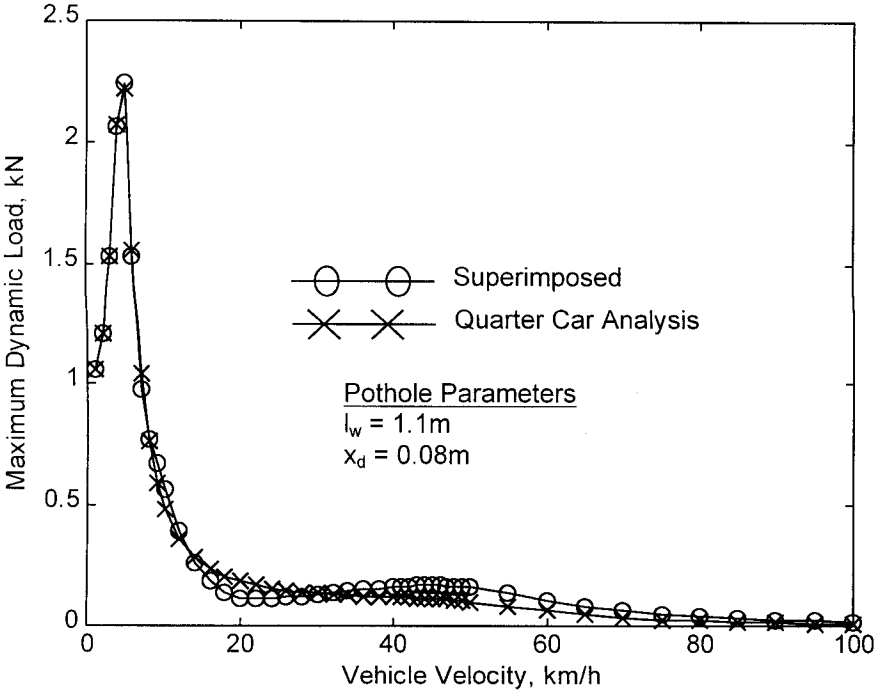

Figure 7.1 Comparison between the Maximum Force for Quarter Car and Superimposed Situations, Front Sprung mass

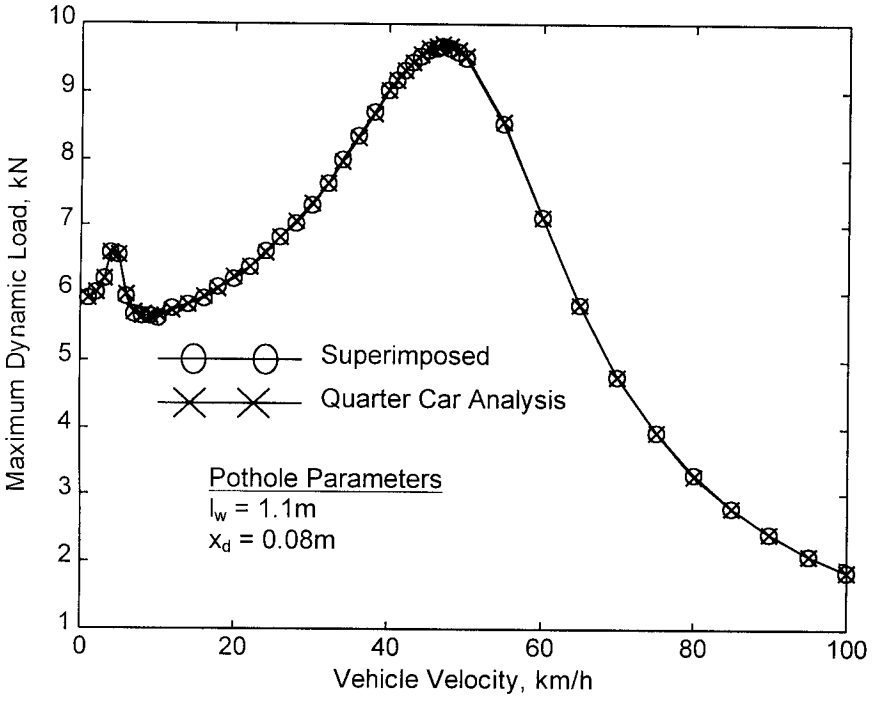

Figure 7.2 Comparison between the Maximum Force for Quarter Car and Superimposed Situations, Front Unsprung mass

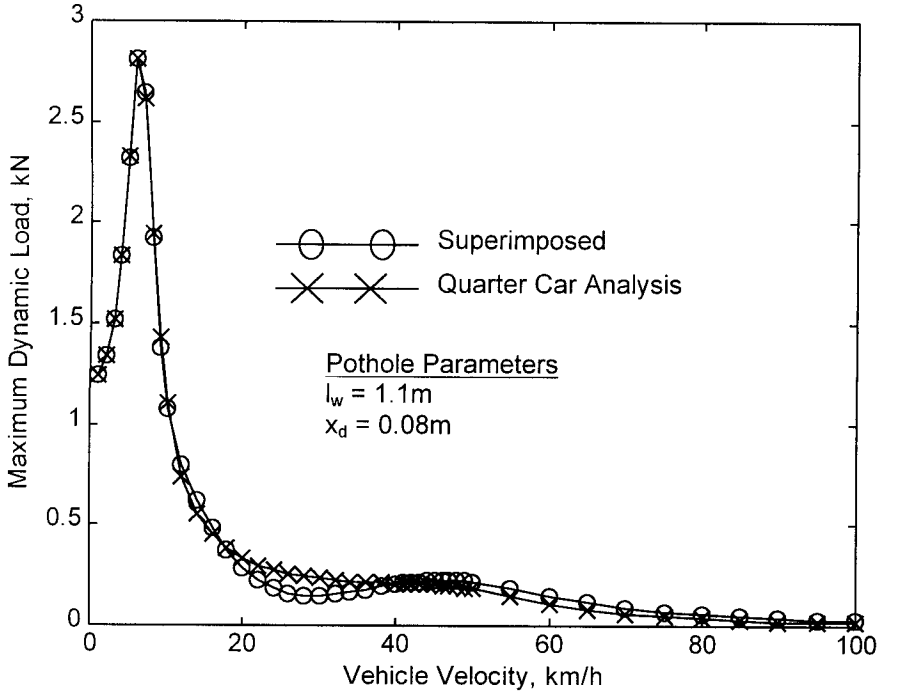

Figure 7.3 Comparison between the Maximum Force for Quarter Car and Superimposed Situations, Rear Sprung mass

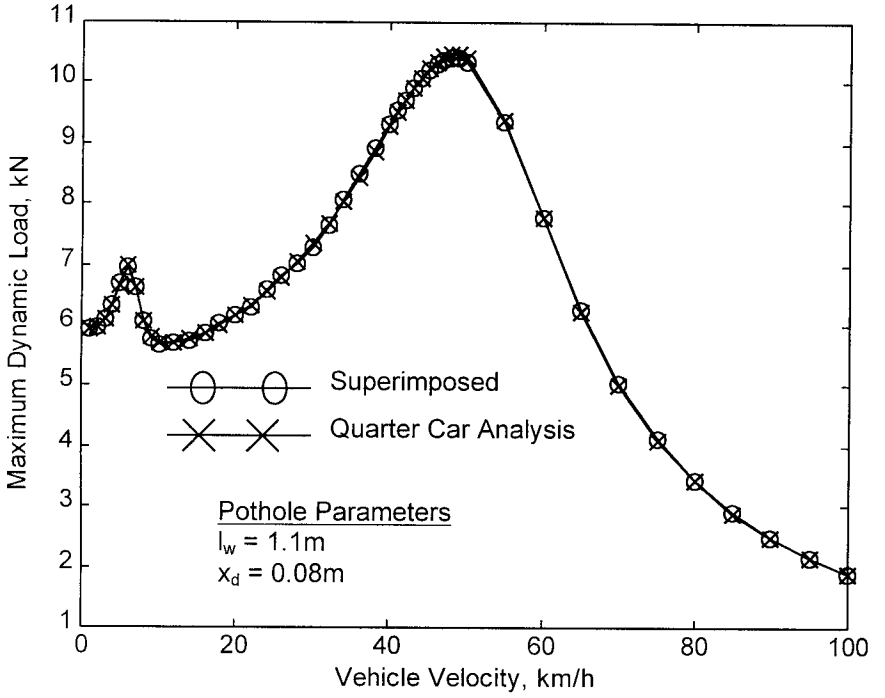

Figure 7.4 Comparison between the Maximum Force for Quarter Car and Superimposed Situations, Rear Unsprung mass

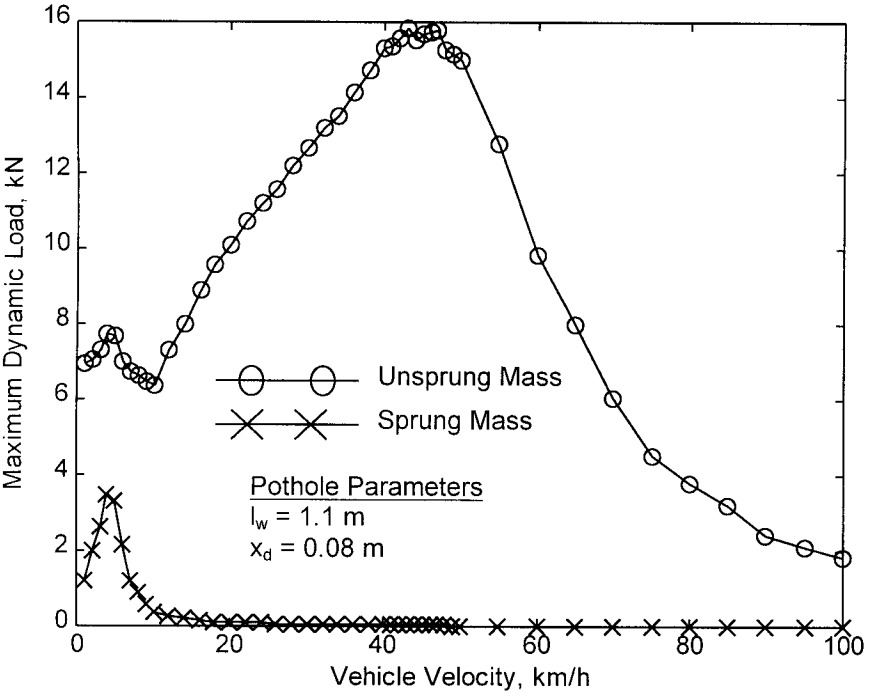

Figure 7.5 Comparison of Maximum Force with A_a Considered between Front Sprung and Unsprung Masses; Quarter Car

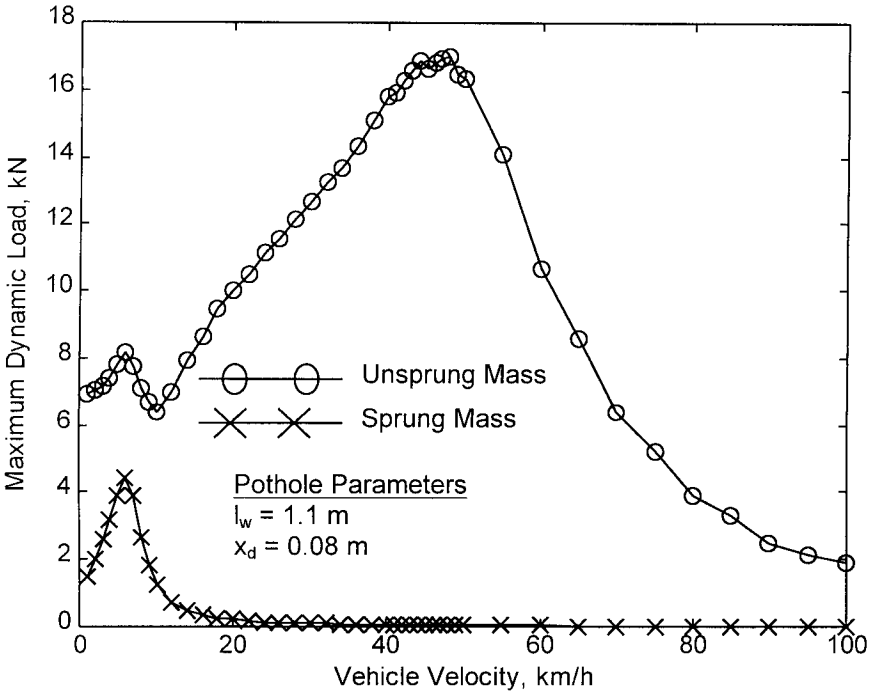

Figure 7.6 Comparison of Maximum Force with A_a Considered between Rear Sprung and Unsprung Masses; Quarter Car

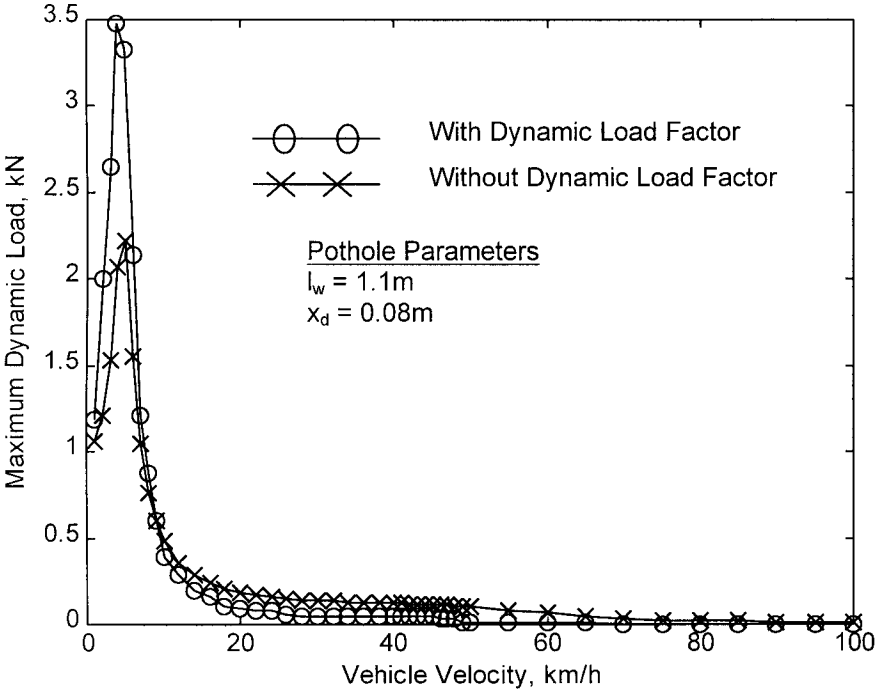

Figure 7.7 Comparison between Max. Force when A_a is considered and when not for Front Sprung Mass, Quarter Car

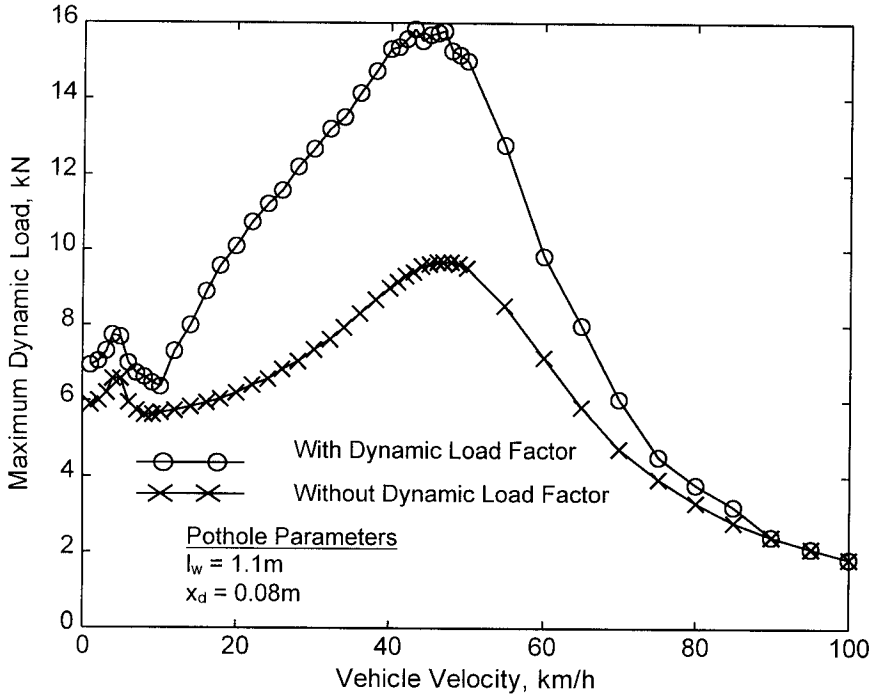

Figure 7.8 Comparison between Max. Force when A_a is considered and when not for Front Unsprung Mass, Quarter Car

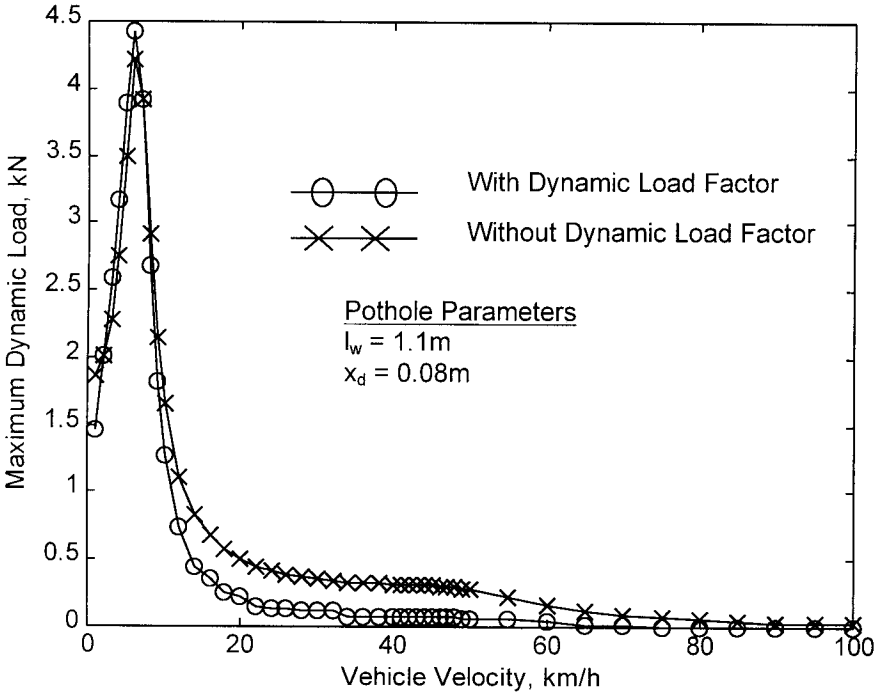

Figure 7.9 Comparison between Max. Force When A_a is considered and when not for Rear Sprung Mass, Quarter Car

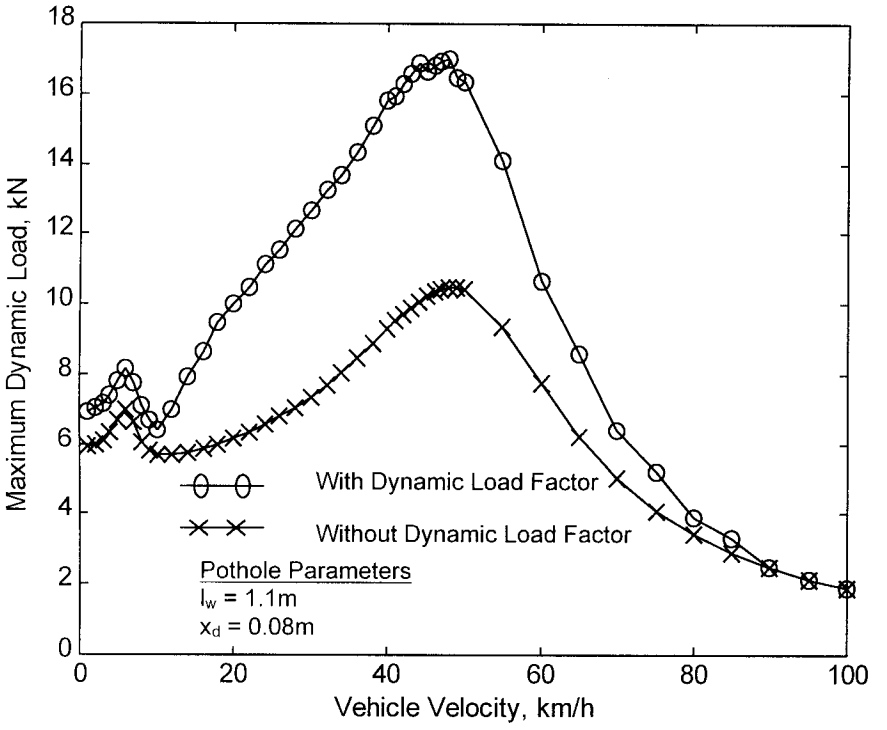

Figure 7.10 Comparison between Max. When A_a is considered and when not for Rear Unsprung Mass, Quarter Car

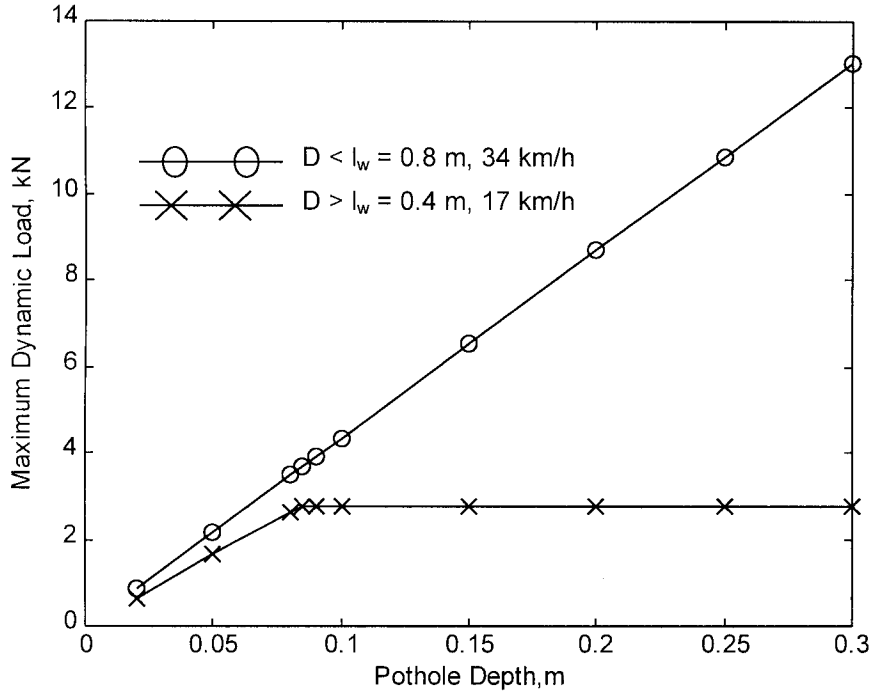

Figure 7.11 Induced Force on the Front Sprung Mass Vs Pothole Depth

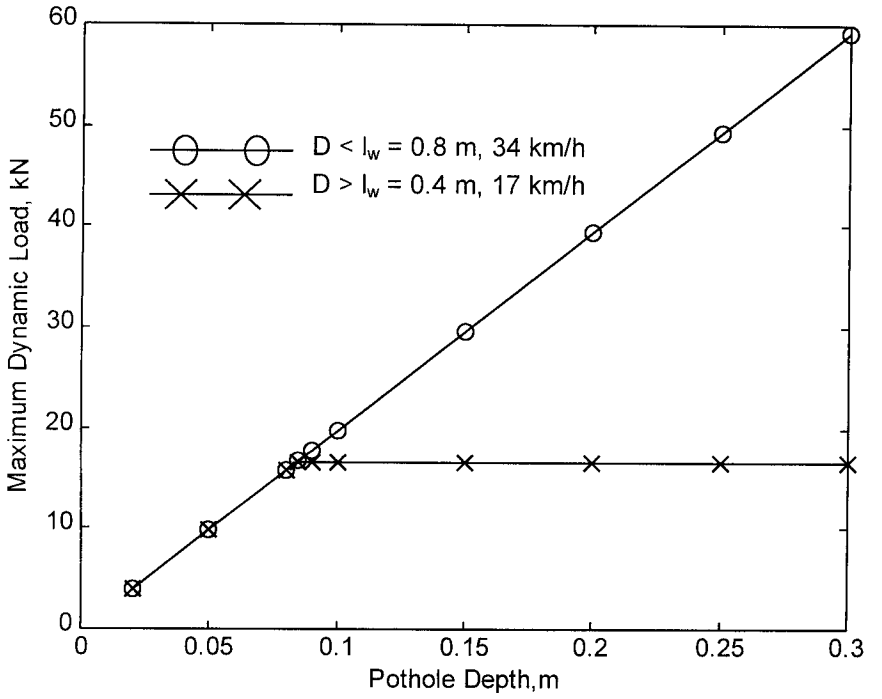

Figure 7.12 Induced Force on the Front Unsprung Mass Vs Pothole Depth

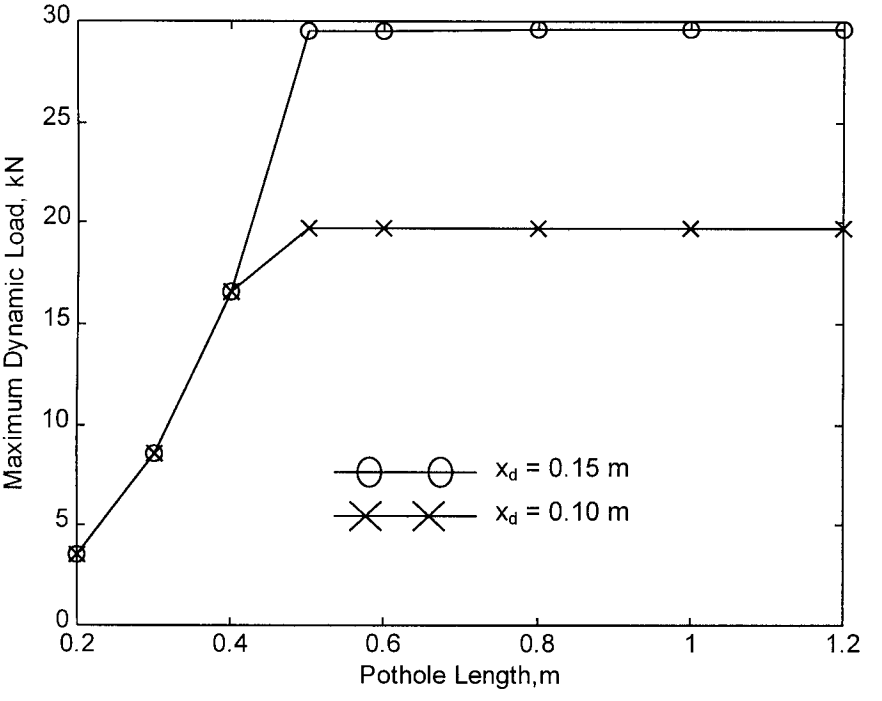

7.13 Induced Force on the Front Unsprung Mass Vs Pothole Length

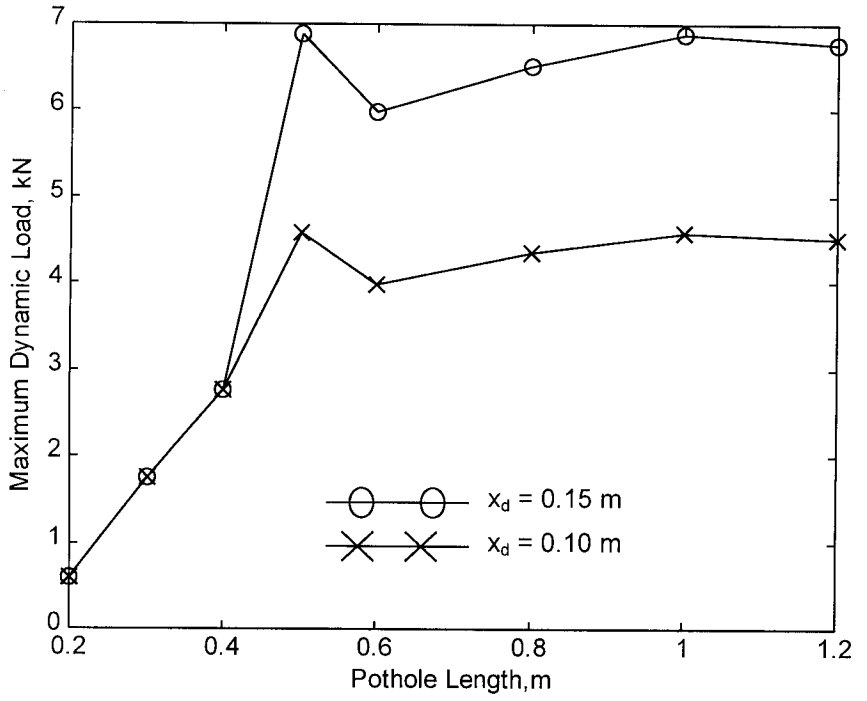

7.14 Induced Force on the Front Sprung Mass Vs Pothole Length

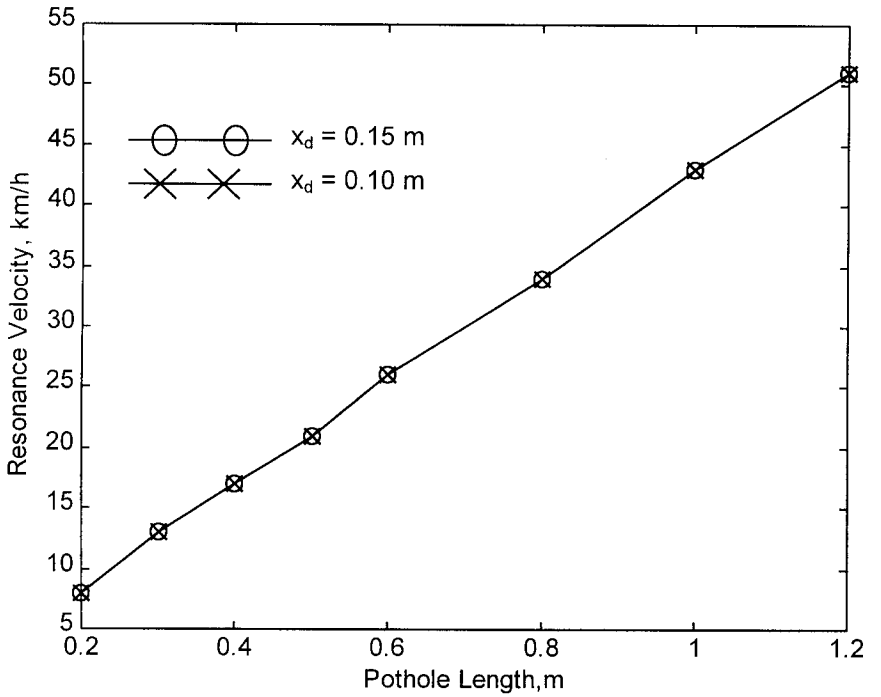

7.15 Front Unsprung Mass Resonance Velocity Vs Pothole Length

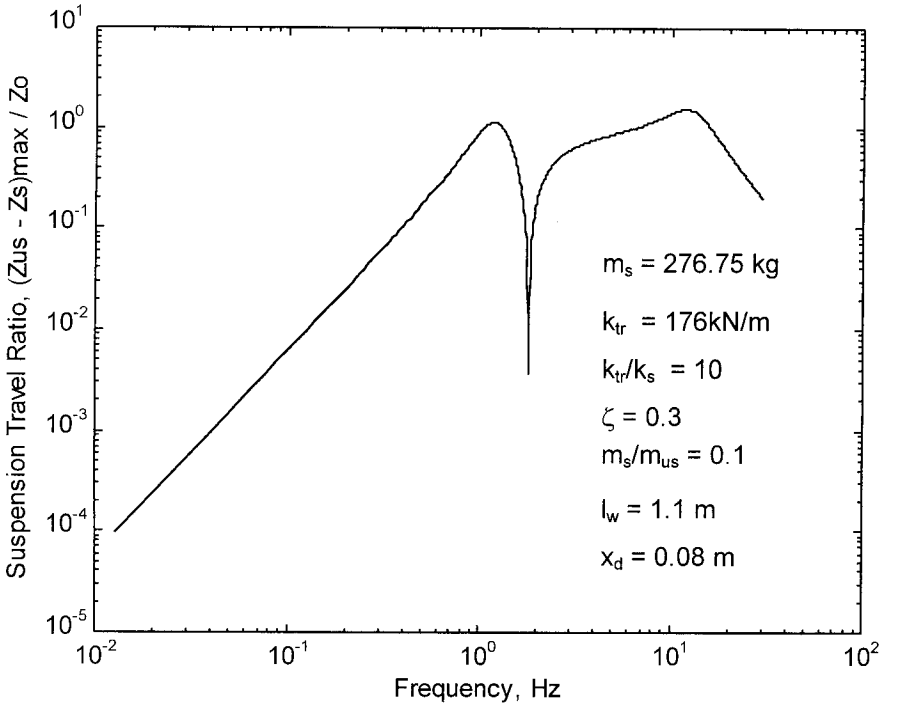

Figure 7.16: Front Suspension Travel Vs Frequency; From the Case Study

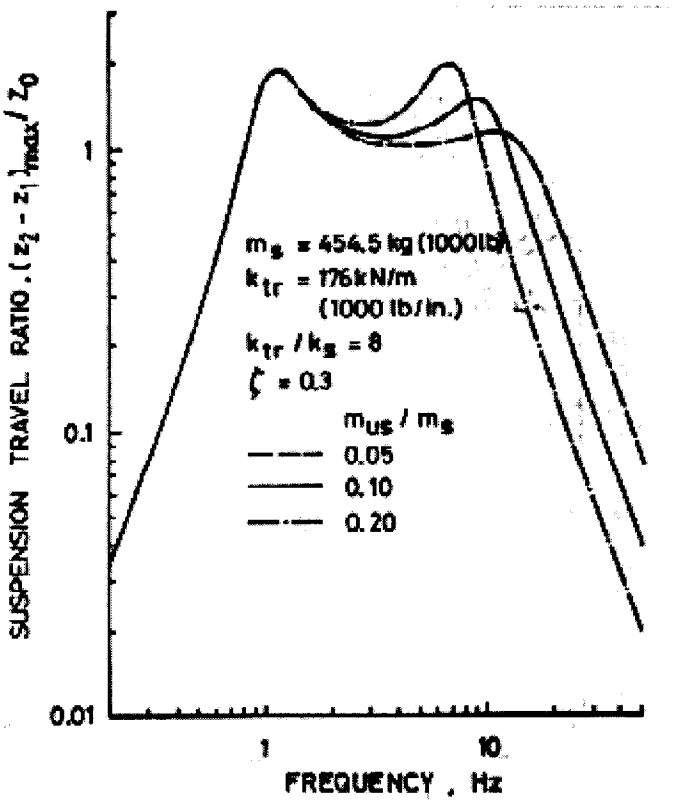

Figure 7.17: Suspension Travel Vs Frequency; Existing Simulation [4]

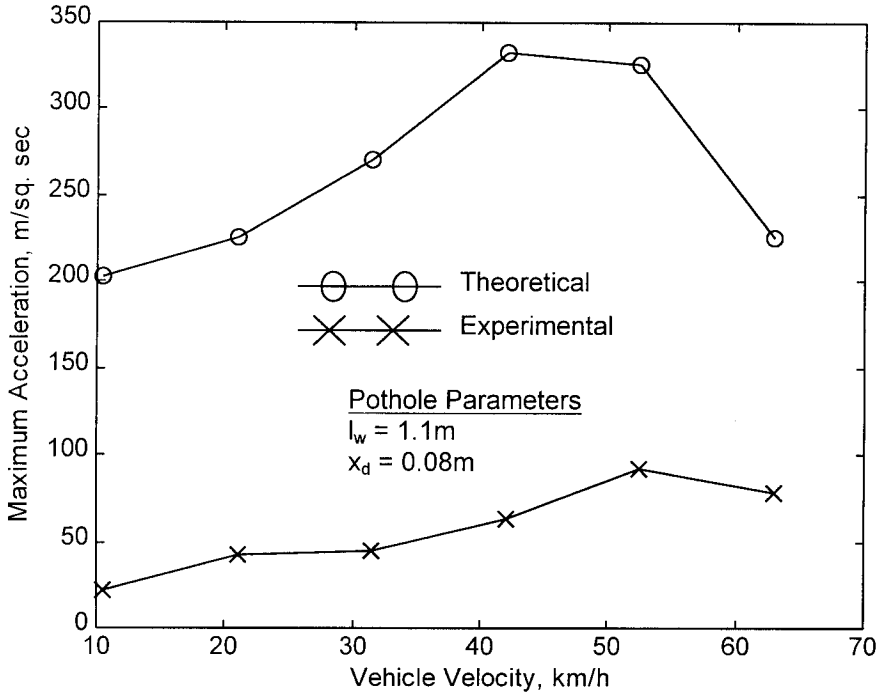

Figure 7.18 Comparison between Experimental and Theoretical Acceleration, Front Unsprung Mass

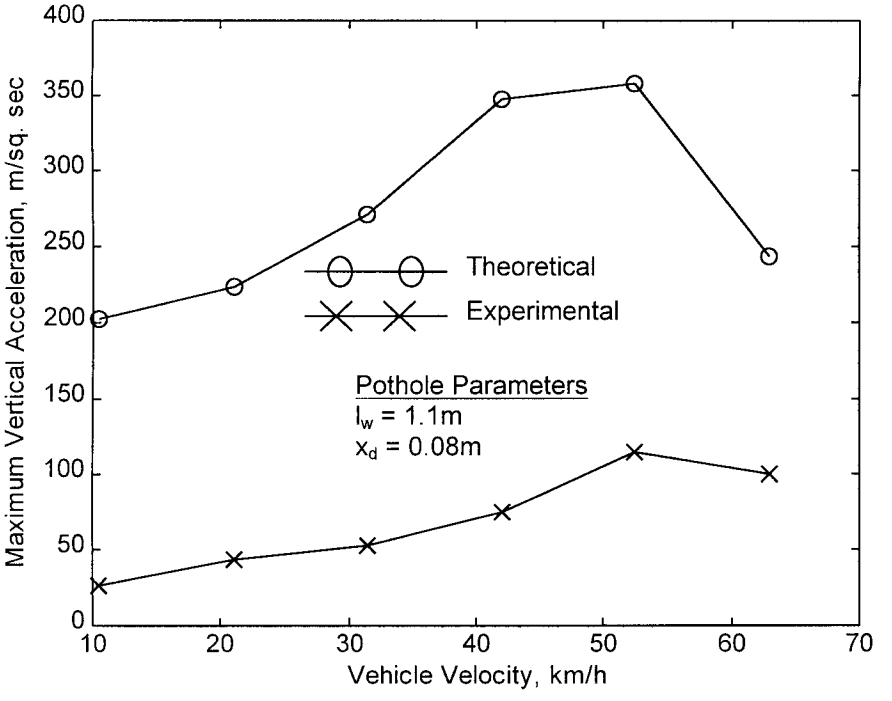

Figure 7.19 Comparison between Experimental and Theoretical Acceleration, Rear Unsprung Mass

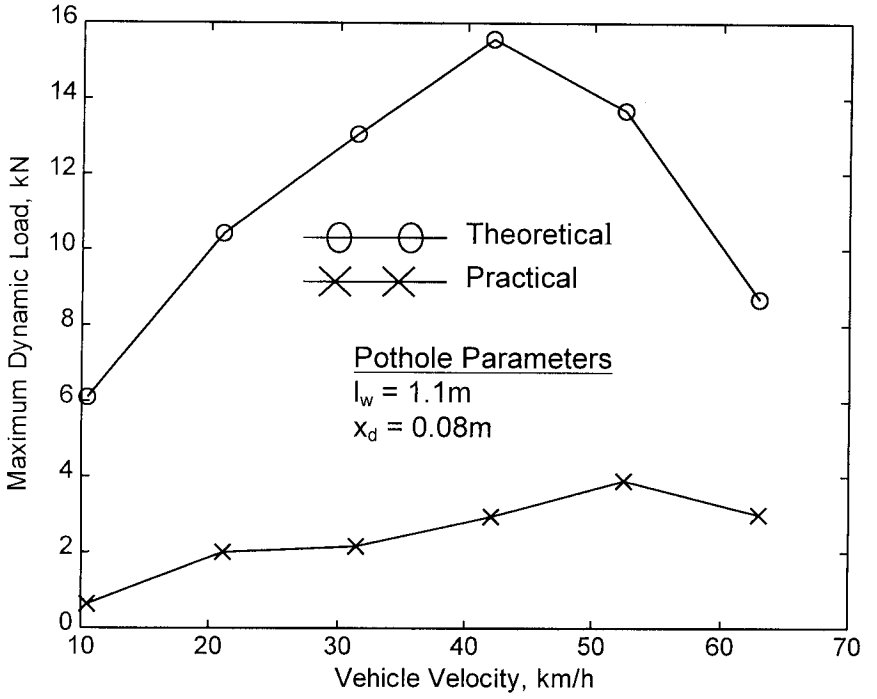

Figure 7.20 Practical vs Theoretical Forces, Front Unsprung Mass

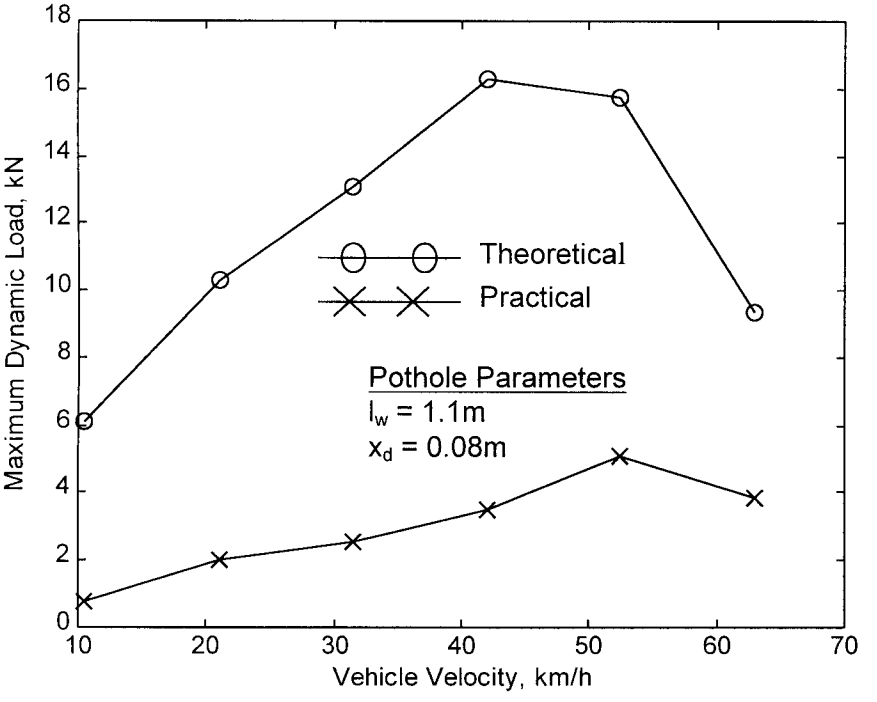

Figure 7.21 Practical vs Theoretical Forces, Rear Unsprung Mass

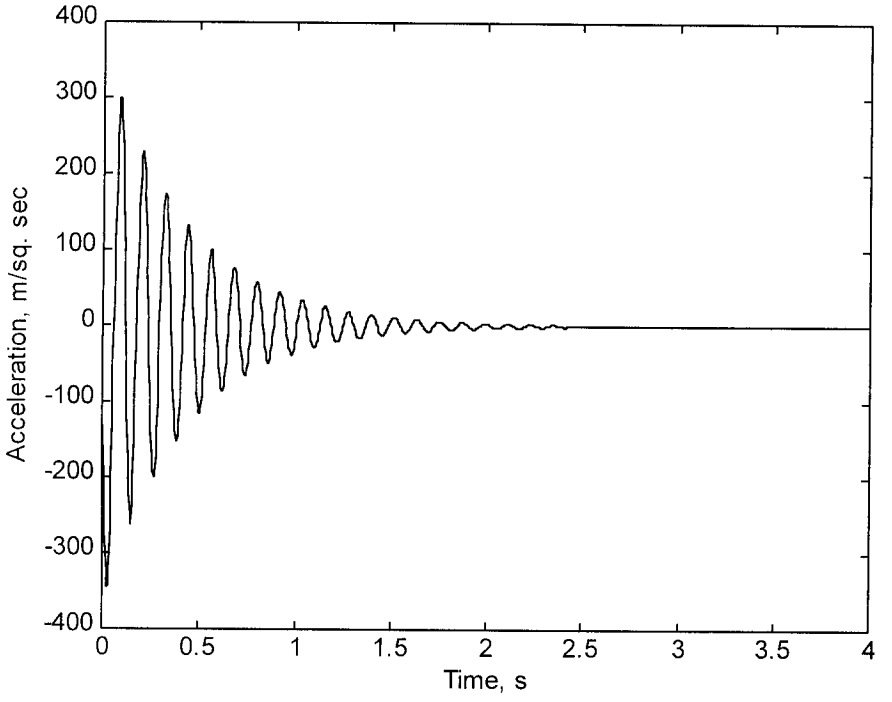

Figure 7.22 Acceleration Vs Time at a resonance velocity of 47km/h for the Front Unsprung Mass (Quarter Car); l_w = 1.1m, x_d = 0.08m

CHAPTER 8

CONCLUSIONS AND RECOMMENDATIONS

8.0 Introduction

This chapter contains the conclusions drawn from this work. Further, it gives recommendations related to the findings of this work, as well as those for future work.

The experiments were conducted in order to compare the results with the simulated ones. Some conclusions were made based on simulations since it was not possible to conduct some experiments aimed at establishing the wheel/pothole dimensions interaction. Ideally, more experiments were required. For example,

(i) It was not possible to carry out experiments to determine how the response changes with increase in pothole dimensions, while keeping the wheel dimensions constant.

(ii) It was not possible to practically show the variation of the response for constant pothole dimensions, while varying the wheel dimensions.

This was due to lack of resources to carry out such extensive experiments. However, it was established from experiments that the response to a vehicle hitting a pothole is approximately sinusoidal. Because of this fact, some conclusions were made based on data obtained from simulations, which used sinusoidal inputs. Otherwise, extensive experiments would be required, and these could be carried out in future work.

8.1 Conclusions

1. The vehicle velocities at which the resonance of each of the sprung and unsprung masses occurs is dependent on the pothole length, irrespective of the pothole depth, up to the limiting length of ripple.
2. From the two cases presented where the pothole length is greater than the wheel diameter, and where the pothole length is smaller than the wheel diameter, it is observed that the magnitude of the maximum dynamic force induced by a pothole is strongly related to the pothole depth. When the vehicle wheel diameter is greater than the pothole length, the deeper the pothole, the higher will be the vertical acceleration and hence the force induced. Another situation occurs when the

wheel diameter of the vehicle is smaller than the pothole length. In this case also, induced acceleration increases with increase in the pothole depth. However, a geometrical condition occurs between the wheel and the pothole dimensions when the value of the induced force becomes constant irrespective of the increase in pothole depth. Therefore, the design of vehicle suspension systems needs to concentrate on the first case where the induced force keeps increasing.

3. When the wheel width is greater than the pothole width, no vertical acceleration, and hence no force is induced to the structure.
4. The excitation due to a vehicle wheel hitting a pothole can be approximated to be a transient sinusoid.
5. It does not necessarily mean that when a vehicle is moving at a low velocity (10 -50km/h), then it is safe from the adverse effects of potholes. From the case study reported in this work, it is clear that for a small saloon car, the maximum induced force falls within this region. Vehicles driving around cities and residential areas are more prone to the said effects as the Highway Code specifies that the maximum velocity in those areas is about 50 km/h [25]
6. When designing a vehicle for such harsh conditions as those that prevail in Zambia, with many potholes, it is necessary to pay much attention to the design of the components which make up the suspension /unsprung mass system as this is where the maximum induced pothole force is exerted.
7. A quarter car model can be adequately used to determine the vibration response of a saloon car when it hits a pothole.
8. When a vehicle passes over a pothole, excessively high vertical loads can be induced. The loads are particularly highest at the resonance velocity. Since most cars are not tailored for such harsh conditions, the loads tend to reduce the life of suspension components with respect to manufacturers' specification. In some cases, instant failure occurs without repeated loading.
9. From the load/stress analysis, it is possible to determine the limiting pothole dimensions above which failure of vehicle suspension components would be expected by taking into account the determined relationship between the wheel diameter and the pothole dimensions.
10. Although the pattern of results obtained experimentally and theoretically is similar, there is a discrepancy between the two. Experimental loads are lower than the theoretical ones. A correction of the theoretical resonance velocity and maximum load in the developed model would produce results that depict the reality.

8.2 Recommendations

In this section, recommendations are presented for the vehicle user as well as the vehicle manufacturer. The last part discusses the recommendations for future work.

8.2.1 Nature of Maintenance

Now that it has been established that the loads due to potholes are expected to be much higher than the design values, it is inevitable that the suspension components discussed should be replaced earlier than the manufacturer's recommendation. Standard tests on the shock absorbers and springs assembly should be carried out at least as frequently as minor vehicle services (after every 5000km).

Although minor vehicle services do not include detailed checks on shock absorbers, shock pads, springs, bearings, bushes/pins, these need to be included. This implies that the cost of vehicle maintenance will also increase.

With Zambia's difficulty economic situation, it will not be possible to maintain all the roads properly. It costs about US$ 26.90 to carry out a $1m^2$ deep-patch pothole repair, while replacement of a paved road costs about US$ 250, 000.00 per kilometer (where US$1 = K2000, in March 2000) [23]. Some paved-road-related costs are shown in Appendix I. This means that it is not envisaged that Zambia shall have good roads all round in the near future.

8.2.2 Recommendations to Manufacturers

In the recent past, Electronic Air Suspensions (EAS) and Electronically Modulated Suspension (EMS) systems have been developed. Using Electro-hydraulics or Electro-pneumatics, they offer superior ride and safety quality. This type of suspension represents the Active type. The fundamental difference between an active and conventional suspension is that active systems provide independent treatment for road-induced forces and for body inertia forces. They therefore have the ability to eliminate the traditional compromise between ride and handling characteristics completely [6]. However, it has become clear that such systems are expensive to install and maintain, and there is need to obtain sufficient performance advantage to justify the high costs [26]. In view of this, vehicles with such suspension systems may not be commonly be used in Zambia.

In most of the systems being investigated, however, road disturbances are treated "passively " as in a conventional system, but with much softer than normal spring and damper settings. Body forces

generated by cornering, braking and acceleration are controlled by the active elements in the system, which resist roll and pitch in both the transient and steady state conditions to maintain the vehicle level and the road wheels more upright, for maximum handling and road holding performance [6].

Due to lack of accurate specifications of motor vehicles, it is not possible to state specifically how the design of motor vehicle suspension systems should be reconsidered. However, an overview of the recommendations is presented here.

8.2.2.1 Shock Absorbers

Using shock absorbers with higher damping constant, without compromising passenger comfort and safety of goods, can reduce the suspension travel, which increases the momentum of the suspension, as well as passenger discomfort.

8.2.2.2 Suspension Springs

In order to increase the suspension's load-bearing capacity, the spring stiffness should be increased, without greatly compromising the ride quality. Note that a spring may not necessarily fracture, but may loose resilience, which is undesirable.

8.2.2.3 Shock Pads

In the case of shock pads, the rubber material used should be of higher shear strength. Similarly, this should be done without greatly reducing the cushioning ability of the material. Hence, tougher rubber is appropriate with minimal change in flexibility. Alternatively, the shock pad dimensions should be increased so as to increase the shear area, and thus reduce the shear stress.

8.2.2.4 Suspension Bushes and Pins

In order to withstand the higher bearing loads on the bushes (and hence pins), larger components should be used. This would, however, increase the unsprung mass. Alternatively, and more preferably, stronger materials could be employed without necessarily increasing the unsprung mass.

8.2.2.5 Wheel Bearings

Bearings with higher static loadability should be used. This may imply using bearings with larger diameters. In such a situation, the bore for the bearing may need to be increased. However, as

above, it would be preferable that bearings with the same size but with higher load-carrying capacity be used in order to accommodate the higher loads due to potholes.

8.2.3 Recommendations for Future Work

In this work, a pothole was treated to be an isolated irregularity on a road. There would be need, however, to consider the treatment of the pothole excitation as a random function. This would assist in taking care of situations where several potholes arise on a particular road portion. Further, the condition where more than one wheel is running over a pothole can be analysed. This represents a highly complex situation.

In order to improve the accuracy of the theoretical results, numerical methods could be considered, e.g. FEM can be used to approximate accelerations and hence forces may yield better correlation. Further, constants or factors to account for inaccuracies arising from the assumptions stated in Chapter 3 should be incorporated. These constants would best be obtained when the experimental work is carried out in an improved manner as suggested in the next section.

8.2.3.1 Collaboration with Research Institutions and Motor Vehicle Manufacturers

Although experimental work was done, it was conducted with some difficult due to lack of appropriate equipment. There would be need to carry out experimental work in conjunction with a research institution or a vehicle manufacturing firm with appropriate equipment to determine the vibration responses as well as the induced force.

Verbal and e-mail interactions with motor vehicle agents working in and outside Zambia showed that it is not possible to have access to technical information unless the manufactures are fully involved in the work. In addition, there would be need to use electronic profilographs for the determination of the exact profile of a pothole. Further, the statistical approach should be incorporated into the study. This would involve categorising vehicles in makes and models, working in conjunction with vehicle manufacturers and motor vehicle garages. In such cases, equipment that can capture both the acceleration and displacement for all the wheel positions at the same time could be used. This way, one is sure that the acceleration determined corresponds to both the displacement and response duration recorded for a given run. This is unlike the equipment used in this work where only one response for one wheel position was captured per run. During such experiments, a new car should be used. This is because when a car is new, the suspension units are more resilient to any form of

shock and load effects and hence the vibration transfer into the main frame at this stage is much less than one with a longer running life.

8.2.3.2 Use of Pothole Dimensions in Road Repair Intervention

Currently in Zambia, the only method of determining the surface condition of a road is by use of *a bump Integrator* [23]. A bump integrator records road bump (ruts, reveling, cracks, potholes, etc, all-inclusive) to produce an International Roughness Index (IRI) measured in m/km. Therefore, road repair intervention is based on the general roughness of a given road. Hence, no measurement of specific potholes is done. Appendix J shows a Decision Tree based on the IRI. In places where potholes are most predominant though, decisions based on suspension failure could be employed, as indicated in the discussion (Section 7.5). Detailed studies in such places can be carried out so that the trend of the failure of motor vehicle suspension components is established. In that case, the impact of the road roughness on these components is based on the extent of potholing.

8.2.3.3 Focus on Specific Motor Vehicle Suspension Components

In order to reduce the error arising from the approximated mechanical properties of the suspension components, on-vehicle tests should be carried out with new components (e.g. shock absorbers, shock pads, tyres, springs etc) that have well known properties.

Having determined the loads arising from hitting a pothole, it would be necessary to have a study to focus on specific components. For example, a detailed study of shock absorbers alone where all common types are considered would enhance understanding of their behaviour under pothole loading. This could be done with a view of designing or redesigning the dampers. It may be the shock absorber orientation, valve actuation, size, etc. Such a study would enable experimentation that would assist in determining the exact effect of potholes on the life span of a suspension component. This would make it easier to give a more precise life span of the component. The work would, however, require significant statistical work. From the experimental results, mathematical models could then be developed to predict the expected life of a given component under pothole loads.

8.2.3.4 General Remarks

From the verbal communication, it was established that specialised companies manufacture certain suspension parts. Parts like shock absorbers, springs and shock pads are manufactured for motor

vehicle companies by different companies. Therefore, to undertake a comprehensive study on these parts, it would be appropriate to carry out the work in collaboration with these companies. During the current work, such companies together with motor vehicle manufacturers were not willing to give out information regarding the technical specifications of the suspension parts as this was taken to be classified information.

REFERENCES

1. National Roads Board (August 1997), **Road Sector Investment Programme (ROADSIP), Core Road Network**, Pages 1-8
2. **Internet (1999),** www.unayton.edu/news/nr/031497.html
3. Rao S.S. (1995), **Mechanical Vibrations**, Third Edition, Addison-Wesley Publishing Company , Pages 191-240, 283,348,358
4. Wong J.Y. (1993),**Theory of Ground Vehicles,** Second Edition, John Wisley and Sons Inc. USA, Pages 348-376
5. Kabondo M.H. (1992) **Computer Simulation Of Effects Of Potholes On The Suspension Systems Of A Passenger Vehicle,** Undergraduate Final Year Project, University of Zambia, Pages 43-67.
6. Bastow D. and Howard G. (1993), **Car Suspension and Handling**, Third Edition, Pentech Press , London , UK, Pages 29-121, 226 - 236
7. Shigley J. E. and Mischke C. R. (1989), **Mechanical Engineering Design,** Fifth Edition, McGraw-Hill Book Company, Singapore, Pages 269-322
8. Chandrupatla T. R. and Belegundu A. D. (1997), **Introduction to Finite Elements in Engineering, Second Edition,** Prentice-Hall International , Inc., USA, Pages 21-290
9. Palm III W. J. (1998), **Introduction To MATLAB For Engineers,** WCB/McGraw-Hill Company, USA Pages 247 - 287
10. The MathWorks Inc (1992),**The Student Edition of MATLAB**, Prentice-Hall, Inc, Paramount Communications Company Englewood Cliffs, NJ, USA, Pages 1-300
11. Campbell C. (1981), **Automobile Suspensions**, 2nd Edition, Chapman and Hall, London
12. Harris C. M. (1996), **Shock and Vibration Handbook**, 4th Edition, McGraw-Hill, New York, U.S.A., Page, 25.28, 31.20
13. Giri N.K. (1996), **Automobile Mechanics (Through Problems)**, 7th Edition, Khannar Publishers, India, Pages 161 - 205, 311 - 330
14. Hillier V.A.W (1991), **Fundamentals of Motor Vehicle Technology**, 4th Edition, Stanley Thornes Publishers Limited, Pages 319, 364 - 366
15. Newton K. et 'al (1989), **The Motor Vehicle**, 11th Edition, Butterworths Limited, U. K., Page 778
16. Robertson A. J. (1985), **Notes on Vehicle Performance**, School of Automotive Studies, Cranfield Institute of Technology, Britain, Pages AJR/CSP/5, AJR/SUS/1-AJR/SUS/2.
17. Bosch (1993), **Automotive Handbook**, 3rd Edition, Robert Bosch GmbH Publishers, Pages 188, 190, 272 - 75

18. Champion R. C and Arnold E. C. (1982), **Motor Vehicle Calculations and Science 2,** 3rd Edition, Pages 299, 301.
19. Van der Zande H. D. (1987), **Handbook for Machine Design,** University of Zambia, School of Engineering, Department of Mechanical Engineering, Lusaka, Pages 3.1-3.25
20. Ashby M. F. and Jones R. H. David (1988), **Engineering Materials 2, An Introduction to Microstructures, Processing and Design**, Pages 10, 11, 206, 207
21. **IRD 885 Analyser/Balancer Manual** (1994), IRD Mechanalysis Company, Ohio, USA.
22. **IRD Fast Track Vibration Machine User's Manual** (1991), IRD Mechanalysis Company, Ohio, USA.
23. Road Repair Database (2000), Department of Roads, Ministry of Works and Supply, Zambia.
24. Cebon David (1999), **Handbook for Vehicle-Road Interaction**, http//rage.eng.cam.ac.uk:80/trg/dcbook
25. **Zambia Highway Code Notes for Motorists**, ZCCM Limited, Mufulira Division, 1997
26. Paulwelussen J. P. and Pacejka H. B. (1995), **Smart Vehicles**, Swets and Zeitlinger Publishers, The Netherlands

APPENDICES

APPENDIX A

DETERMINATION OF CORRECTION FACTORS

A.1 THE SPEEDOMETER CALIBRATION FACTOR

Results

Table A.1: Speedometer Calibration Results

Run	Time(s)	
	Watch 1	Watch 2
1	7	7
2	7	7
3	7	6

Analysis

Average time, T = (7+7+7+7+7+6)/6 = 6.83 s

Hence the speed, V = distance / time = (80 / 6.83) * 3.6 km/h

Therefore, V = 41.17 km/h

The calibration factor is given by:

C = 41.17/40 = 1.05

Hence, the calibration factor is 1.05

A.2 CORRECTION FACTOR FOR UNSPRUNG MASS EXPERIMENTAL RESULTS

Reference is made to Figure A.1. Since the transverse link rotates about a pivot, the angular acceleration at the accelerometer position is the same as that of the wheel hub.

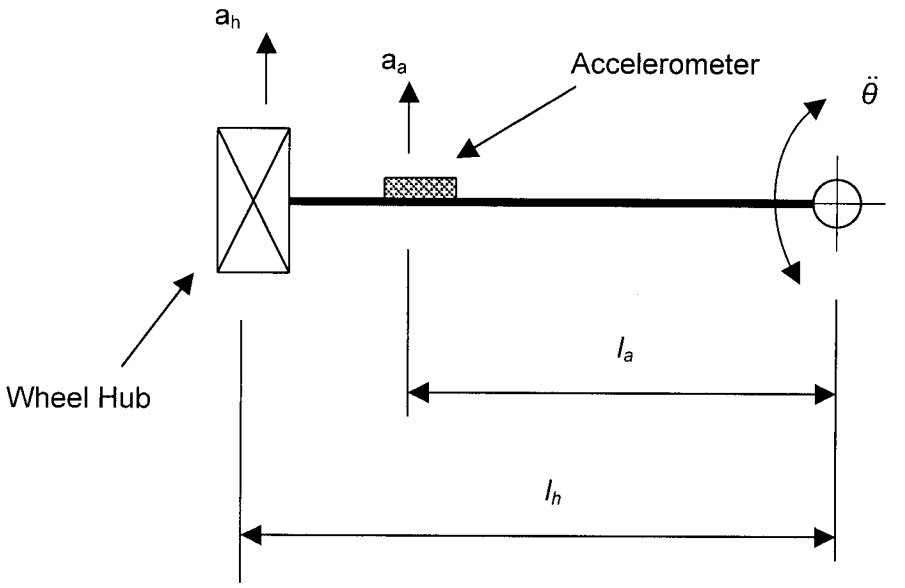

Figure A.1: Transverse link motion

Let,

l_a = the distance from the transverse link pivot to the position of the accelerometer

l_h = the distance from the transverse link pivot to the wheel hub

a_a = linear acceleration at the accelerometer

a_h = linear acceleration of the wheel hub

$\ddot{\theta}$ = angular acceleration of the transverse link

From applied mechanics,

$$a_a = l_a \ddot{\theta} \qquad A.1$$

$$a_h = l_h \ddot{\theta} \qquad A.2$$

From equations A.1 and A.2,

$$\ddot{\theta} = \frac{a_a}{l_a} = \frac{a_h}{l_h}$$

$$\Rightarrow a_h = \left(\frac{l_h}{l_a}\right) a_a \qquad A.3$$

The ratio $\left(\frac{l_h}{l_a}\right)$ is the correction factor.

A.2.1 Front Wheel

Since the distance from the wheel hub to the accelerometer was 0.09m,

$l_a = (l_h - 0.09)$

Therefore, the correction factor is given by,

$$C_a = \frac{l_h}{l_h - 0.09} \qquad A.4$$

But the distance l_h was measured to be 32cm. Replacing the value of l_h into Equation A.4 gives,

C_a = 1.39

Therefore, in this work, for every given experimental value of acceleration on the front unsprung mass, the following relationship applies:

$a_h = 1.39\ a_a$ *A.5*

And thus were the obtained results corrected.

A.2.2 Rear Wheel

The method of calculating C_a is the same as that of the front wheel. The only difference is that the distance of the accelerometer from the wheel hub is 9.5cm while the length l_a = 44cm.

Carrying out similar working as for the front wheel gives:

C_a = 1.28

Therefore, in this work, for every given experimental value of acceleration on the rear unsprung mass, the following relationship applies:

$a_h = 1.28\ a_a$ *A.6*

APPENDIX B

SAMPLES OF THE COLLECTED RESPONSES

B.1 Acceleration Plots

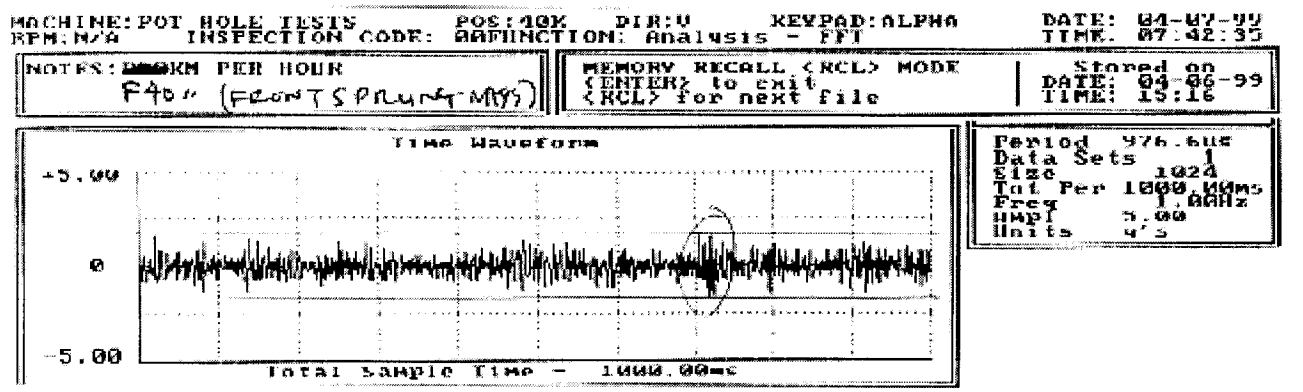

Figure B.1: Acceleration response of the front sprung mass at 40 km/h

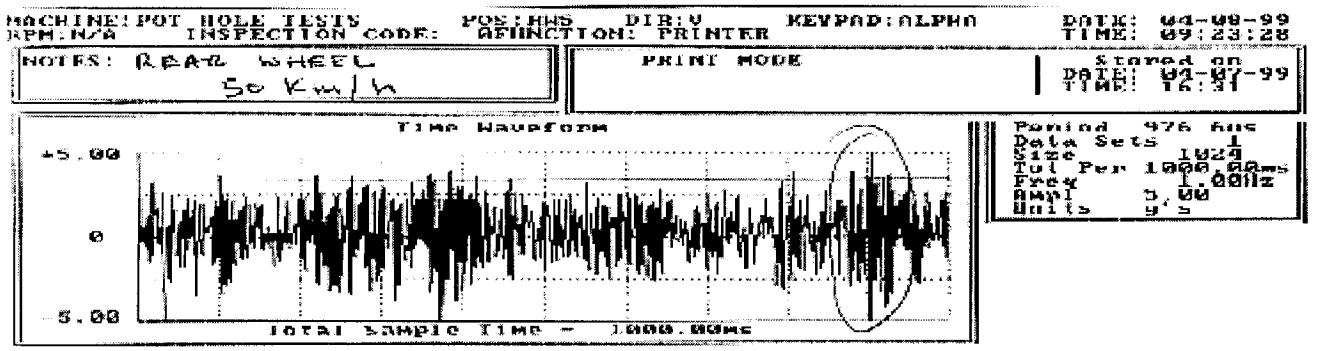

Figure B.2: Acceleration response of the rear unsprung mass at 50km/h

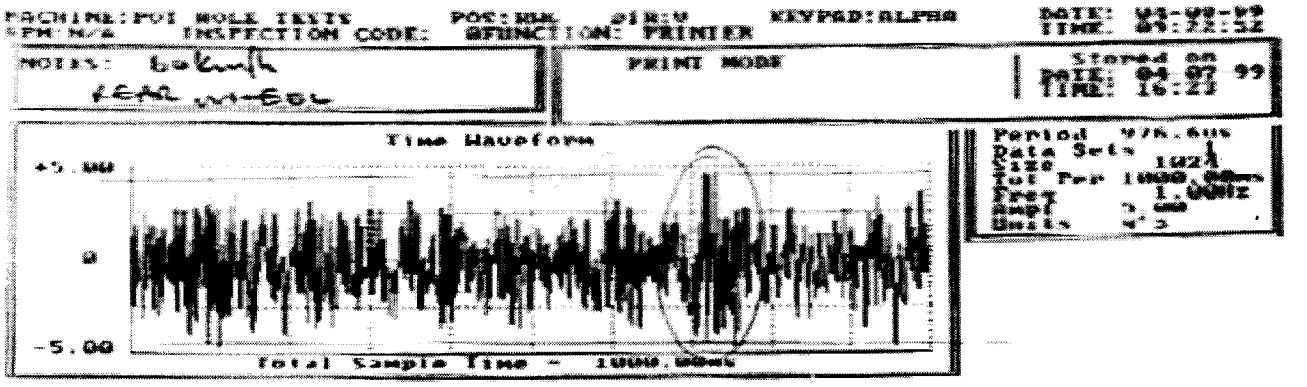

Figure B.3: Acceleration response of the rear unsprung mass at 60km/

B.2 Displacement Plots

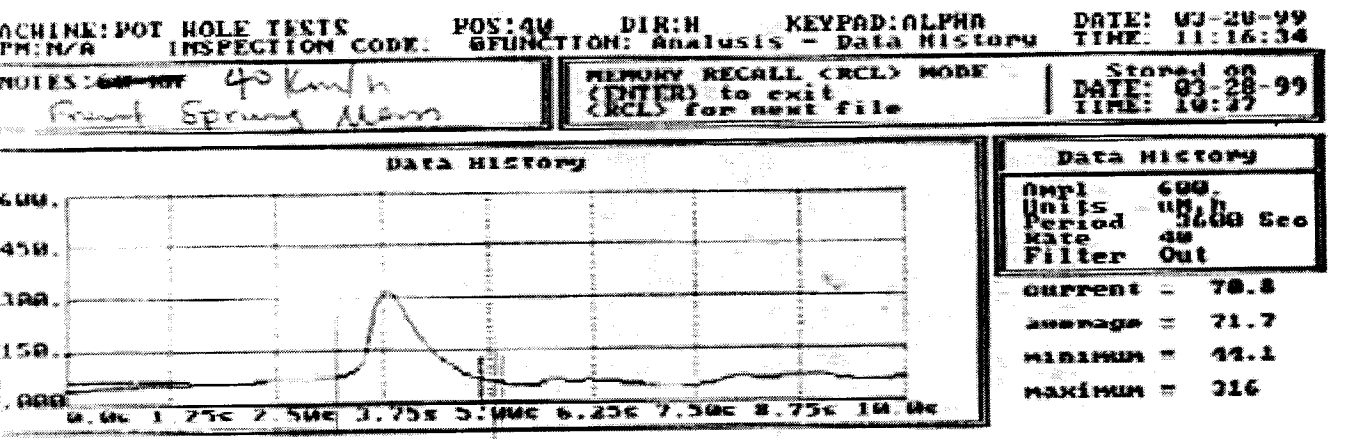

Figure B.4: Displacement response of the front sprung mass at 50km/h

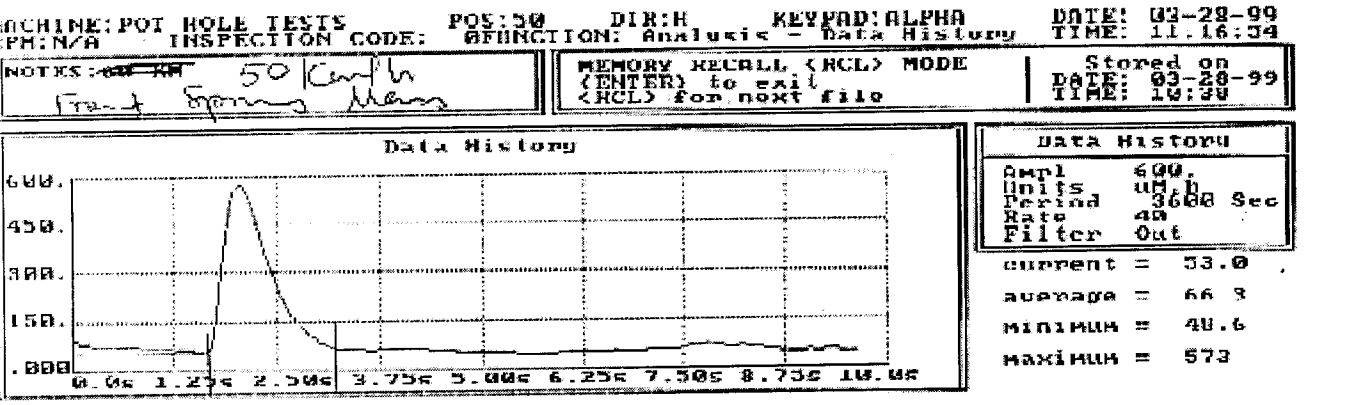

Figure B.5: Displacement response of the front sprung mass at 50km/h

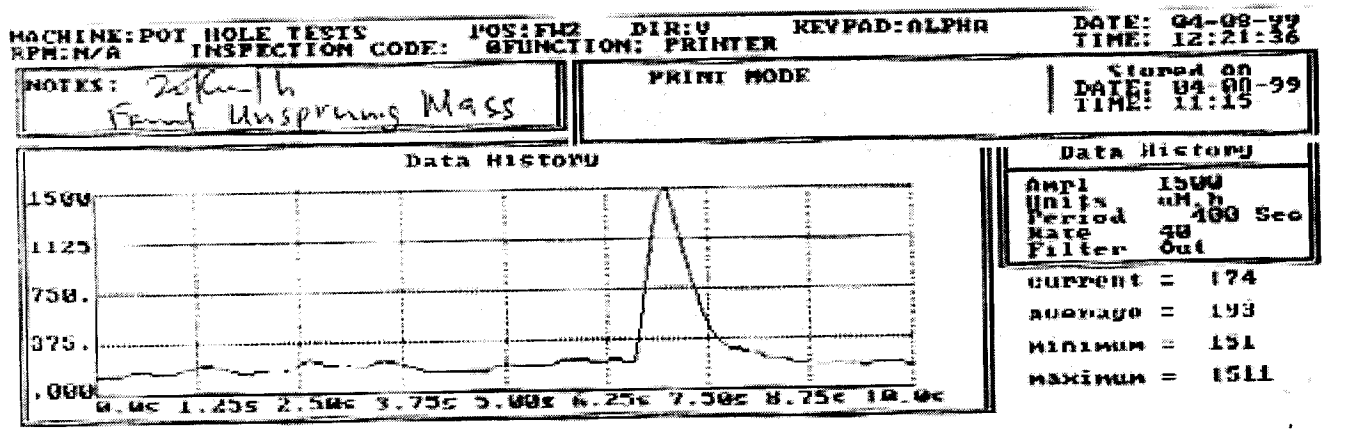

Figure B.6: Displacement response of the front unsprung mass at 20km/h

APPENDIX C

COLLECTED EXPERIMENTAL RESULTS FOR THE CASE STUDY

Table C.1: Maximum Acceleration of the Front Sprung Mass When the Front Wheel Hits a Pothole

Vehicle Speed (km/h)	Acceleration (g's)*				
	Run ➢	1	2	3	Average
10		1.538	1.538	1.346	1.474
20		1.538	1.923	1.731	1.731
30		1.731	2.115	2.308	2.051
40		3.462	2.692	2.692	2.949
50		-	3.846	3.320	3.583
60		3.462	3.846	3.462	3.590

Table C.2: Maximum Acceleration of the Front Unsprung Mass When the Front Wheel Hits a Pothole

Vehicle Speed (km/h)	Acceleration (g's)*				
	Run ➢	1	2	3	Average
10		1.538	1.635	1.538	1.570
20		3.262	3.120	3.142	3.175
30		3.654	3.077	3.077	3.269
40		4.615	4.231	5.000	4.615
50		6.731	6.538	7.115	6.795
60		5.385	5.538	5.192	5.372

* - Acceleration due to gravity; $1g \approx 9.81\ m/s^2$

Table C.3: Maximum Acceleration of the Rear Sprung Mass When the Rear Wheel Hits a Pothole

Vehicle Speed (km/h)	Acceleration (g's)*				
	Run ➢	1	2	3	Average
10		0.538	0.577	0.692	0.602
20		0.846	0.846	0.654	0.782
30		1.231	1.231	1.077	1.180
40		1.934	-	2.154	2.044
50		2.992	3.061	3.300	3.118
60		2.885	2.308	2.308	2.500

Table C.4: Maximum Acceleration of the Rear Unsprung Mass When the Rear Wheel Hits a Pothole

Vehicle Speed (km/h)	Acceleration (g's)*				
	Run ➢	1	2	3	Average
10		2.692	2.308	2.125	2.375
20		3.077	3.462	3.846	3.462
30		4.231	4.240	4.231	4.234
40		6.154	5.962	5.769	5.962
50		9.423	8.846	9.231	9.167
60		8.269	7.981	7.692	7.981

* - Acceleration due to gravity; $1g \approx 9.81\ m/s^2$

APPENDIX D

DETERMINATION OF MEAN VALUES AND STANDARD DEVIATIONS

The mean value, $\bar{x}$, is expressed as,

$$\bar{x} = \frac{\sum x}{n}$$

Where,
x - the value or score
n - the number of values or scores
$\sum$ - the summation, sigma

The standard deviation, σ is given by the following expression,

$$\sigma = \sqrt{\frac{\sum d^2}{n}}$$

where, d is the difference between any value and the mean value ($x - \bar{x}$)

By applying these equations for each data set, the standard deviations were determined for the acceleration values. Since only one run was done for the displacement, calculation of mean values and standard deviations was not applicable.

EXAMPLE

Taking the values of the accelerations obtained for the rear unsprung mass at 10km/h (Table D.3).

Acceleration values for three runs: 1.538g, 1.635g, 1.538g

$$\bar{x} = \frac{1.538 + 1.635 + 1.538}{3} = \underline{\underline{1.570g}}$$

Table D.1 shows the deviations of the values from the mean and their squares.

Table D.1: Deviations of the Values from the Mean

Value (x)	$x - \bar{x}$	$(x - \bar{x})^2$
1.538	-0.032	0.001024
1.635	0.065	0.004225
1.538	- 0.032	0.001024
		$\sum(x - \bar{x})^2 = 0.006273$

Therefore, the standard deviation, $\sigma = \sqrt{\frac{0.006273}{3}}$

$\sigma = \underline{0.046}$ g, which in m/s^2 is (0.065x9.81) = $\underline{0.449 m/s^2}$

The percentage deviation is given by $\frac{0.449}{1.570} x100 = \underline{2.9\%}$

In this case, since $\sigma << \bar{x}$, the three values obtained are not very dispersed. Therefore, the determination of these values was reasonably accurate. The standard deviations for the other data sets are shown below:

Table D.2: Deviations of Front Sprung Mass Acceleration

Velocity (km/h)	Acceleration (g's)			$\bar{x}$, mean (g's)	$x - \bar{x}$, (Value – mean) (g's)			$\sum(x - \bar{x})^2$	σ (g's)	Acceleration (m/s^2)			σ (m/s^2)	Percentage deviation (%)
	Run>	1	2	3		1	2	3			1	2	3		
10		1.538	1.538	1.346	1.474	0.064	0.064	-0.128	0.025	0.091	15.088	15.088	13.204	0.888	6.1
20		1.538	1.923	1.731	1.731	-0.193	0.192	0.000	0.074	0.157	15.088	18.865	16.981	1.542	9.1
30		1.731	2.115	2.308	2.051	-0.320	0.064	0.257	0.173	0.240	16.981	20.748	22.641	2.353	11.7
40		3.462	2.692	2.692	2.949	0.513	-0.257	-0.257	0.395	0.363	33.962	26.409	26.409	3.561	12.3
50		3.269	3.846	2.692	3.269	0.000	0.577	-0.577	0.666	0.577	32.069	37.729	26.409	5.660	7.7
60		3.462	3.846	3.462	3.590	-0.128	0.256	-0.128	0.098	0.181	33.962	37.729	33.962	1.776	5.0

Table D.3: Deviations of Front Unsprung Mass Acceleration

Velocity (km/h)	Acceleration (g's)			$\bar{x}$, mean (g's)	$x - \bar{x}$, (Value – mean) (g's)			$\sum(x-\bar{x})^2$	σ (g's)	Acceleration (m/s^2)			σ (m/s^2)	Percentage deviation (%)
	Run>	1	2	3		1	2	3			1	2	3		
10		1.538	1.635	1.538	1.570	-0.032	0.065	-0.032	0.006	0.046	15.088	16.039	15.088	0.449	2.9
20		3.462	2.500	3.462	3.141	0.321	-0.641	0.321	0.617	0.453	33.962	24.525	33.962	4.449	14.4
30		3.654	3.077	3.077	3.269	0.385	-0.192	-0.192	0.222	0.272	35.846	30.185	30.185	2.668	8.3
40		4.615	4.231	5.000	4.615	0.000	-0.384	0.385	0.296	0.385	45.273	41.506	49.050	3.772	8.3
50		6.731	6.538	7.115	6.795	-0.064	-0.257	0.320	0.173	0.240	66.031	64.138	69.798	2.353	3.5
60		5.385	6.538	5.192	5.705	-0.320	0.833	-0.513	1.059	0.594	52.827	64.138	50.934	5.830	10.4

Table D.4: Deviations of Rear Sprung Mass Acceleration

Velocity (km/h)	Acceleration (g's)			$\bar{x}$, mean (g's)	$x - \bar{x}$, (Value – mean) (g's)			$\sum(x-\bar{x})^2$	σ (g's)	Acceleration (m/s^2)			σ (m/s^2)	Percentage deviation (%)
	Run>	1	2	3		1	2	3			1	2	3		
10		1.15	1.35	1.250	1.250	-0.096	0.096	0.000	0.018	0.078	11.321	13.204	12.263	0.769	6.3
20		1.54	1.35	1.442	1.442	0.096	-0.096	0.000	0.018	0.078	15.088	13.204	14.146	0.769	5.4
30		1.54	1.54	1.520	1.532	0.006	0.006	-0.012	0.000	0.008	15.088	15.088	14.911	0.083	0.6
40		1.92	1.92	1.918	1.921	0.002	0.002	-0.003	0.000	0.003	18.865	18.865	18.816	0.025	0.1
50		3.08	2.69	2.308	2.693	0.384	0.000	-0.385	0.296	0.314	30.185	26.418	22.641	3.080	11.7
60		3.46	3.65	3.558	3.558	-0.096	0.096	0.000	0.018	0.078	33.962	35.846	34.904	0.769	2.2

Table D.5: Deviations of Rear Unsprung Mass Acceleration

Velocity (km/h)	Acceleration (g's)			$\bar{x}$, mean (g's)	$x - \bar{x}$, (Value – mean) (g's)			$\sum(x-\bar{x})^2$	σ (g's)	Acceleration (m/s^2)			σ (m/s^2)	Percentage deviation (%)
	Run>	1	2	3		1	2	3			1	2	3		
10		2.692	2.308	2.125	2.375	0.317	-0.067	-0.250	0.167	0.236	26.409	22.641	20.846	2.318	9.9
20		3.077	3.462	3.846	3.462	-0.385	0.000	0.384	0.296	0.314	30.185	33.962	37.729	3.080	9.1
30		4.231	4.240	4.231	4.234	-0.003	0.006	-0.003	0.000	0.004	41.506	41.594	41.506	0.000	0.1
40		6.154	5.962	5.769	5.962	0.192	0.000	-0.193	0.074	0.157	60.371	58.487	56.594	1.888	2.6
50		9.423	8.846	9.231	9.167	0.256	-0.321	0.064	0.173	0.240	92.440	86.779	90.556	2.354	2.6
60		8.269	7.981	7.692	7.981	0.288	0.000	-0.289	0.166	0.236	81.119	78.294	75.459	2.311	3.0

APPENDIX E

TYPICAL VALUES OF DAMPING COEFFECIENTS OF TYRES

TABLE E.1 Damping Coefficient of Tyres

Tire	Inflation Pressure	Damping Coefficient
Bias-ply	103.4 kPa (15 psi)	4.59 kN · s/m (315 lb · s/ft)
5.60 × 13	137.9 kPa (20 psi)	4.89 kN · s/m (335 lb · s/ft)
	172.4 kPa (25 psi)	4.52 kN · s/m (310 lb · s/ft)
	206.9 kPa (30 psi)	4.09 kN · s/m (280 lb · s/ft)
	241.3 kPa (35 psi)	4.09 kN · s/m (280 lb · s/ft)
Radial-ply	103.4 kPa (15 psi)	4.45 kN · s/m (305 lb · s/ft)
165 × 13	137.9 kPa (20 psi)	3.68 kN · s/m (252 lb · s/ft)
	172.4 kPa (25 psi)	3.44 kN · s/m (236 lb · s/ft)
	206.9 kPa (30 psi)	3.43 kN · s/m (235 lb · s/ft)
	241.3 kPa (35 psi)	2.86 kN · s/m (196 lb · s/ft)

Source Reference: [4]

APPENDIX F

PROPERTIES OF SOME ENGINEERING MATERIALS

TABLE F.1 PROPERTIES OF METALS

Metal	Cost (UK£ (US$) tonne^{-1})	Density (Mg m^{-3})	Young's modulus (GPa)	Yield strength (MPa)	Tensile strength (MPa)	Ductility	Fracture toughness (MPa m$^{1/2}$)	Melting temperature (K)	Specific heat (J kg^{-1} K^{-1})	Thermal conductivity (W m^{-1} K^{-1})	Thermal expansion coefficient (MK^{-1})
Iron	100 (140)	7.9	211	50	200	0.3	80	1809	456	78	12
Mild steel	200–230 (260–300)	7.9	210	220	430	0.21	140	1765	482	60	12
High-carbon steel	150 (200)	7.8	210	350–1600	650–2000	0.1–0.2	20–50	1570	460	40	12
Low-alloy steels	180–250 (230–330)	7.8	203	290–1600	420–2000	0.1–0.2	50–170	1750	460	40	12
High-alloy steels	1100–1400 (1400–1800)	7.8	215	170–1600	460–1700	0.1–0.5	50–170	1680	500	12–30	10–18
Cast irons	120 (160)	7.4	152	50–400	10–800	0–0.18	6–20	1403			
Copper	1020 (1330)	8.9	130	75	220	0.5–0.9	>100	1356	385	397	17
Brasses	750–1060 (980–1380)	8.4	105	200	350	0.5	30–100	1190		121	20
Bronzes	1500 (2000)	8.4	120	200	350	0.5	30–100	1120		85	19
Nickel	3200 (4200)	8.9	214	60	300	0.4	>100	1728	450	89	13
Monels	3000 (3900)	8.9	185	340	680	0.5	>100	1600	420	22	14
Superalloys	5000 (6500)	7.9	214	800	1300	0.2	>100	1550	450	11	12
Aluminium	910 (1180)	2.7	71	25–125	70–135	0.1–0.5	45	933	917	240	24
1000 Series	910 (1180)	2.7	71	28–165	70–180	0.1–0.45	45	915			24
2000 Series	1100 (1430)	2.8	71	200–500	300–600	0.1–0.25	10–50	860		180	24
5000 Series	1000 (1300)	2.7	71	40–300	120–430	0.1–0.35	30–40	890		130	22
7000 Series	1100 (1430)	2.8	71	350–600	500–670	0.1–0.17	20–70	890		150	24
Casting alloys	1100 (1430)	2.7	71	65–350	130–400	0.01–0.15	5–30	860		140	20
Titanium	4630 (6020)	4.5	120	170	240	0.25		1940	530	22	9
Ti–6 Al 4 V	5780 (7510)	4.4	115	800–900	900–1000	0.1–0.2	50–80	1920	610	6	8
Zinc	330 (430)	7.1	105		120	0.4		693	390	120	31
Lead–tin solder	2000 (2600)	9.4	40					456			27

Source reference [20]

TABLE F.2 PROPERTIES OF PLASTICS

Polymer	Cost (UK£ ($US) tonne^{-1})	Density (Mg m^{-3})	Young's modulus (20°C 100 s) (GPa)	Tensile strength (MPa)	Fracture *toughness* (20°C) (MPa m$^{1/2}$)	Glass temperature T_g (K)	*Softening* temperature T_s (K)	Specific heat (J kg^{-1} K^{-1})	Thermal conductivity (W m^{-1} K^{-1})	Thermal expansion *coefficient* (MK^{-1})
Thermoplastics										
Polyethylene, PE (low density)	560 (780)	0.91–0.94	0.15–0.24	7–17	1–2	270	355	2250	0.35	160–190
Polyethylene, PE (high density)	510 (700)	0.95–0.98	0.55–1.0	20–37	2–5	300	390	2100	0.52	150–300
Polypropylene, PP	675 (950)	0.91	1.2–1.7	50–70	3.5	253	310	1900	0.2	100–300
Polytetrafluoroethylene, PTFE	—	2.2	0.35	17–28	—	—	395	1050	0.25	70–100
Polystyrene, PS	650 (910)	1.1	3.0–3.3	35–68	2	370	370	1350–1500	0.1–0.15	70–100
Polyvinylchloride, PVC (unplasticised)	425 (595)	1.4	2.4–3.0	40–60	2.4	350	370	—	0.15	50–70
Polymethylmethacrylate, PMMA	1070 (1550)	1.2	3.3	80–90	1.6	378	400	1500	0.2	54–72
Nylons	2350 (3300)	1.15	2–3.5	60–110	3–5	340	350–420	1900	0.2–0.25	80–95
Resins or thermosets										
Epoxies	1150 (1600)	1.2–1.4	2.1–5.5	40–85	0.6–1.0	380	400–440	1700–2000	0.2–0.5	55–90
Polyesters	930 (1300)	1.1–1.4	1.3–4.5	45–85	0.5	340	420–440	1200–2400	0.2–0.24	50–100
Phenolformaldehyde	750 (1050)	1.27	8	35–55	—	—	370–550	1500–1700	0.12–0.24	26–60
Elastomers (rubbers)										
Polyisoprene	610 (850)	0.91	0.002–0.1	≈10	—	220	≈350	≈2500	≈0.15	≈600
Polybutadiene	610 (850)	1.5	0.004–0.1		—	171	≈350	≈2500	≈0.15	≈600
Polychloroprene	1460 (2050)	0.94	≈0.01		—	200	≈350	≈2500	≈0.15	≈600
Natural polymers										
Cellulose fibres		1.5	25–40	≈1000	—	—	—	—	—	—
Lignin		1.4	2.0	—	—	—	—	—	—	—

Source reference: [20]

TABLE F.3 PROPERTIES OF PLASTIC MATERIALS USED FOR BUSHES IN AUTOMOBILES

	Oil-impregnated sintered bearings		Polymer bearings		Metal-backed composite bearings Liner		Synthetic carbons
	Sintered iron	Sintered bronze	Thermoplastic polyamide	Duroplastic polyimide	PTFE + additive	Acetal resin	
Comp. strength N/mm²	80 ... 180		70	110	250	250	100 ... 200
Max. sliding velocity m/s	10	20	2	8	2	3	10
Typical load N/mm²	1 ... 4 (10)		15	50 (at 50°C) 10 (at 200°C)	20 ... 50	20 ... 50	50
Permissible operating temperature °C Short-term	−60 ... 180 (depends on oil) 200		−130 ... 100 120	−100 ... 250 300	−200 ... 280	−40 ... 100 130	−200 ... 350 500
Coefficient of friction without lubrication	with lubrication 0.04 ... 0.2		0.2 ... 0.35	0.2 ... 0.5 (unfilled) 0.1 ... 0.4 (filled)	0.04 ... 0.2	0.07[1]) ... 0.2 [1]) PTFE filled	0.1 ... 0.35
Thermal conductivity W/(m · K)	20 ... 40		0.3	0.4 ... 1	46	2	10 ... 65
Corrosion resistance	poor	good	very good		good	good	very good
Chemical resistance	no		very good		conditional	conditional	good
max. $p \cdot v$ (N/mm²) · (m/s)	20		0.05	0.2	1.5 ... 2		0.4 ... 1.8
Embeddability of dirt and abraded material	poor		good	good	poor	good	poor

Source reference [17]

TABLE F.4 PROPERTIES OF SPRING STEEL

Spring steel

Materials	DIN	Primary alloying constituents, approx. in % by wt.; E and G in N/mm²	Diameter mm	R_m [1] min. N/mm²	Z [2] %	σ_b [3] N/mm²	τ_{kh} [4] N/mm²	τ_{perm} [5] N/mm²	Characteristic properties, applications
Spring steel wire D patented and springy drawn [6]	17 223 Sheet 1	0.8 C, 0.6 Mn, < 0.35 Si E = 206 000 G = 81 500	1 3 10	2230 1840 1350	40 40 30	1590 1280 930	380 [7] 360 [7] 320	1115 920 675	For high maximum stresses (see page 280)
Stainless-steel spring wire	17 224	< 0.12 C, 17 Cr, 7.5 Ni E = 185 000 G = 73 000	1 3	2000 1600	40 40	1400 1130	– –	1000 800	Stainless-steel springs
Oil-tempered valve-spring steel wire [6]	17 223 Sheet 2	0.65 C, 0.7 Mn; < 0.30 Si E = 206 000 G = 80 000	1 3 8	1720 1480 1390	45 45 38	1200 1040 930	380 [8] 380 [8] 360 [8]	860 740 690	For severe fatigue loading
Oil-tempered, alloyed valve-spring steel wire VD Si Cr [6]	–	0.55 C; 0.7 Mn, 0.65 Cr, 1.4 Si E = 200 000 G = 79 000	1 3 8	2060 1920 1720	50 50 40	– – –	430 [8] 430 [8] 380 [8]	1030 960 860	For most severe fatigue loading and high temperatures
Oil-tempered, alloyed valve-spring steel wire VD Cr V [6]	–	0.7 C, 0.7 Mn, 0.5 Cr; 0.15 V, ≤ 0.30 Si E = 200 000 G = 79 000	1 3 8	1860 1670 1420	45 45 40	– – –	470 [8] 470 [8] 400 [6]	930 835 710	For severe fatigue loading
Spring steel strip Ck 85	17 222	0.85 C, 0.55 Mn; 0.25 Si E = 206 000	h ≤ 2.5	1470		1270	σ_{bh} = 640		Highly stressed leaf springs
Stainless-steel spring strip	17 224	< 0.12 C; 17 Cr; 7.5 Ni E = 185 000	h ≤ 1	1370	–	1230	σ_{bh} = 590	–	Stainless steel leaf springs.

[1] Tensile strength [2] Reduction of area at fracture. [3] Permissible bending stress [4] Permissible lift stress for stress cycles endured $N \geq 10^7$.
[5] Permissible maximum stress for temperatures to approx. 30 °C and 1 ... 2 % relaxation in 10 hrs.; for higher temperatures see page 280.
[6] See pages 280 and 281 for fatigue-strength diagrams. [7] 400 N/mm² for peened springs [8] Approx. 40 % higher for peened springs.

Source reference [17]

APPENDIX G

ESTIMATION OF MAXIMUM POTHOLE DIMENSIONS

G.1 Determination of the Maximum Pothole Length

Normally, a pothole should not go beyond an area of 1 m^2 before a maintenance intervention is carried out [23]. Assuming a pothole to be circular, the equivalent diameter, d_{eq}, is calculated as given below:

$$\frac{\pi d_{eq}^{2}}{4} = 1,$$

$$\Rightarrow d_{eq} = \frac{2}{\sqrt{\pi}}$$

$$d_{eq} = 1.13m$$

Hence the maximum practical length was taken to be 1.2m

G.2 Determination of the Maximum Pothole Depth

Table G.1 Paved Road Layers

Layer	Typical Height (m)
Overlay	0.040
Stabiliser	0.150
Sub-layer	0.150
Total	**0.340**

Since the total height is 0.340m [23], the maximum depth was assumed to be 0.30m

APPENDIX H

SIMULATED DYNAMIC TYRE FORCES OF A TRUCK

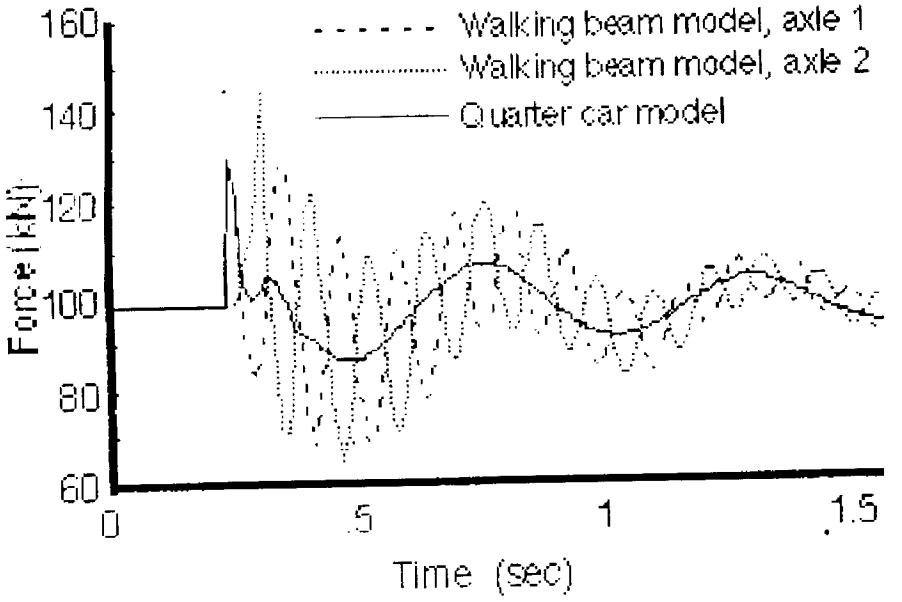

(a) Response to a 10mm step

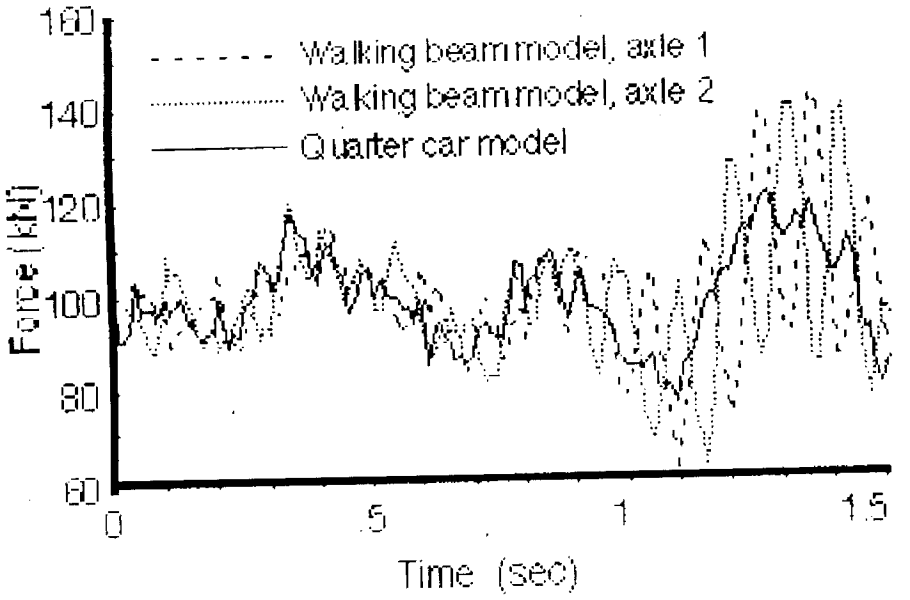

(b) Response to a sample of 'good' random road

Figure H.1: Dynamic tyre force histories generated by the simple vehicle models at 80 km/h [24]

APPENDIX I

COST OF REPAIRING AND REPLACING OF PAVED ROADS

Table I.1 Cost of Repairing and Replacement of Paved Roads in Zambia

Intervention	**Type of Intervention**	**Cost (US$)**
Road Resurfacing	Slurry Seal	0.95 /m^2
	Surface dressing without levelling	2.6/m^2
	Surface dressing with levelling	9.4/m^2
Pothole Patching	Shallow patching	6.5/m^2
	Deep patching	26.9/m^2
Total Rehabilitation	Replacement of Paved Road	250, 000/km

Source reference: Department of Roads, Ministry of Works and Supply, Zambia [23]

APPENDIX J

DECISION TREE FOR PAVED ROAD DAMAGE INTERVENTION

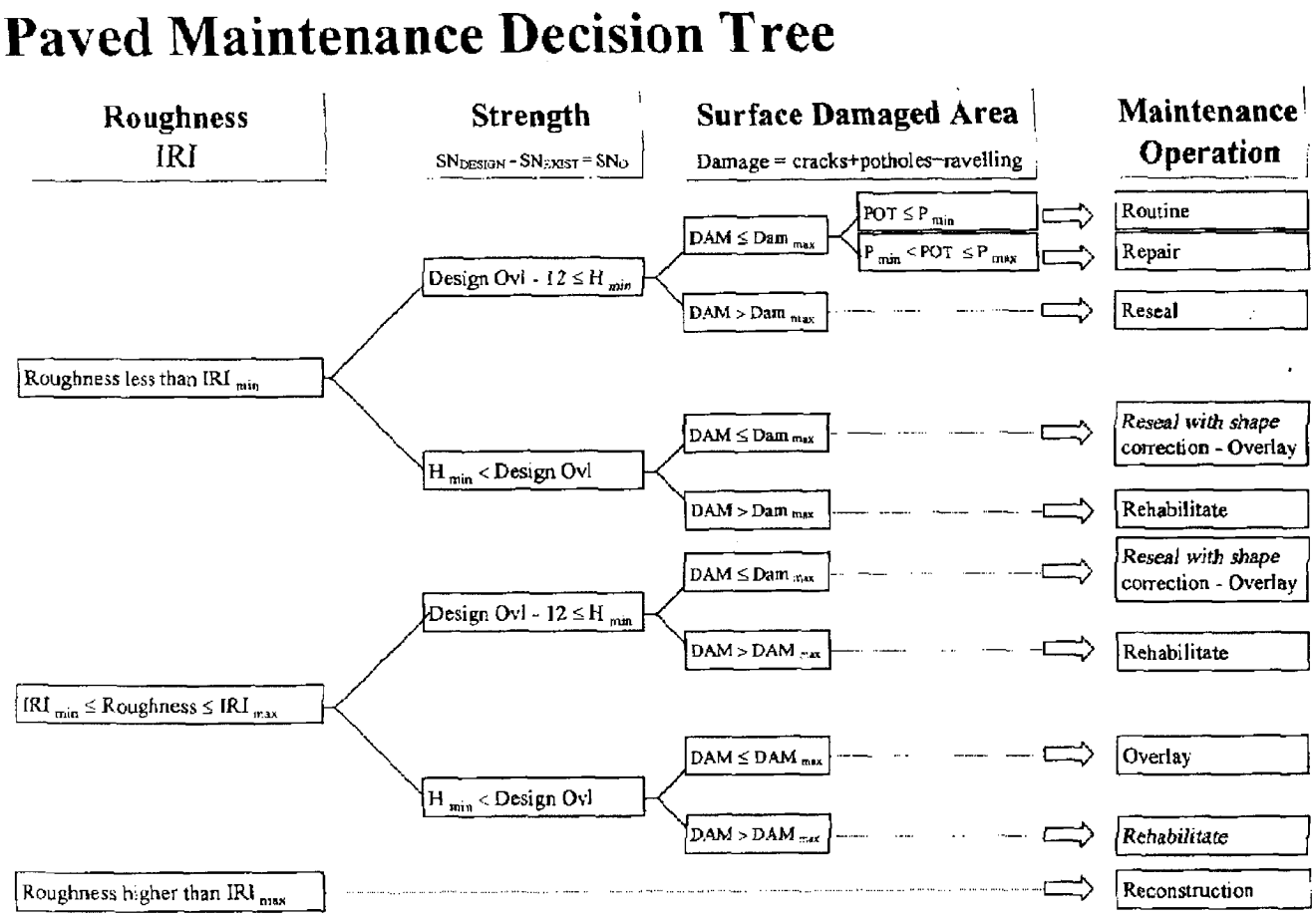

Figure J.1 Paved Road Maintenance Decision Tree

Source reference: Ministry of Works and Supply, Department of Roads, Zambia [23]